

2008

Micropiles: Case Studies

Daniela Ramirez
Western University

Follow this and additional works at: <https://ir.lib.uwo.ca/digitizedtheses>

Recommended Citation

Ramirez, Daniela, "Micropiles: Case Studies" (2008). *Digitized Theses*. 4326.
<https://ir.lib.uwo.ca/digitizedtheses/4326>

This Thesis is brought to you for free and open access by the Digitized Special Collections at Scholarship@Western. It has been accepted for inclusion in Digitized Theses by an authorized administrator of Scholarship@Western. For more information, please contact wlsadmin@uwo.ca.

Micropiles: Case Studies

(Thesis format: Monograph)

by

Daniela Ramirez

Graduate Program in Engineering Science
Department of Civil and Environmental Engineering

Submitted in partial fulfillment
of the requirements for the degree of
Master of Engineering Science

Faculty of Graduate Studies
The University of Western Ontario
London, Ontario
April, 2008

© Daniela Ramirez 2008

THE UNIVERSITY OF WESTERN ONTARIO
FACULTY OF GRADUATE STUDIES

CERTIFICATE OF EXAMINATION

Joint-Supervisor

Dr. Sean Hinchberger

Joint-Supervisor

Dr. K.Y. Lo

Supervisory Committee

Dr.

Examiners

Dr. M. Hesham El Naggar

Dr. Tim Newson

Dr. Anthony H. Tawil

The thesis by

Daniela Ramirez

entitled:

Micropiles: Case Studies

is accepted in partial fulfilment of the
Requirements for the degree of
Master of Engineering Science

Date _____

Chair of the Thesis Examination Board

ABSTRACT

Micropiles are small diameter bored piles. This type of deep foundation is increasingly being adopted in North America to retrofit existing structures, because of minimal installation vibration, excellent load capacity for seismic upgrades and low headroom and tight access applications. The main objective of this thesis is to investigate and analyze the results of full-scale load tests on micropiles to gain insight into factors affecting the development of axial load capacity. This thesis examines in detail the response of 9 micropiles in soil and 7 micropiles in rock during compressive axial load tests. The micropiles in soil are analyzed using the finite element software PLAXIS. The rock micropiles are analyzed using a closed form solution. Some of the micropiles were instrumented with a device called Contractometer, which permitted measurement of the distribution of axial compression along the pile at various axial loads. The internal contractometer measurements provide information on the structural performance of the pile. This study suggests that a significant portion of the axial capacity of micropiles comes from pile enlargement and post-yield dilatancy of the pile-to-soil interface.

Key Words: Micropiles (minipiles) , Deep Foundations, Bored, Grouted, Piles, PLAXIS, Finite Element

DEDICATION

To my Husband and
The Memory
of my
Father

ACKNOWLEDGEMENTS

The author would like to sincerely thank and acknowledge Dr. Sean D. Hinchberger, Professor of the Geotechnical Research Centre at The University of Western Ontario, for guidance, patience and perseverance; Isherwood Associates for general funding, specially Nadir Ansari for encouragement and support; Jim Bruce, whose company Geo-Foundations Contractors Inc. funded the majority of micropile tests presented in this thesis, and Peter Lausch, of Mine Design Technologies, for supply and insights into the Contractometer.

TABLE OF CONTENTS

CERTIFICATE OF EXAMINATION	ii
ABSTRACT	iii
DEDICATION	iv
ACKNOWLEDGEMENTS	v
TABLE OF CONTENTS	vi
LIST OF FIGURES.....	viii
LIST OF TABLES.....	xii
CHAPTER 1.....	1
1.1 Overview of Thesis.....	2
1.2 Thesis Layout	3
1.3 Original Contributions.....	4
1.4 Definitions.....	5
CHAPTER 2.....	7
2.1 Introduction	8
2.2 History of Micropiles.....	8
2.3 Micropile Classification	10
2.4 Current Design Methodology	14
2.4.1 Design Considerations	14
2.4.2 Axial Capacity.....	14
2.4.3 Methods of Interpreting Pile Load Tests.....	19
2.4.4 Methods of Estimating Pile Deflection For Design.....	20
2.5 Contractometer	25
2.6 Grout Properties	28
2.7 Summary and Conclusions	31
CHAPTER 3.....	33
3.0 Introduction to Micropile Case Studies in Soil.....	34
3.1 Methodology.....	34
3.1.1 Pile Construction	34
Method II - Injection-bored, Hollow Core Bar Method	37
3.1.2 Pile Enlargement.....	39
3.1.3 Pile Load Tests	40
3.1.4 Finite Element (FE) Analysis.....	43
3.1.5 Strain in the Micropiles.....	49
3.2 Case 1 - Nipigon, Ontario.....	49
3.3 Case 2 - Point Edward, Ontario	63
3.4 Case 3 - Kitchener, Ontario	68
3.5 Case 4 - Alliston, Ontario.....	73
3.6 Case 5 - Pembroke, Ontario.....	77
3.7 Conclusions.....	82
CHAPTER 4.....	84
4.0 Case Studies of Micropiles Tested in Rock	85

4.1.1 Methodology	85
4.1.2 Rock Micropile Installation Methods	88
4.2 Case 1 - Intersection of Dundas and McCaul, (Toronto)	92
4.3 Case 2 - Micropile in Metamorphic Rock in Thunder Bay, Ontario	100
4.4 Case 3 - Intersection of Yonge and Dundas Toronto Micropile	104
Confirmation Cases	108
4.5 Case 4 – Tip Top Lofts, Toronto	108
4.6 Case 5 - Exhibition Place, Toronto	109
4.7 Case 6 - Mississauga, Ontario	110
4.9 Conclusions	112
CHAPTER 5	114
5.1 Summary	115
5.2 Conclusions	116
5.3 Recommendations	117
REFERENCE	119
APPENDIX A	121
GROUT COMPRESSION RESULTS	121
APPENDIX B	123
RAW LOAD TEST RESULTS	123
APPENDIX C	128
SENSITIVITY ANALYSIS	128
CV	130

LIST OF FIGURES

Figure 1.1 Typical Micropile Geometry.....	6
Figure 2.1 Fernando Lizzi Example of Pali Radice (Lizzi 1982).....	9
Figure 2.2 Types of Grouting Procedures (FHWA 2000).....	13
Figure 2.3 Bearing capacity factor (After Berezantsev et al, 1961).....	19
Figure 2.4 Davisson's Method (Poulos 1980).....	20
Figure 2.5 Poulos Influence Factor R_v	22
Figure 2.6 Poulos Influence Factor I_o	23
Figure 2.7 Poulos Influence Factor R_b	23
Figure 2.8 Poulos Influence Factor R_k	24
Figure 2.9 Poulos Influence Factor R_h	24
Figure 2.11 Schematic of Contractometer Inner Workings.....	27
Figure 2.12 Effects of Water to Cement Ratio on the Strength of Grout (FHWA 2000)	29
Figure 2.13 Test Set Up.....	30
Figure 2.14 Stress Strain Curve for Grout Cylinder.....	31
Figure 2.15 Stress Strain Curve for Grout Cylinder.....	31
Figure 3.1 Installation of Rotary Duplex Micropile.....	36
Figure 3.2 Diagram Illustrating the Installation of Grout.....	37
Figure 3.3 Injection bored Hollow Core bar.....	38
Figure 3.4 Hollow Core Bar Method showing Pile Enlargement (Contech Systems Titan Bar Website).....	39
Figure 3.5. Actual and Idealized Pile Geometry	40
Figure 3.6 Schematic Set-Up for Applying Loads to Test Piles Using a Hydraulic Jack Acting Against an Anchored Reaction Frame.....	41
Figure 3.7 Typical Micropile Compression Test Set Up. (Note: The timbers were used temporarily to support the reaction beam prior to jacking).....	42

Figure 3.8 Material Zones and FE Mesh.	45
Figure 3.9. Typical F.E. Load-Displacement Response For $\psi = 0^\circ$ and $\psi \neq 0^\circ$	47
Figure 3.10 Plastic zones (in red) at point “A”.....	48
Figure 3.11 Plastic zones (in red) at Point “B”.....	48
Figure 3.12 Installation Details for East Nipigon-Micropile 1.....	53
Figure 3.13 Load Displacement Behaviour for the East Nipigon-Micropile 1.	54
Figure 3.14 Strain Depth for East- Nipigon Micropile 1.....	55
Figure 3.15 Installation Details for East Nipigon Micropile 2.	57
Figure 3.16 Load Displacement Behaviour East-Nipigon Micropile 2.....	58
Figure 3.17 Installation Details for the West-Nipigon Micropile 3.	61
Figure 3.18 Load Displacement Behaviour for West-Nipigon Micropile 3.....	62
Figure 3.19 Strain Depth for West-Nipigon Micropile 3.	62
Figure 3.20 Installation Details For The Point Edward Case.	66
Figure 3.21 Load Displacement Behaviour For Point Edward-Micropile 4.	67
Figure 3.22 Load Displacement Behaviour for Point Edward Micropile 5.....	67
Figure 3.23 Installation Details for Kitchener Micropiles.....	71
Figure 3.24 Load Displacement Behaviour for Kitchener-Micropile 6.	72
Figure 3.25 Load Displacement Behaviour for Kitchener-Micropile 7.	73
Figure 3.26 Installation Details for The Alliston Case.....	76
Figure 3.27 Load Displacement Behaviour for Alliston Micropile.....	77
Figure 3.28 Installation Details for Pembroke-Micropile 9.	80
Figure 3.29 Load Displacement Behaviour For Pembroke-Micropile 9.	81
Figure 3.30 Strain vs. Depth Graph for Pembroke-Micropile 9.....	81
Figure 4.1 General Geometry of Rock Micropiles.	86
Figure 4.2 Elastic Settlement Influence Factors (after Pells and Turner).....	87

Figure 4.3 Distribution of Side wall Shear (Pells and Turner 1995).....	88
Figure 4.4 Injection Bored Hollow Core Bar.	89
Figure 4.5 Installation of a Rotary Duplex Micropile in Rock.....	91
Figure 4.6 Installation of Micropile in Rock - Pressure Grouting.....	91
Figure 4.7 Installation Details for AGO-Micropile 1.	94
Figure 4.8 Load Displacement for AGO-Micropile 1.	95
Figure 4.9 Strain vs. Depth Graph for AGO-Micropile 1.	95
Figure 4.10 Installation Details for AGO- Micropile 2.	98
Figure 4.11 Load Displacement for AGO-Micropile 2.	99
Figure 4.12 Strain vs. Depth for AGO-Micropile 2.	99
Figure 4.13 Installation Details for Thunder Bay-Micropile 3.....	102
Figure 4.14 Load Displacement for Thunder Bay-Micropile 3.....	103
Figure 4.15 Strain vs. Depth for Thunder Bay-Micropile 3.	103
Figure 4.16 Installation Details for Yonge and Dundas Toronto Micropile.	106
Figure 4.17 Load Displacement Behaviour for Yonge and Dundas Toronto Micropile.	107
Figure 4.18 Strain vs. Depth Graph for Yonge and Dundas Toronto Micropile.....	107
Figure 4.19 Load Displacement Behaviour for Bathurst and Lakeshore Toronto Micropile.	109
Figure 4.20 Load Displacement Behaviour for Exhibition Place Toronto Micropile..	110
Figure 4.21 Load Displacement Behaviour for Mississauga Micropile.....	112
Figure C1. Sensitivity Analysis for psi angle.....	129
Figure C2. Sensitivity Analysis for phi angle.....	130
Figure C3. Sensitivity Analysis for Elastic Modulus	131
Figure C4. Sensitivity Analysis for Diameter of the pile	132
Figure C5. Sensitivity Analysis for the Ko.....	133

LIST OF TABLES

Table 2.1. Values of Soil to Ground Adhesion (FHWA 2000).....	18
Table 2.2 Grout Sample Results.....	30
Table 3.1 Parameters Used for the Micropiles at Nipigon.....	54
Table 3.2 Parameters Used for Micropiles 2 at Nipigon.....	58
Table 3.3 Parameters Used for Micropile 3 at Nipigon.....	63
Table 3.4. Parameters used for Point Edward.....	68
Table 3.5. Parameters used for Kitchener Micropile 6.....	72
Table 3.6 Parameters used for Kitchener Micropile 7.....	73
Table 3.7 Parameters used for Alliston Case.....	77
Table 3.8 Parameters used for Pembroke.....	79
Table 3.9 Calculated Theoretical Micropile Capacities.....	82
Table 4.1 Theoretical and Measured Strains along the casing for Micropile 1.....	93
Table 4.2 Theoretical and Measured Strains along the casing for Micropile 2.....	97
Table 4.4 Theoretical and Measured Strains along the casing for Micropile 4.....	105

CHAPTER 1
OVERVIEW OF THESIS

1.1 Overview of Thesis

Micropiles are a type of deep foundation that originated in the 1950's after WWII when many structures in Europe were being rebuilt and/or retrofitted. At that time, micropiles were used in groups of small diameter (up to 100 mm) piles that worked collectively to reinforce the earth. Micropiles have since changed to be up to 300 mm diameter piles that are more heavily loaded and that mostly work independently from one another.

The use of micropiles in North America has increased in recent years along with the number of projects involving retrofitting existing structures. Retrofitting projects can involve upgrading the compressive or uplift capacity of foundations as a result of, for example, either upgraded seismic design accelerations (see CNBCC 2006) or construction of additional floors on top of existing structures. Retrofits are typically done in low headroom settings with restrictions on vibrations to minimize settlement or disturbance of nearby structures. Micropiles are an ideal foundation alternative for such installations since they can be installed with low headroom (typically one floor height - 2.7 m) using small drill rigs. In addition, micropiles can be installed with minimal vibration and consequent disturbance to nearby sensitive structures. In general, it is anticipated that the use of micropiles will increase with time in North America as the infrastructure ages. It is envisioned that the contributions of this thesis will help improve the design of these foundations.

The objective of this thesis is to study and gain an improved understanding of micropile construction methods, the load-displacement behaviour of micropiles, and the distribution of strain in micropiles during loading.

1.2 Thesis Layout

This section describes the layout of this thesis. Chapter 2 provides an overview of micropiles. This overview includes the history of micropiles, current design and construction practices, and typical approaches to the analysis of load data. Chapter 2 describes the Contractometer; an instrument used to measure compression along the length of some of the micropile load tests presented in Chapter 3 and 4. The last section of Chapter 2 describes the properties of grout and some compression tests that were performed on grout used to build some of the micropiles studied in Chapters 3 and 4.

Chapter 3 describes cases of micropiles constructed in permeable soils (sands, sands with silt and sands and gravels) and the analysis of micropile load tests from each case using the commercial software PLAXIS. The first section of Chapter 3 describes the two different pile construction procedures considered, the procedures for pile testing, and how strain calculations were made based on Contractometer readings. This is followed by a detailed evaluation of 9 micropile load tests using the finite element program PLAXIS. From this analysis the main considerations for the design of micropiles is summarized. Four of the tested micropiles were instrumented with a Contractometer to obtain compression measurements along the length of the micropile. These measurements provide additional insight into the structural performance of the piles.

Next, Chapter 4 describes detailed testing and analysis of 7 micropiles socketed into rock. Four of these cases had Contractometers embedded in the piles to measure compression along the length during loading. In most of the cases, it is shown that a classic rock socket is mobilized in hard rock and in soft rock there is yielding of the pile

at the tip. Also, in this Chapter a brief description is given in table format of several other micropiles tested in rock, not instrumented with a Contractometer.

Finally, Chapter 5 summarizes conclusions made from the analysis and observations contained in this thesis and identifies potential areas for future research.

1.3 Original Contributions

The main contribution of this thesis is to present and analyze full scale instrumented micropile tests done in rock and soil in Ontario, Canada. The in-depth analysis of each full scale micropile test includes details of the pile installation including in some cases the grouting takes, the soil stratigraphy, drilling methodology, the load displacement curves, and internal strain measurement. It is shown that the load capacity of micropiles is strongly affected by the installation method and grouting procedure.

The load-deflection plots based on micropile results show that Davisson's criterion is not always accurate when estimating the ultimate capacity of micropiles from pile load test results. In addition, the estimation of pile deflection cannot always be calculated using Poulos and Davis solutions since the slenderness of some micropiles lies outside the range of parameters reported in their graphs.

The use of a Contractometer to measure compression is an original contribution. The compression measurement gives a basis for identifying the probable load carrying mechanisms of micropiles. For example, it has been observed that there are high strains calculated from the contractometer measurements in the tip of micropiles socketed into weak rock.

The finite element analyses presented in this thesis demonstrate that the diameter enlargement effect of micropiles installed in permeable soils causes significant increased

axial load capacity. The analysis also indicates that the friction angle of the pile-to-soil interface is the same as that of the surrounding soil. Finite element analysis further suggests that a significant portion of the axial capacity of micropiles occurs after yielding due to dilatancy of the pile-to-soil interface.

1.4 Definitions

Figure 1.1 illustrates the typical geometry of a micropile. Micropiles usually have a cased length to prevent buckling or bending in the top where the micropile will be connected to a pile cap or to a superstructure. Below the cased section it has an uncased length where there is direct contact between the grout and the surrounding soil or rock. The main structural member of a micropile is usually a concentric steel bar embedded in the pile during construction. The steel bar may be solid or hollow. In cases where the load is very large there may be several steel bars. The micropile typically supports load by means of friction between the grout and the surrounding soil or rock. There may also be a contribution from end bearing at the tip of the micropile. Figure 1.1a shows typical micropile geometry and Figure 1.1b illustrates the skin friction and end-bearing components of axial load capacity.

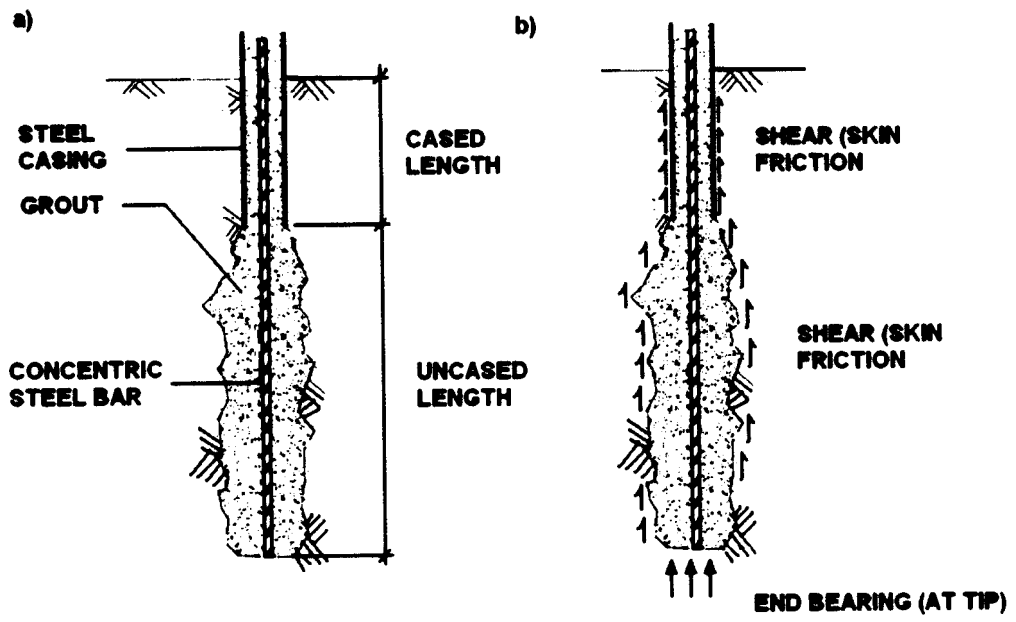


Figure 1.1 Typical Micropile Geometry

CHAPTER 2
MICROPILE BACKGROUND

2.1 Introduction

This Chapter summarizes the history of micropiles, and the current state-of-the-art for micropile design. The first section describes where micropiles originated and how micropiles have changed over time. The second section provides a description of how micropiles are categorized and a brief introduction of installation techniques. The next section lists closed form solutions typically used for large diameter piles to estimate pile capacity and pile settlement. In some of the micropile load cases presented in Chapters 3 and 4 a Contractometer was used to measure relative movement within micropiles. In Chapter 2 the inner workings of the Contractometer are described. The last section describes the results of unconfined compression tests on grout specimens that were the basis of grout properties used in the finite element analysis of each micropile tested in Chapter 3.

2.2 History of Micropiles

Micropiles were first conceived and used by Fernando Lizzi to retrofit structures in Italy after World War II (FHWA 2000). Lizzi used root piles (*pali radice*) which are small diameter piles (from 100 mm diameter to 250 mm) with lengths typically varying from 6m to 30 m. Lizzi describes the installation of a root pile as rotary drilling through existing structures into the soil below (Lizzi 1982). The holes were filled with cement grout and a steel bar. It was hypothesized that *Pali radice* behave like tree roots since they were usually installed in groups of inclined micropiles forming a lattice. Lizzi reinforced both the foundations of existing structures and elements of the above-grade superstructure together to make a more competent structure as a whole. F.Lizzi also reinforced the walls of existing structures with a method he called “*Reticolo cementato*”. An example of a structure that was restored by F.Lizzi is illustrated in

Figure 2.1. Figure 2.1 depicts church “Sant’Andrea delle Fratte” located in Rome. In this Figure the “pali radice” is shown below the structure and “Reticolo Cementato” is shown within the walls of the structure.

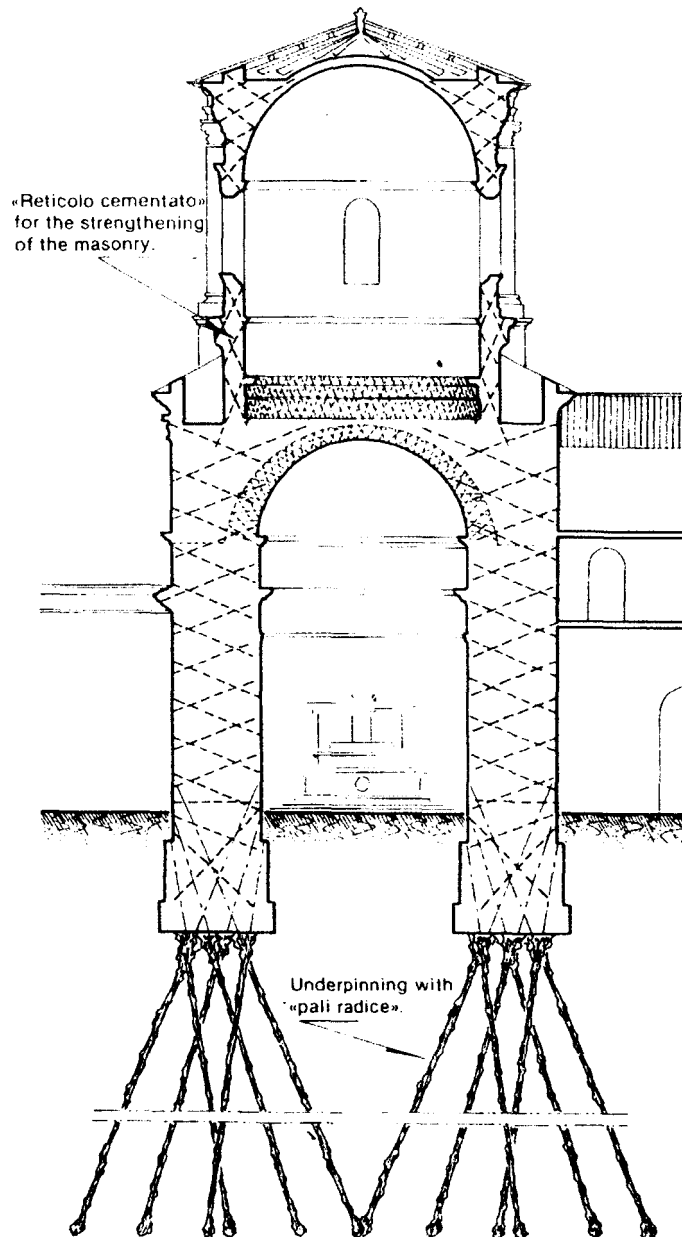


Figure 2.1 Fernando Lizzi Example of Pali Radice (Lizzi 1982).

Modern micropiles are typically of larger diameter (up to 300 mm), longer and of higher axial capacity than envisioned by Lizzi and, they are most similar to drilled shaft

foundations. The difference between a micropile and a drilled shaft is typically the installation method, which in turn influences how load is distributed along the pile. Drilled shafts are typically constructed using auger equipment to drill a large diameter hole, which is filled with cast-in-place concrete reinforced with a steel cage. The bored hole may stand open or be supported using Bentonite Slurry or a steel casing. Micropiles are bored and grouted piles that can be installed in various ways, as illustrated in Chapters 2, 3 and 4. Due to their small diameter, micropiles are typically designed as friction piles whereas drilled shaft foundations can have significant end-bearing capacity in addition to skin resistance. Micropiles resist compression in end bearing as well, however end bearing is usually ignored in design due to the small diameter.

2.3 Micropile Classification

The Federal Highway Administration (FHWA) implementation manual is the main document referenced in the design of micropiles in North America (FHWA 2000). This manual is intended as a “practitioner-oriented” document containing information on micropile design, construction specifications, inspection and testing procedures, cost data, and contracting methods to facilitate the implementation and cost effective use of micropiles (FHWA Technical Report Documentation Page). The FHWA manual classifies micropiles into two categories denoted as Case I and Case II. Case I micropiles are loaded directly and the pile resists the applied load in accordance with conventional pile theory or mechanics. Case II micropile elements circumscribe and internally reinforce the soil to make a reinforced soil composite or reticulated pile network that resists the applied load (FHWA, 2000). This thesis deals with Case I micropiles only.

Case I micropiles are further subdivided into Types A through D depending on their grouting construction. Type A micropiles are bored piles tremie grouted under gravity head only. The grout is pumped into the drill hole through a pipe that extends to the bottom of the hole. Type A micropiles are sometimes constructed by drilling or boring a hole with a steel casing to stabilize the hole. If a casing is used, the hole is filled with grout as the casing is retracted. Typically the casing is left in place for only the upper 25% to 35% of the pile see Figure 2.2. Type B micropiles are tremie grouted and pressure grouted using grout pressures up to 1 MPa as the drill casing is withdrawn. The grout pressure is applied by attaching a pressure cap to the top of the drill casing and injecting additional grout into the soil formation and casing under controlled pressure. Type C micropiles, most commonly used in France, are tremie grouted and then, 15 to 25 minutes later, grout is injected using pressures greater than 1 MPa through a tube-a-manchette installed in the pile. A tube-a-manchette is a small (usually 25 mm diameter) plastic tube, which has one way ports along its length that open when the pressure grout is inserted. Typically the casing is left in place for only the upper 25% to 35% of the pile (see figure 2.2). Finally, Type D micropiles are tremie and pressure grouted (similar to type B) and then post-grouted using a tube-a-manchette, which is typically inserted in the pile and attached to the central reinforcing bar during construction. The post grouting is usually done after the initial grout has cured (usually after 24 hours). In addition, grout can be injected numerous times through the tube-a-manchette. It is typical to record pressures of 2 to 8 MPa, especially at the beginning of each treatment when the surrounding primary grout must be ruptured for the first time. The different grouting procedures are illustrated in Figure 2.2.

There is another common method of installing micropiles where the reinforcing element is a hollow core bar with a drill bit at the end. This method is categorized as a Type A micropile according to the FHWA manual. Further description of this method of installation is given since many of the cases presented in Chapters 3 and 4 were installed using this procedure. As the bar is drilled into the ground, a high water to cement grout is injected inside the bar and jetted out of the drill bit. The borehole is advanced by the rotary action of a percussive drill bit and the jetting action of the grout, which serves as the drilling fluid. Once the bar is drilled to the desired depth, the grout is flushed from the borehole with a lower water to cement ratio grout to complete the micropile construction.

Although micropiles are classified depending on the grouting method, their performance is also affected by the method of drilling. Some typical drilling methods include: single tube advancement, rotary duplex, rotary percussive concentric and eccentric duplex, double head duplex and hollow stem auger (FHWA 2000). Water, air, drill slurries, foam, or grout may be used as the drill fluid to clean and flush the hole. When using air as the drill fluid it is important to avoid injecting excessive quantities of air into the surrounding ground since this may cause fracturing and heaving. When water is used as the drilling fluid, it may be necessary to clean the hole thoroughly before grouting to reduce the chance of leaving a weak layer of mud around the hole which may decrease the pile-to-soil bond depending on the soil conditions.

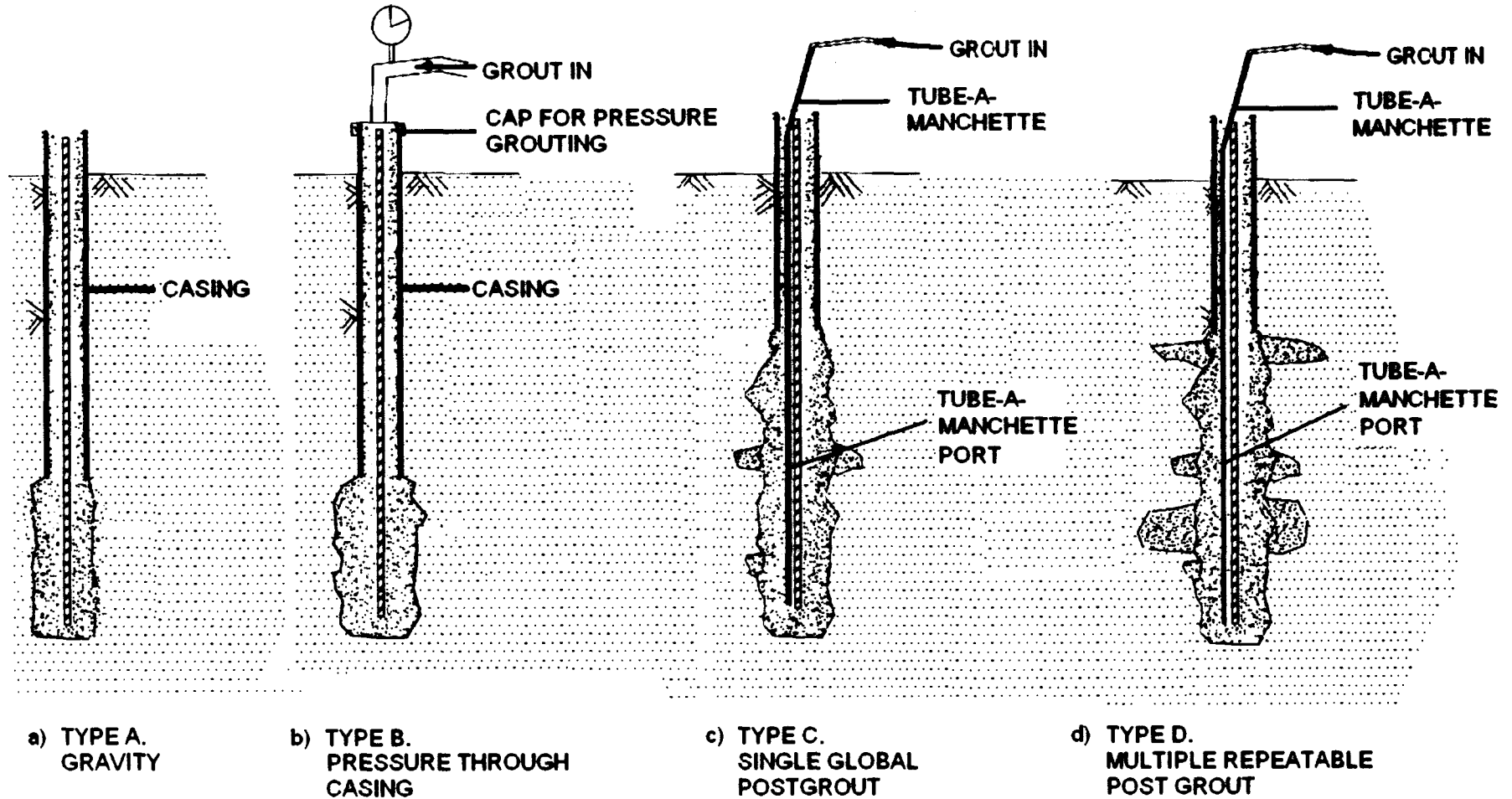


Figure 2.2 Types of Grouting Procedures (FHWA 2000).

2.4 Current Design Methodology

2.4.1 Design Considerations

There are three basic considerations in micropile design: structural capacity, geotechnical or pile-to-soil capacity, and pile head deflection. Equations provided for each of these considerations are described below.

Structurally, the steel and grout in a micropile must be checked for yielding, buckling (eg. if micropiles are drilled in weak soils or karstic rock) and bending (eg. if lateral load is to be carried by the micropile). Corrosion is also a consideration since micropiles are often drilled into corrosive environments (eg. highway bridges where there is salt used for deicing purposes). Corrosion can be mitigated by either using epoxy coated steel reinforcement, installing double corrosion protected steel reinforcement or by designing the steel with a sacrificial area. According to AASHTO Section 4.5.7.4 (16th Edition), for concrete filled pipe piles, where corrosion may be expected, 1.6 mm shall be deducted from the shell thickness to allow for reduction in the steel section due to corrosion. (FHWA page 4-39). The corrosion shell may vary depending on the service life and soil classification (eg. not aggressive to very aggressive), which depends on the chloride content.

The following section focuses on methods of estimating the structural axial capacity, and geotechnical capacity of micropiles.

2.4.2 Axial Capacity

Considering the compressive structural capacity only, the allowable load of a micropile according to FHWA and AASHTO is:

$$P_s = 0.40 f_c A_g + 0.47 f_y A_s \quad [2.1]$$

In Equation 2.1, f_c is the compressive strength of the grout, A_g is the cross section area of the grout, f_y is the compressive yield stress of steel and A_s is the cross section area of steel (the calculated area after corrosion is taken into account if this is the corrosion method of choice).

Generally, the ultimate capacity of the soil-grout interface is calculated using Equation 2.2:

$$P_{ult} = A_{soil} f_b \quad [2.2]$$

where, A_{soil} is the surface area of the pile in contact with soil (skin area) and f_b is generally referred to as the adhesion (in most cases friction) between the pile and the soil. In clays, f_b can be estimated from Equation 2.3.

$$f_b = \alpha C_u \quad [2.3]$$

where α is the reduction factor for adhesion and C_u is the undrained shear strength of the clay. Micropiles are often designed satisfactorily with α values of 0.6 to 0.8 (see FHWA 1997).

In sands, f_b can be estimated from Equation 2.4.

$$f_b = \int k_s \sigma'_{vz} \tan \delta \, dz \quad [2.4]$$

where k_s is the coefficient of horizontal soil stress, σ'_{vz} is the effective vertical overburden pressure over the length of the soil layer, and δ is the interface friction angle between the soil and the pile.

According to Tomlinson (1995), the ratio of k_s/k_o varies between 0.71 to 1 for bored and cast-in-place piles, while for jetted piles it varies from 0.5 to 0.7. In addition, the ratio of ϕ of the soil and the pile interface (ϕ / δ) is 1 for cast-in-place concrete in contact with sand (Tomlinson 1995). Equation 2.4 implies that, in a uniform cohesionless soil, the unit skin friction continues to increase linearly with increasing depth; However, this is not always the case and can generate increasingly unsafe load estimates as the penetration depth exceeds about 20 pile diameters (Tomlinson 1995). This is the case for micropiles since they are up to 300 mm in diameter and usually longer than 6m.

O'Neill and Hassan (1994) also suggested an empirical relationship between f_b and SPT blow counts (N) as shown by Equations 2.5 and 2.6.

$$K_o \tan \phi = 1.5 - 0.42 [z \text{ (m)}]^{0.34}, \quad 1.2 \geq K_o \tan \phi \leq 0.25 \quad \text{for } N > 15 \text{ or,} \quad [2.5]$$

$$K_o \tan \phi = 1.5 - 0.42 [z \text{ (m)}]^{0.34} * N/15, \quad \text{for } N < 15 \quad [2.6]$$

where z is the depth in meters.

Soil pile adhesion values obtained from pile load tests for different soils are summarized in Table 1 from the FHWA manual (FHWA 1997). Since the values in Table 1 can vary depending on the drilling technique, soil-to-pile adhesion values should always be checked by load tests as recommended by the FHWA design manual. It can

be seen that the values provided in Table 1 have a large range and hence it is difficult to use such tables for practical design purposes.

Table 2.1. Values of Soil to Ground Adhesion (FHWA 2000).

Soil / Rock Description	Typical Range of Grout-to-Ground Bond Nominal Strengths (kPa)			
	Type A	Type B	Type C	Type D
Silt & Clay (some sand) (soft, medium plastic)	35-70	35-95	90-120	90-145
Silt & Clay (some sand) (stiff, dense to very dense)	50-120	70-190	95-190	95-190
Sand (some silt) (fine, loose-medium dense)	70-145	70-190	95-190	95-240
Sand (some silt, gravel) (fine-coarse, med.-very dense)	95-215	120-360	145-360	145-385
Gravel (some sand) (medium-very dense)	95-265	120-360	145-360	145-385
Glacial Till (silt, sand, gravel) (medium-very dense, cemented)	95-190	95-310	120-310	120-335
Soft Shales (fresh-moderate fracturing, little to no weathering)	205-550	N/A	N/A	N/A
Slates and Hard Shales (fresh-moderate fracturing, little to no weathering)	515-1,380	N/A	N/A	N/A
Limestone (fresh-moderate fracturing, little to no weathering)	1,035-2,070	N/A	N/A	N/A
Sandstone (fresh-moderate fracturing, little to no weathering)	520-1,725	N/A	N/A	N/A
Granite and Basalt (fresh-moderate fracturing, little to no weathering)	1,380-4,200	N/A	N/A	N/A

As micropiles have a small cross section the end bearing is usually neglected; however when the bearing stratum is very dense it is important to consider end bearing as it can contribute to the capacity of the micropile. The base resistance can be calculated using the following equation:

$$Q_b = N_q \sigma'_{vo} A_b \quad [2.7]$$

N_q is the bearing capacity factor according to Figure 2.3, σ'_{vo} is the average effective overburden pressure at the pile tip, and A_b is the base area.

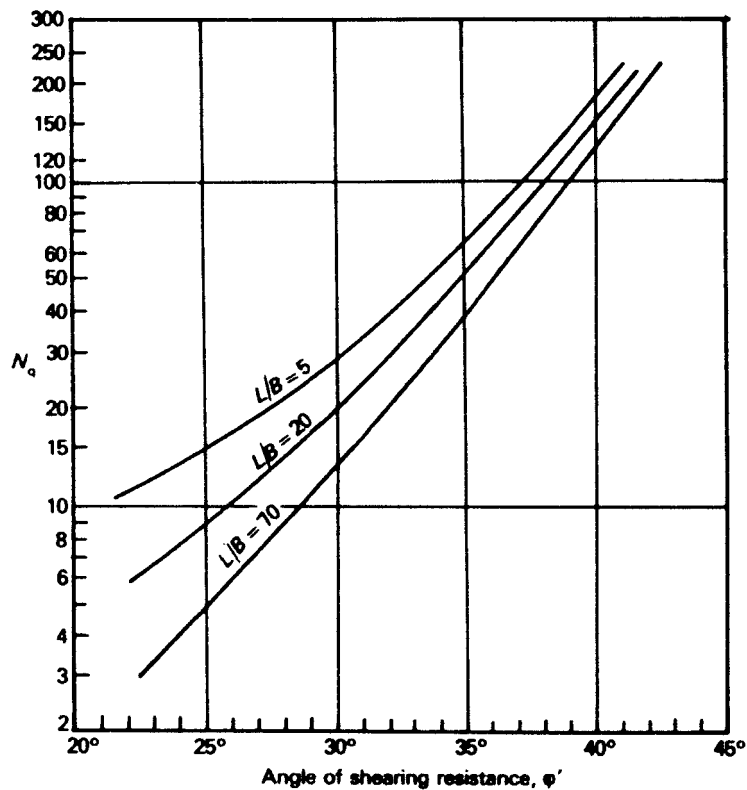


Figure 2.3 Bearing capacity factor (After Berezantsev et al, 1961).

2.4.3 Methods of Interpreting Pile Load Tests

Terzaghi suggested that the ultimate load of a pile can be defined as that which causes a settlement of one-tenth the pile diameter or width (Tomlinson 1995). This is a fairly good estimate for most of the cases presented in this Thesis. As well as using Terzaghi's equation the following criteria was used to calculate the capacity of a pile.

Davisson's Criterion

Davisson's criterion is a common method used to estimate the capacity of a pile from load tests. This criterion utilizes Equation 2.8 and accounts for soil deformation by adding 4mm of displacement plus the diameter of the pile divided by 120 to the compression one would expect if the pile were a free column.

$$\Delta = 4\text{mm} + B/120 + P L / (A_s * E_s + A_g * E_g) \quad [2.8]$$

In question 2.8, the variable B is the diameter of the pile, P is the constant load in the pile, L is the length of the pile, A_s is the area of steel including the bar and casing if present, E_s is the elastic modulus of steel, A_g is the area of grout and E_g is the elastic modulus of confined grout.

Figure 2.4 below summarizes the application of Davisson's method to pile load test data. Other methods of estimating the capacity of piles have been presented by Fellenius (2002).

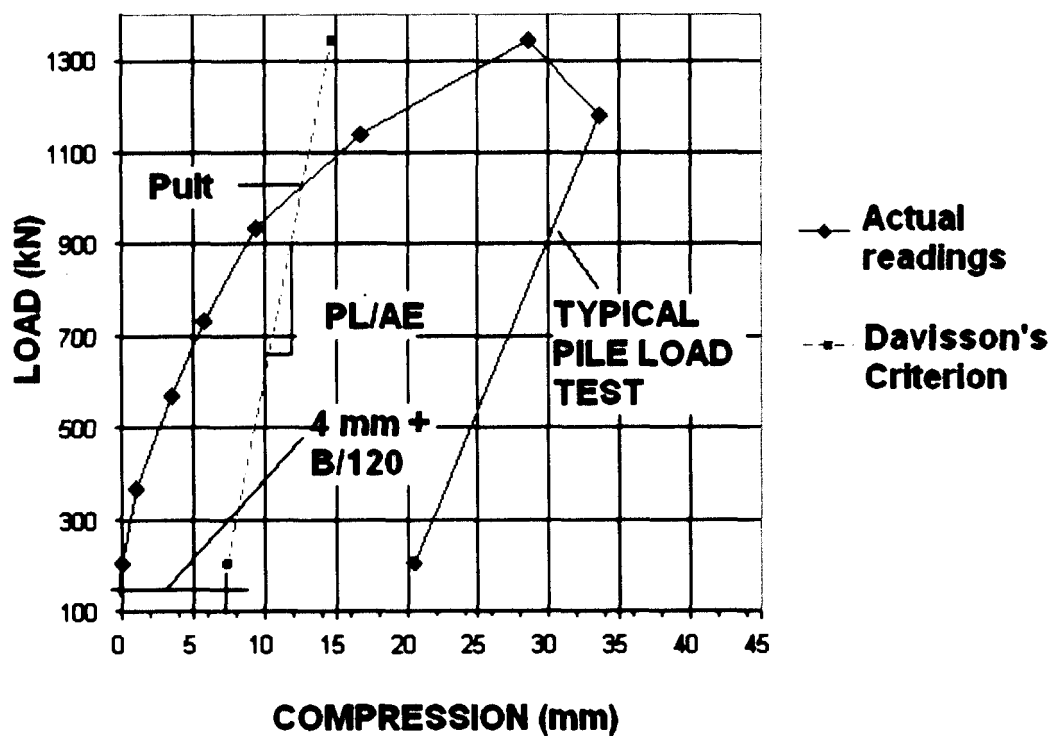


Figure 2.4 Davisson's Method (Poulos 1980)

2.4.4 Methods of Estimating Pile Deflection For Design

From elastic theory, the compression of a pile can be estimated during the initial linear elastic range of loading using Equation 2.9. (see below) Equation 2.9 is typically used for columns where the load is constant along the length of the member; however, for piles, the axial load is higher at the top of the pile and it decreases towards the tip.

Therefore Equation 2.9 may be used in lengths of the pile where there is no load shedding to the soil.

$$\Delta = P L / (A_{\text{steel}} E_{\text{steel}} + A_{\text{grout}} E_{\text{grout}}) \quad [2.9]$$

In Equation 2.9, P is the constant load along the pile, L is the plunge length, A_{steel} is the area of steel including the bar and casing if present, E_{steel} is the elastic modulus of steel, A_{grout} is the area of grout and E_{grout} is the elastic modulus of confined grout. Plunge length is that length of the pile that is free to compress.

There are several methods for calculating the settlement of a single pile as described in Tomlinson (1986), Craig (1997) and Poulos (2004). This section summarizes the method developed by Poulos (2004) which is based on elastic theory. Equation 2.10 can be used to calculate the pile head displacement for a floating (friction) pile in a uniform infinite deep layer.

$$\Delta = P I_o R_k R_h R_v / r * E_s \quad [2.10]$$

Whereas Equation 2.11 can be used to calculate the pile head displacement for an end-bearing pile in a uniform finite layer:

$$\Delta = P I_o R_k R_b R_v / r * E_s \quad [2.11]$$

In Equations 2.10 and 2.11, R_v is the effect of Poisson's ratio of soil (Fig 2.5), I_o is the influence factor (see Fig. 2.6), R_b is the bearing factor (Fig. 2.7), R_k is the pile compressibility factor which is very important for longer piles (see Fig. 2.8), R_h is the finite layer which has relatively little effect for long compressible piles (Fig.2.9), r is the radius of the pile and E_{soil} is the elastic modulus of the soil.

Figures 2.5 to Figures 2.9 summarize typical graphs for estimating the influence factors. For some micropiles, the slenderness ratio for micropiles lies outside the extents of these graphs. For example, in Chapter 4 the slenderness ratio for a micropile drilled

in rock is 285. Thus, these graphs do not always cover the slenderness ratios (L/d) common for micropiles. Note that K is the ratio of the Elastic modulus of the pile and the elastic modulus of the soil.

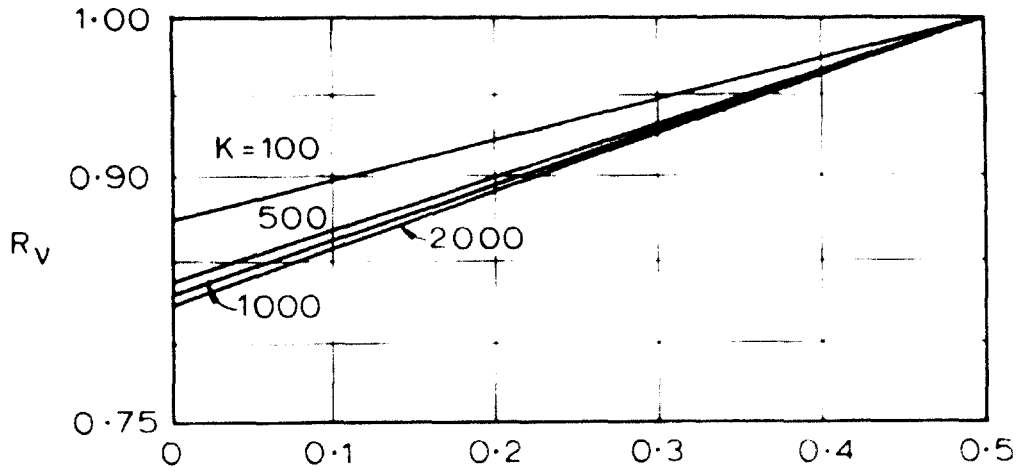


Figure 2.5 Poulos Influence Factor R_v .

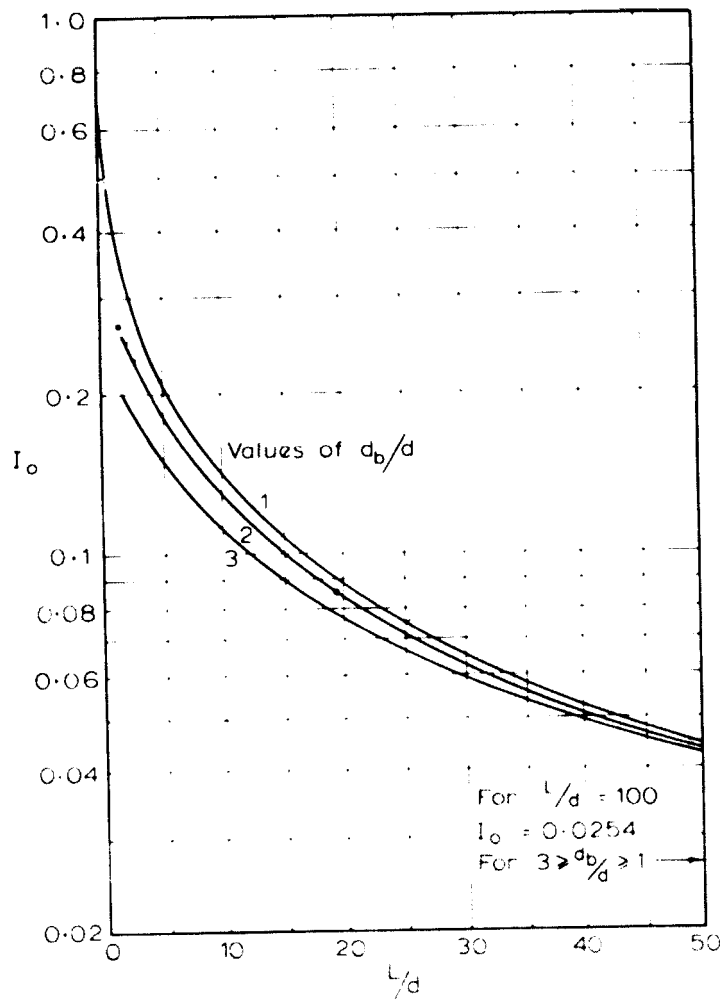


Figure 2.6 Poulos Influence Factor I_o .

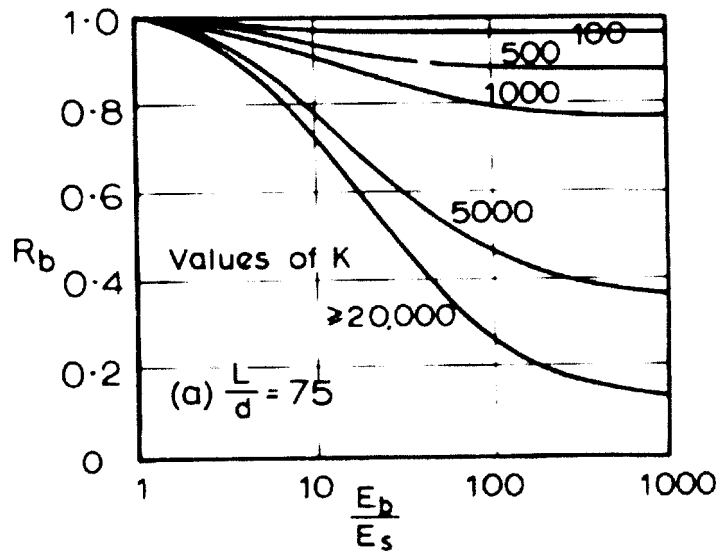


Figure 2.7 Poulos Influence Factor R_b .

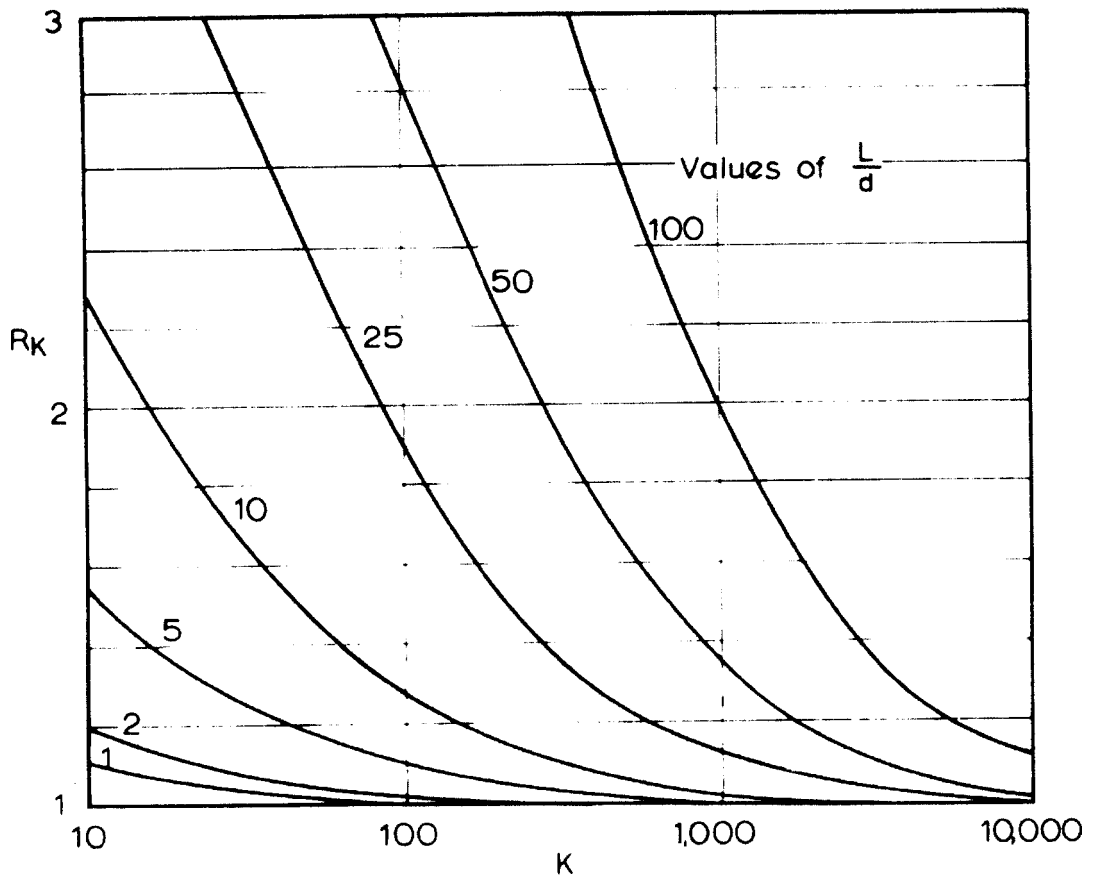


Figure 2.8 Poulos Influence Factor R_k .

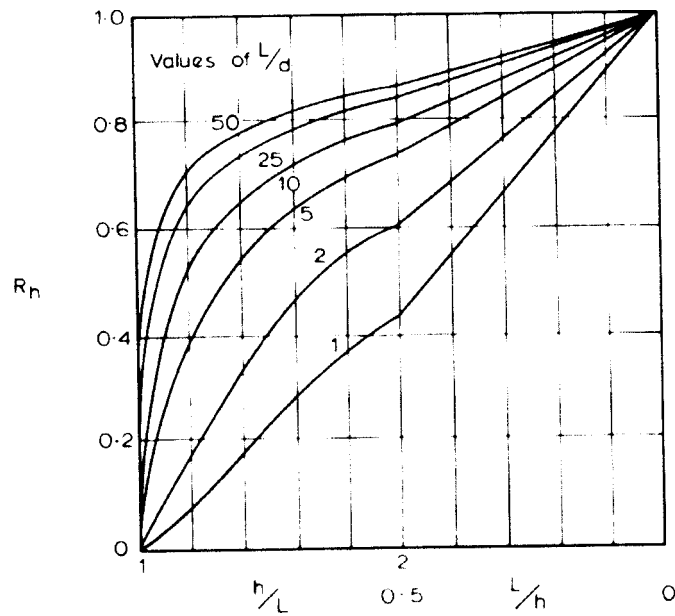


Figure 2.9 Poulos Influence Factor R_h .

2.5 Contractometer

Typically, to measure strain within a pile, strain gauges are attached to the steel elements of a pile or telltale rods are installed inside the length of a pile. Strain gauges usually provide an indication of the strain of the steel; however, they are often damaged during construction of a pile. Telltale rods extend from the top of the pile to some specified depth and are encased in a protective sleeve (Coduto 2001). By comparing the difference in movement of these rods the average strain between the anchor points can be calculated.

Some of the cases described and analyzed in Chapters 3 and 4 were instrumented with a new device called the Contractometer. The schematics of a Contractometer are shown in Figure 2.10 and Figure 2.11. In principle, a Contractometer acts like a tell-tale system. A Contractometer comprises custom spaced nodes (eg. depends on the pile geometry etc) made of aluminum. Each node is connected to a fiber glass rod that runs from the node to the pile head where it is placed in contact with a potentiometer. The fiber glass rods are encased in PVC tubing to allow them to move freely and to protect the instrument from damage during handling and high pressure grouting. As each node in the pile moves the end of the fiber glass rods also move sliding along the potentiometers. The potentiometer voltage changes and the change in voltage is proportional to the movement of the tip of the fiber glass rods. Consequently, the instrument gives the average node to node deformation.

In this thesis, rather than showing the relative compression between nodes the strains are shown. The strains are calculated by subtracting the movement between nodes. These strains are plotted at the midpoint between adjacent nodes since they are the average strain between nodes.

A wide range of potentiometers are available ranging from 32 mm to 190 mm in length. The manufacturer states that the instrument accuracy is 1.0% of potentiometer length; however this accuracy can be affected by handling of the Contractometer during installation. Displacement data can be captured during load tests using either a hand-held reader, or automated data logger.

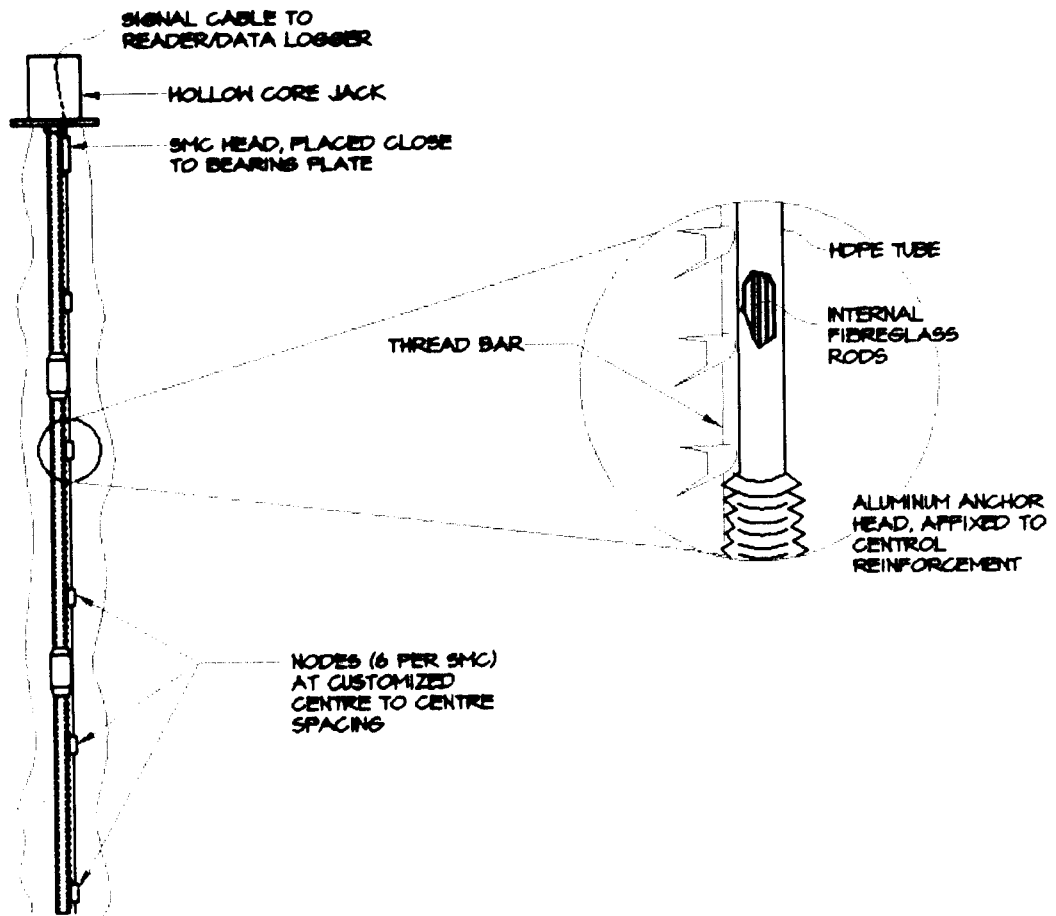


Figure 2.10 Schematic of the Contractometer.

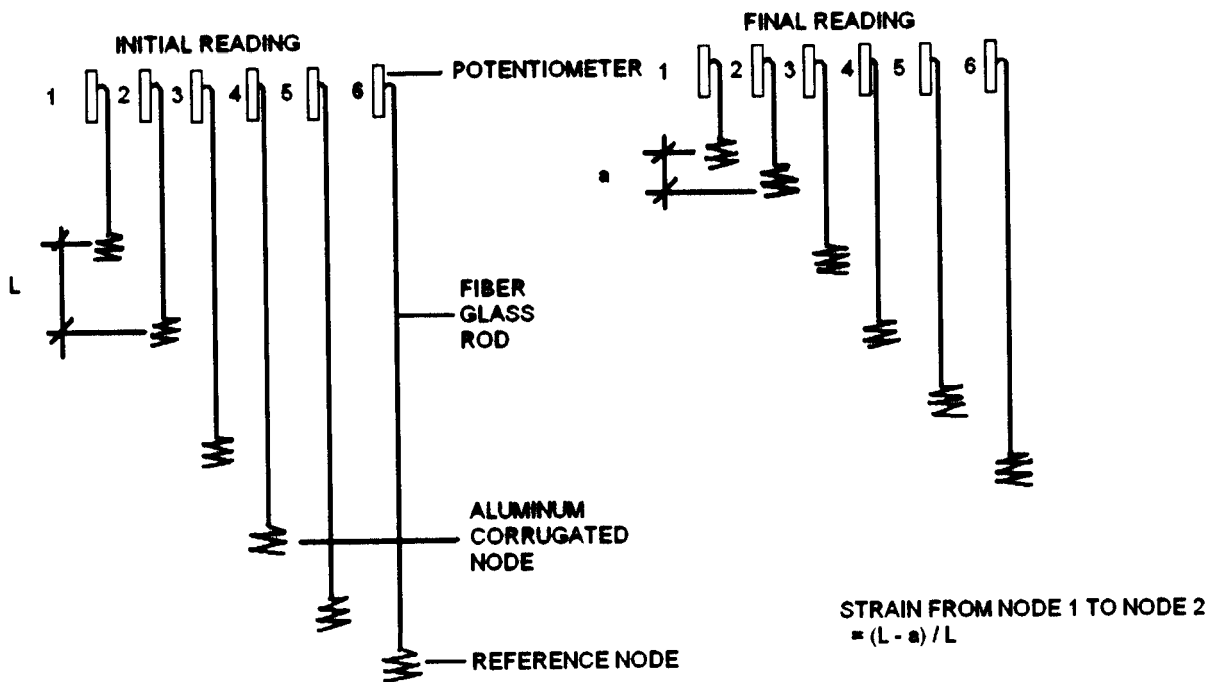


Figure 2.11 Schematic of Contractometer Inner Workings.

2.6 Grout Properties

Two types of grout were typically used to construct the micropiles presented in this thesis. The most common grout type was type 10 portland cement mixed with water and the second type was an ultra fine cement grout (eg. King grout) that permitted the use of very low water to cement ratios (as low as 0.3). For grout, reducing the water to cement ratio increases the strength as illustrated in Figure 2.12. Type 10 portland cement can also be used in water to cement ratio as low as 0.45 and can be further lowered with water reducing agents such as fly-ash, pumice, slag, bentonite, clay, and tailings (FHWA 2000) In this Chapter, the elastic modulus of the grout was verified by testing unconfined grout cylinders in a loading apparatus. Twelve samples of type 10 cement grout were taken from a site in Oakville, Ontario on September 7, 2005. The grout was mixed using a colloidal mixer. The water to cement ratio was 0.45 and the specific gravity was 1.92. The grout was placed in 75 mm diameter by 150 mm high cylinders. The cylinders were kept in a cooler under water until they were brought to a steam room at the University of Western Ontario on September 15, 2005.

For each compression test, the cylinders were sulfur-caped prior to testing in accordance with ASTM C39, SSA.A23.13. Figure 2.13 shows a photograph of the test setup. Radial and vertical deformations were measured during compression using LVDT's mounted on each sample and the compressive load was measured using a load cell. The results of these tests are presented in Table 2.2.

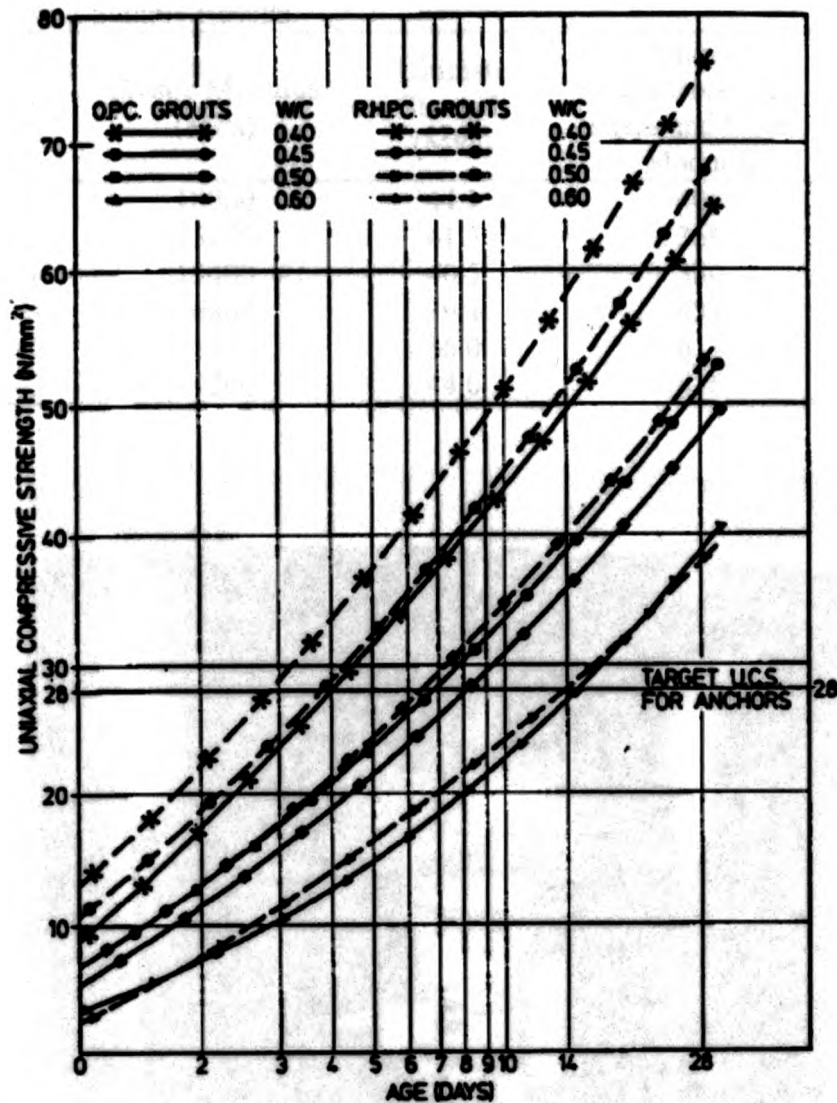


Figure 2.12 Effects of Water to Cement Ratio on the Strength of Grout (FHWA 2000)

From Table 2.2, the average strain at failure after 7 days is $1950\mu\epsilon$ and the average elastic modulus was roughly 16,000 MPa. The ratio of compressive stress and elastic modulus obtained from the tests was about 450. Figure 2.14 and Figure 2.15 summarize typical compression test results. The end of the graph is indicative of sudden brittle failure. Additional stress-strain graphs are reported in Appendix A. Poisson's ratio was also calculated from the tests. The average Poisson's ratio is roughly 0.3, although it was generally not constant during each test.

Table 2.2 Grout Sample Results.

Grout Sample	Elastic Modulus (MPa)	Ultimate Strength (MPa)	Ratio of compressive stress and Elastic Modulus	Microstrain At Failure
7 days - 1	18000	44.1	408	1400
7 days - 2	15200	41.3	368	2350
7 days - 3	15400	40.5	380	2080
24 days - 1	16800	39.4	431	1880
24 days - 2	22200	36.0	613	1470
24 days - 3	19200	44.0	436	1720



Figure 2.13 Test Set Up.

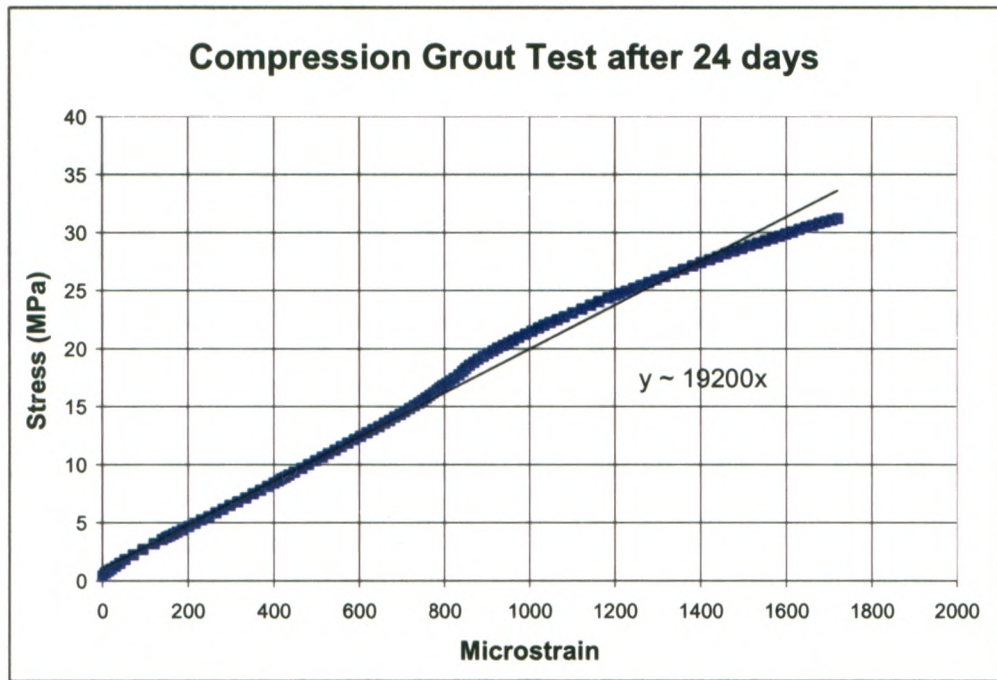


Figure 2.14 Stress Strain Curve for Grout Cylinder.

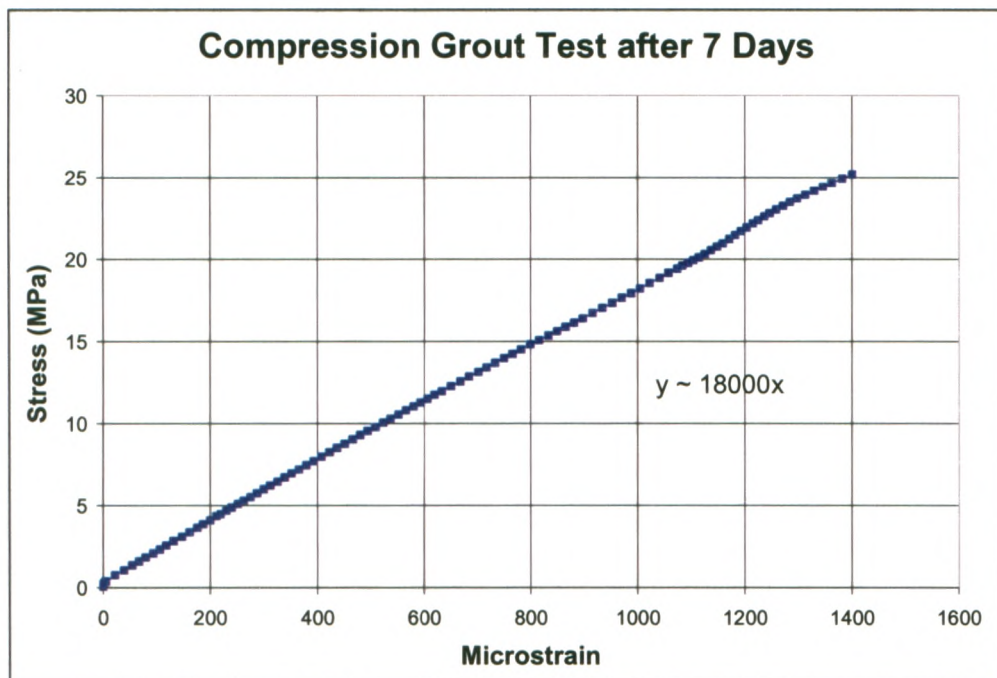


Figure 2.15 Stress Strain Curve for Grout Cylinder.

2.7 Summary and Conclusions

Chapter two has given an overview of the history, classification, and design methodology for micropiles. This Chapter has also given a brief description of the

Contractometer (used to measure strain in some micropiles) and has concluded with grout properties from compression test on cylindrical grout samples.

Pile deflection estimation cannot always be done using Poulos and Davis (1980) solutions since the slenderness ratio of some micropiles lies outside those in the graphs. The geotechnical capacity of micropiles can be estimated from adhesion values given in the FHWA manual (FHWA 1997), as well as using equations from the literature. The FHWA manual gives rather large ranges of adhesion capacities and hence creates difficulty for practical design purposes.

The average modulus of elasticity for grout obtained from compression tests was 16000 MPa and the poisson's ratio was 0.3. These values will be used in the analysis of the micropile load tests described in Chapters 3 and 4.

CHAPTER 3
MICROPILE CASE STUDIES

3.0 Introduction to Micropile Case Studies in Soil

This Chapter examines five cases involving the construction of nine floating or friction micropiles in mainly cohesionless soils. As discussed in Chapter 2, micropiles are suitable for retrofitting old or existing structures where the load carrying capacity of existing foundations must be upgraded to support additional loads (e.g. either due to the addition of floors to existing buildings or due to upgraded seismic design forces). All of the cases described in this Chapter involved projects where the use of conventional drilled shaft foundations was deemed too costly or impractical due to limited overhead clearance and/or due to the presence of sensitive structures nearby. In one case, micropiles were used to retrofit an existing railway bridge that had undergone significant settlement and was deemed sensitive to vibrations. For each of the cases examined, load-displacement data is available from pile load tests on full-scale micropiles. For two cases, the micropiles were instrumented with a Contractometer (see Chapter 2), which provided information to calculate the internal strain in each pile during loading. In the following sections, details of the micropile cases are presented and the response of the piles during loading is interpreted using the finite element (FE) program PLAXIS with the objective to gain insight into factors affecting the developed axial capacity of micropiles. The cases and finite element analyses described in this study highlight some key factors affecting the performance of micropiles, which should be of interest to foundation engineers and the geotechnical community.

3.1 Methodology

3.1.1 Pile Construction

Two different construction methods were used to build the micropiles described in this Chapter. The following is a summary of these methods.

Method I - Rotary Duplex Drilling Method

The micropiles described in Case 1 (see below) were constructed by advancing a steel casing through overburden soil using a rotary duplex drilling machine in conjunction with a super jaw drilling bit (retractable bit) and down-the-hole hammer. For this installation method, the super jaw drill bit was used to under-ream the casing creating a borehole with a slightly larger diameter than the casing. The casing was advanced behind the drill bit using rotary action. Water was the drilling fluid. After advancing the casing to the required depth, the drill string (bit and drill rods) was retracted and a threaded solid bar was installed centered in the finished borehole (with casing). For some piles as described below, a tube-a-manchette (TAM) was also installed in the casing. Figure 3.1 shows the schematics of the Case 1 micropiles at this stage in their construction.

For the first pile in Case 1, the casing was filled with tremied grout after finishing the borehole. Then, the casing was subsequently retracted in 3 m increments, and the grout was topped up in the casing during each increment. When the casing was retracted to a depth of 9.9m, a pressure cap was installed at the top of the casing and grout was injected under pressure into the foundation soil. The resultant micropile is classified as Type B according to the FHWA (2000) manual. Figure 3.2 illustrates a typical finished micropile constructed by Method 1.

For the second and third piles described in Case 1, the construction proceeded as described above with the exception of the grouting phase. For these piles, the casing was filled with tremied grout after completing the drilling. Then, the casing was retracted in 3m intervals. During each interval, the grout in the casing was topped up, a pressure cap was installed at the top of the casing, and grout was injected into the soil

formation under pressure. In addition, the second and third micropiles in Case 1 were post-grouted 12 hours after the pressure grouting was finished. The post-grouting was performed by injecting grout through a TAM embedded in the pile during construction (see Fig. 3.1). The resultant pile is classified as Type D according to FHWA (2000) manual. Figure 3.2 shows a drawing of the completed Case 1 piles, which comprised grout, grouted soil, an upper cased length, and a lower uncased length with a steel bar centred in the pile extending from the pile head to toe.

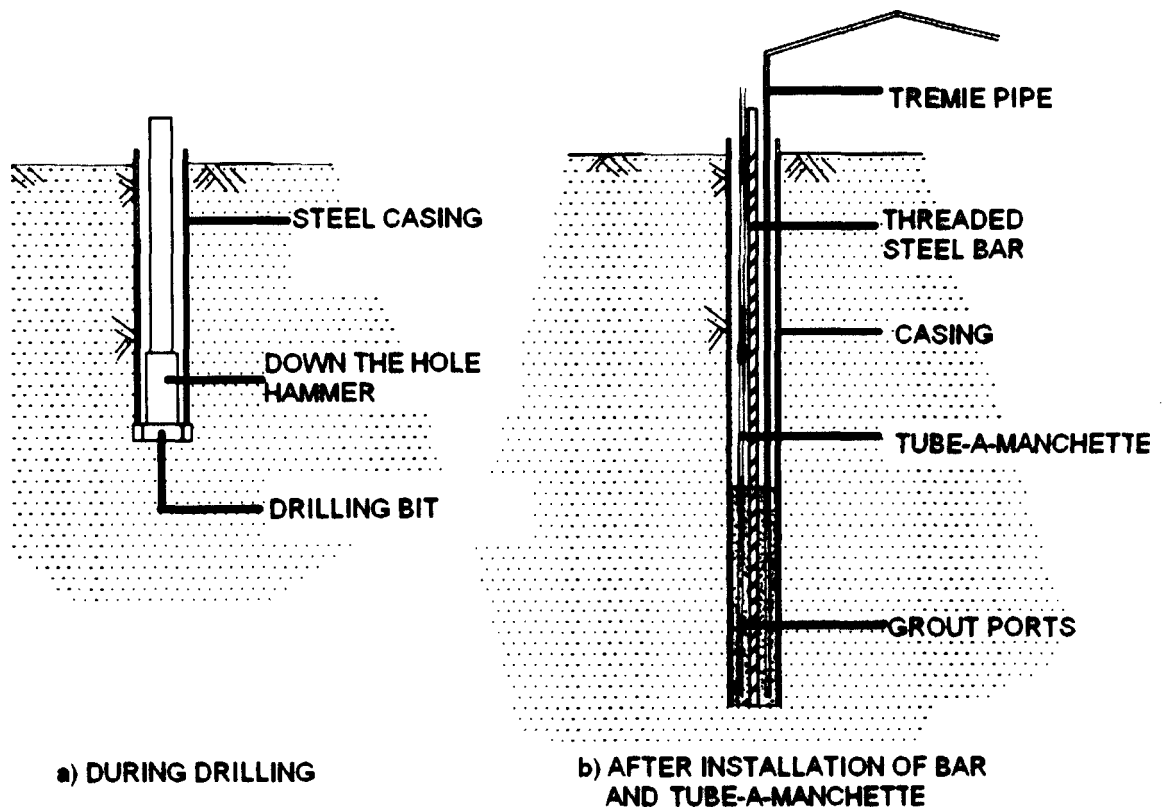


Figure 3.1 Installation of Rotary Duplex Micropile.

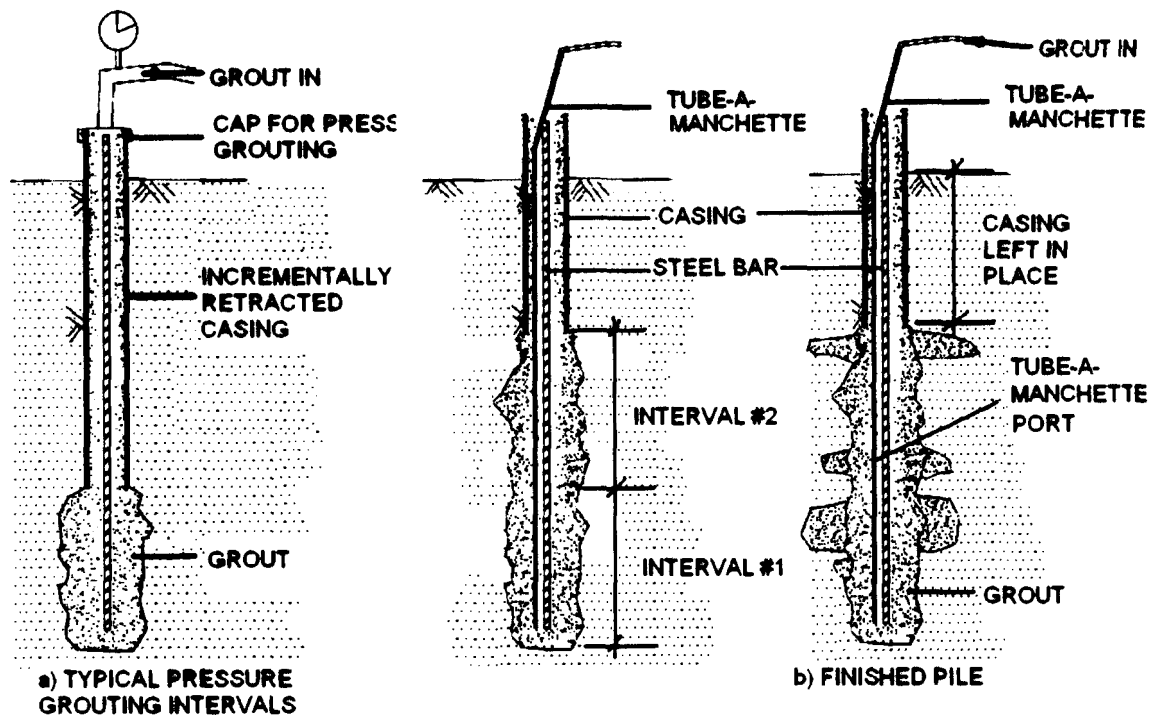


Figure 3.2 Diagram Illustrating the Installation of Grout.

Method II - Injection-bored, Hollow Core Bar Method

The second method of installation is called the injection-bored, hollow core bar method. This is a common method of constructing micropiles because it has been found to result in good grout-to-soil adhesion and it is relatively quick. This method, which is illustrated in Figure 3.3, involved using a hollow threaded steel bar fitted with a disposable drill bit at the tip forming the drill string. The drill string was advanced through the ground by rotation and percussive drilling using high water to cement ratio (w/c) grout as the drilling fluid (typically w/c=0.6). During drilling, the drill fluid was continuously circulated through the hollow core bar to the bit where it was jetted out of the bit. After reaching the desired depth, the lean grout in the borehole was flushed with structural grout that had a water to cement ratio (w/c) between 0.3 and 0.45 depending on the case. The structural grout was pumped through a tube inserted to the bottom of the borehole and the flushing proceeded until the grout flowing from the top

of the hole had the required specific gravity. To complete the micropile construction by Method 2, a casing was installed in the upper part of the pile by pushing the casing into the ground. As shown in Figures 3.3b and 3.4, this construction method results in a pile that is augmented by some grouted soil adjacent to the pile (for permeable soils). The piles described in Cases 2 through 5, inclusive, were constructed using this method.

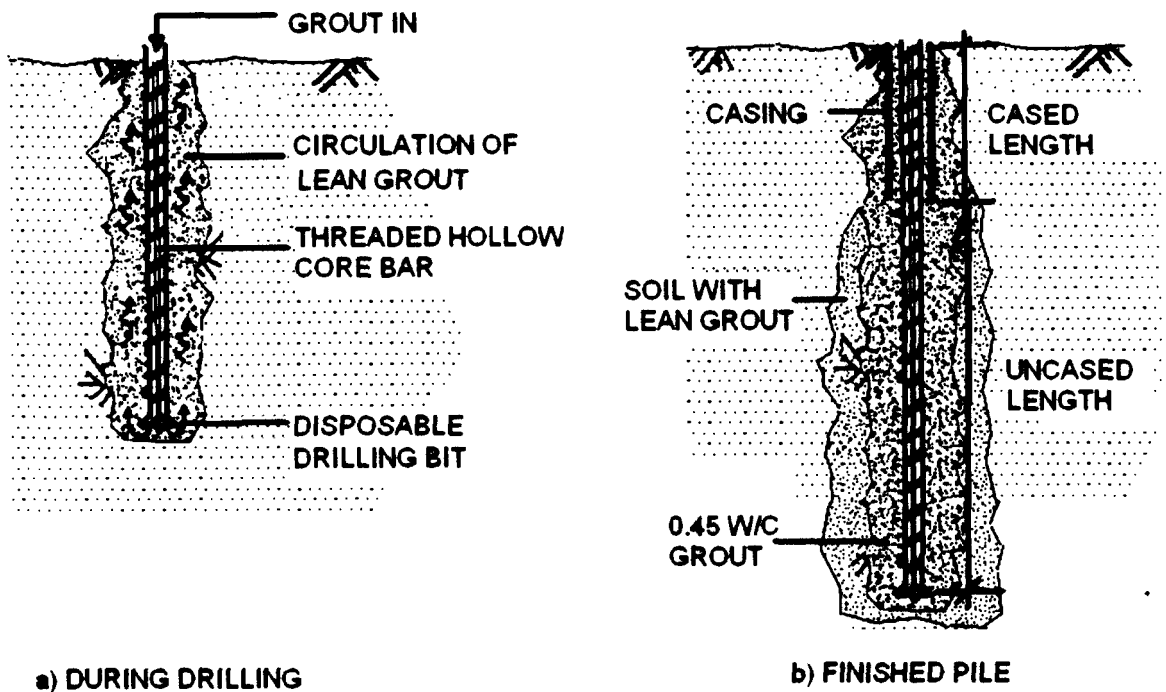


Figure 3.3 Injection bored Hollow Core bar.

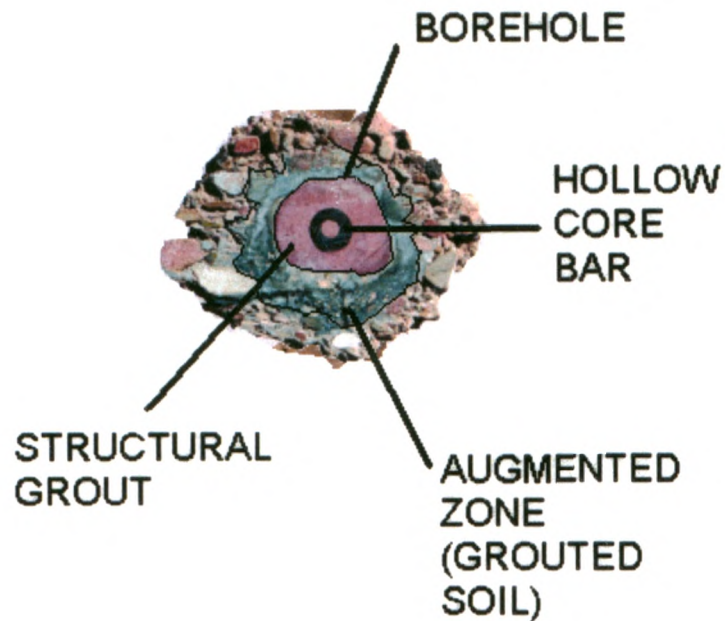


Figure 3.4 Hollow Core Bar Method showing Pile Enlargement (Contech Systems Titan Bar Website)

3.1.2 Pile Enlargement

The geometry of a micropile is complex compared to that of conventional driven piles. Consequently, some idealization was required to interpret the load tests described below. Referring to Figure 3.5 (a), the minimum diameter of a micropile is governed by the diameter of the drill bit used for construction. However, during construction of a micropile, the bored diameter is usually enlarged due to the jetting and flushing action of the drilling fluid. As a result, the diameter of a micropile is typically larger than that of the corresponding drill bit. For micropiles constructed in permeable soils, grout can also penetrate into the soil surrounding the borehole. Such conditions are shown in Figure 3.5(a). Lastly, due to soil variability, the shape of the pile can be variable over its length. As a result, micropiles constructed in permeable soils typically possess a diameter that is significantly larger than that estimated from the drill bit diameter.

Figure 3.5 (b) shows the idealized micropile geometry adopted in this study. For analytical purposes, each micropile was idealized as having a uniform circular cross-section with enlarged diameter, D' , to account for pile enlargement caused by grouting and grout penetrating into the soil formation. For Case 1, the volume of grout was recorded during construction of each pile. As a result, a lower bound pile diameter, D' , could be estimated from the volume of grout consumed during construction, the length of the pile, and the volume of steel in each pile, neglecting the influence of porosity on the injected grout volume.

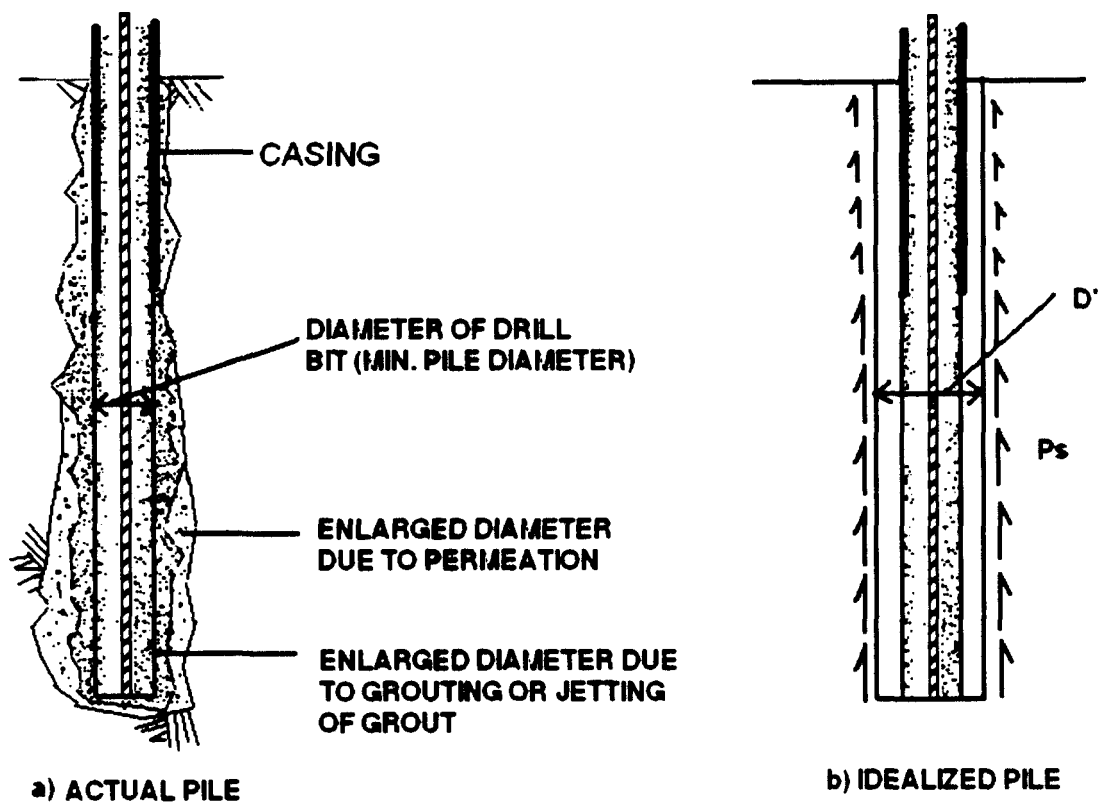


Figure 3.5. Actual and Idealized Pile Geometry

3.1.3 Pile Load Tests

For each case described below, pile load tests were conducted in accordance with test procedure described in the Post-Tensioning Institute Manual (PTI 2004). The pile

load test set up was according to ASTM 1143 (ASTM 1987). Each micropile was typically tested at least 7 days after installation. The axial load was applied in eight equal increments up to twice the design load using an electrically controlled jack. At each load increment, the load was cycled (eg. The pile was unloaded to a seating load and then re-loaded to the new level) to determine the elastic and inelastic deformation during each increment. Each load was held for 10 minutes except the design load (100%) and 2 times (200%) the design load, which were both held for at least 1 hour. Each test typically comprised either 3 or 5 micropiles: e.g. either 2 or 4 micropiles were used as reaction piles in tension. A typical 3-pile set up is shown in Figure 3.6 and Figure 3.7.

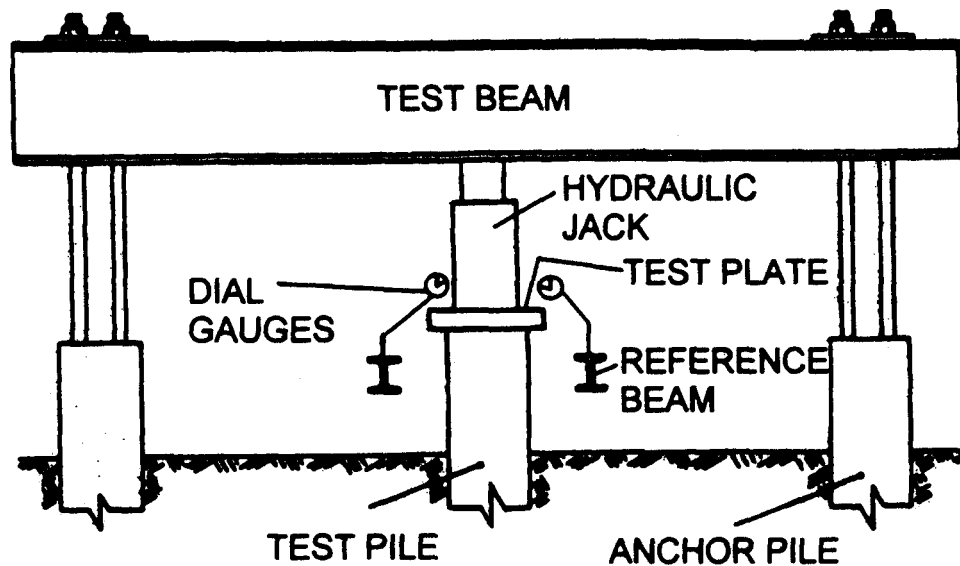


Figure 3.6 Schematic Set-Up for Applying Loads to Test Piles Using a Hydraulic Jack Acting Against an Anchored Reaction Frame.



Figure 3.7 Typical Micropile Compression Test Set Up. (Note: The timbers were used temporarily to support the reaction beam prior to jacking)

The pile head movement of the compression micropile was recorded after a seating load (typically 25% of the design load) was applied to tighten the reaction frame. Two, and in some cases four, dial gauges were used to measure the deflection of a steel plate placed on the top of the micropile between the hydraulic jack and pile head. The dial gauges had 0.0254 mm divisions and were mounted on reference beams anchored outside the influence of the loading (typically 1.5 m from the pile head).

In all the load movement graphs shown in Chapter 3 and 4 the different cycles have been omitted for clarity. The compression measured during the creep test is shown in all the graphs. For complete cycling data refer to Appendix B where all the cycles are shown.

3.1.4 Finite Element (FE) Analysis

FE Mesh

The commercial 2D finite element (FE) program PLAXIS (Version 8) was used to analyze each of the micropile load tests reported below. The FE analyses were done to interpret mechanisms of load transfer and factors affecting pile performance. In most cases, the soil profile was layered and the pile cross-section was not uniform. In addition, most of the cases involved significant plasticity in the soil.

In this study, each pile load test was modelled assuming axisymmetric conditions and using triangular 6-noded linear strain elements both in the pile and in the surrounding soil. The final run was completed using 15-noded triangular elements. The lateral mesh boundary was placed 60 pile diameters from the pile centreline and the depth (minimum of 10 pile diameters) of the model was extended below the toe of the pile to sufficient distance that it did not influence the calculated behaviour. Smooth rigid boundary conditions were assumed at all mesh boundaries. In all cases, the number of finite elements was increased until the calculated behaviour converged.

Materials

The material zones considered in each analysis are summarized in Figure 3.8 (a). Figure 3.8 (b) shows a typical FE mesh. In total, a minimum of 4 zones were typically modelled: the cased length of the micropile, the uncased length of the micropile, a zone of augmented or grouted soil around the micropile and the soil deposit. The elastic modulus and the yield stress of the cased and uncased portions of each micropile were calculated based on the ratio of steel and grout area as follows:

$$E_{pile} = \rho_s * E_s + \rho_g * E_g \quad [3.1]$$

$$\sigma_{yp} = (\rho_s E_s + \rho_g E_g) \epsilon_g \quad [3.2]$$

where ρ_s is the area of steel divided by the gross area of the pile, E_s (200000 MPa) is the elastic modulus of steel, ρ_g is the area of grout divided by the gross area of the pile, E_g (16000 MPa) is the elastic modulus of grout, and σ_{yp} is the minimum yield stress of the pile. As a result, the pile was assumed to yield when the axial strain exceeded the yield strain of the grout.

In many cases, the diameter of each micropile was enlarged to consider a zone of grouted soil around the pile. To simplify the analysis, the section properties for the augmented diameter of the pile were calculated in accordance with Equations 3.1 and 3.2 above assuming the grouted soil and grout had identical properties. An elastoplastic interface was assumed between the soil and pile over its entire length. However, the interface friction angle, δ_i , was assumed equal to the effective friction angle of the soil, ϕ'_s , for the uncased length of each micropile; whereas $\tan(\delta_i)/\tan(\phi'_s)$ was taken to be 0.1 between the upper steel casing and the soil, based on interpretation of the actual pile behaviour during loading.

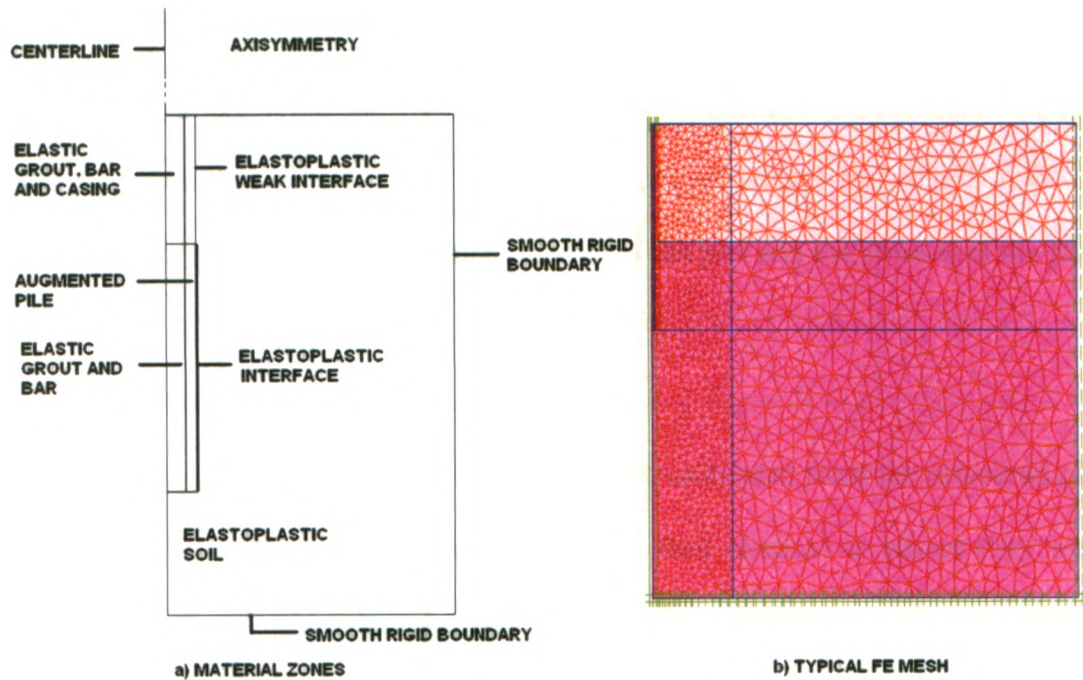


Figure 3.8 Material Zones and FE Mesh.

All materials were modelled as elastoplastic materials with Young's modulus, E , and Poisson's ratio, ν . Failure was assumed to be governed by the Mohr Coulomb failure criterion, (c' and ϕ') and a non-associated flow rule was typically assumed by specifying a dilatancy angle, ψ , that was less than the effective friction angle, ϕ' , of the soil. For each material, the parameters include Young's modulus (E), the effective cohesion intercept (c'), Poisson's ratio (ν) and the dilatancy angle (ψ). Specific values of each parameter are summarized during the analysis of each case. For the pile, ϕ' was taken to be 0° , and c' was set equal to $\sigma_{yp}/2$, although the FE analysis did not show yielding in the pile (eg. $\epsilon_{axial} < \epsilon_g$).

Solution Sequence

Each FE analysis involved setting up the initial stresses. This was done by specifying the bulk density of the soil above the groundwater table and the buoyant

weight below the groundwater table. The ratio of horizontal to vertical stress was established using K'_o , estimated from Poisson's ratio (eg. $K_o = \nu / (1 - \nu)$). The pile loading was simulated by prescribing pile head displacement and allowing PLAXIS to iteratively solve for the reaction forces on the top of the pile and the stresses in the pile-soil system.

Estimation of the Soil Parameters

For each case, the soil parameters were back-calculated from the measured pile response using FE analysis. The parameters were then checked to ensure they were consistent with the SPT N-values (blows/foot of penetration) measured for the soils in each case. The unknown variables in each of the FE analyses were: the enlarged micropile diameter D' , the elastic modulus, E , and effective friction angle, ϕ' , of the soil, and the dilation angle, ψ_i , of the pile-soil interface.

Figure 3.9 illustrates the calculated (by FE Analysis) load versus pile-head displacement curve for a typical micropile. Appendix C presents the results of additional sensitivity study. Referring to Figure 3.9, the initial slope of the load-displacement curve was found to be governed by the elastic modulus of the soil, E , and the augmented pile diameter, D' . For each calculated load-displacement curve, there was a yield point (see Point A in Figure 3.9) which was governed by the friction angle of the pile-soil interface, δ_i , and the effective friction angle of the soil, ϕ' . At point A, most of the friction along the pile is mobilized as shown in Figure 3.10 and there is some local yielding near the tip. Since $\delta_i = \phi'$ has been assumed (see above), the yield point was governed primarily by ϕ' of the soil. The slope of the load-displacement curve beyond Point B (see Fig. 3.9) was found to be governed by the dilation angle of the soil-pile interface, ψ_i . If ψ_i is set to zero, a classic elastic-plastic response is obtained (see Curve

1 in Fig. 3.9). Figure 3.11 shows the plastic zones in the soil at point B. From Fig. 3.11, it can be seen that the pile-soil interface and the tip have fully yielded at Point B and the subsequent post yield stiffness of the micropile is derived from dilatancy along the interface and in the soil at the tip.

In the first 3 cases described below, at least 2 micropiles were tested and a unique set of parameters (D' , E , ϕ' and ψ_i) could be deduced using trial-and-error for these cases. The term unique is used to denote that all piles in the case could be simulated numerically using the same (or unique) set of parameters. For the last two cases, however, only one pile load test was performed. As a result, pile enlargement (percent increase in the bored diameter) similar to that deduced from cases with multiple pile tests was assumed and only E , ϕ' and ψ_i were back-calculated from the measured load-deflection response.

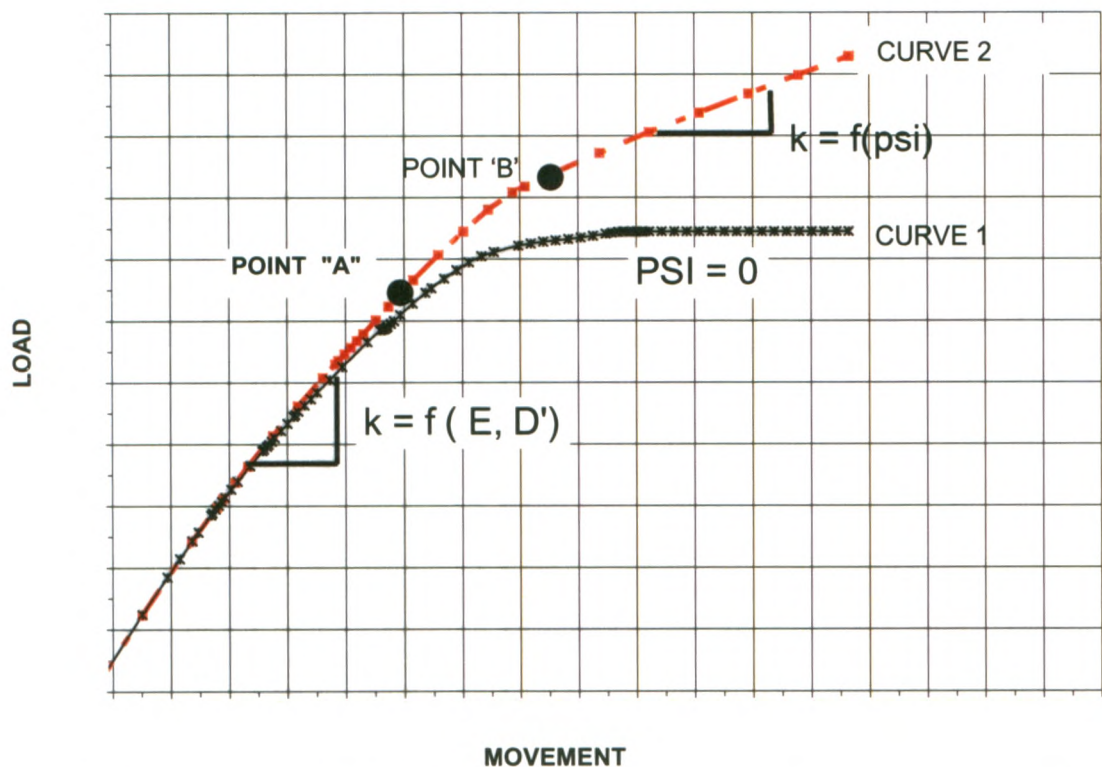


Figure 3.9. Typical F.E. Load-Displacement Response For $\psi = 0^\circ$ and $\psi \neq 0^\circ$

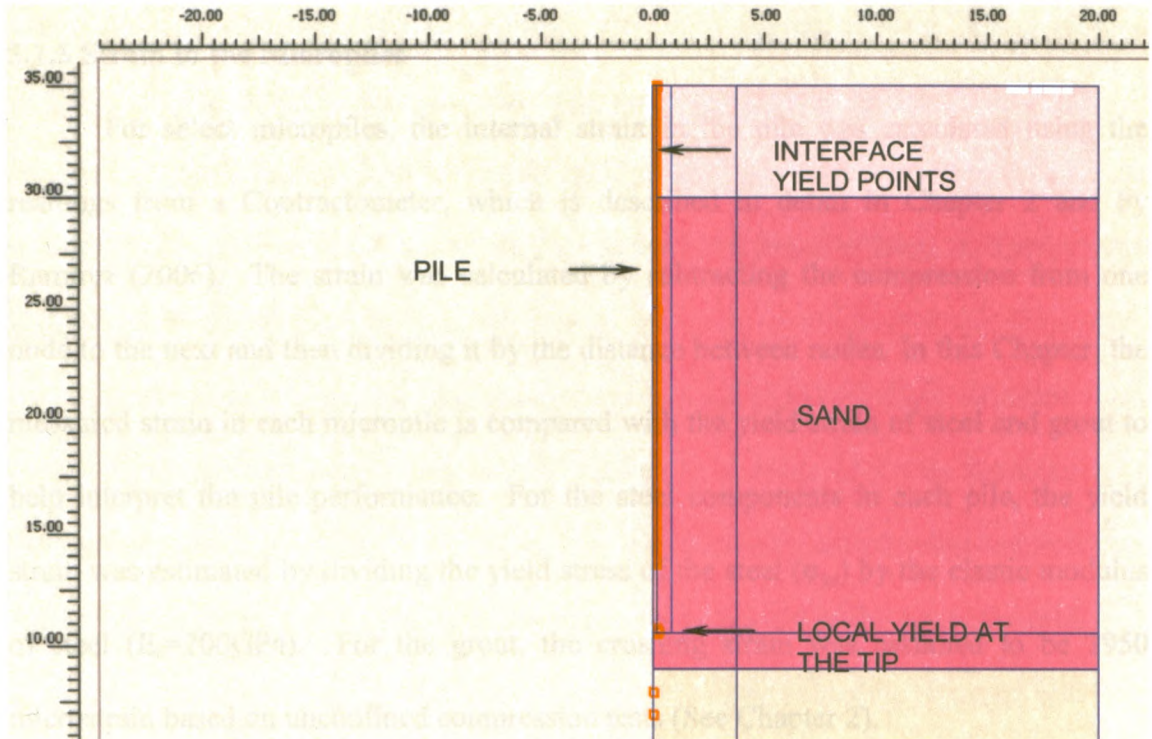


Figure 3.10 Plastic zones (in red) at point "A"

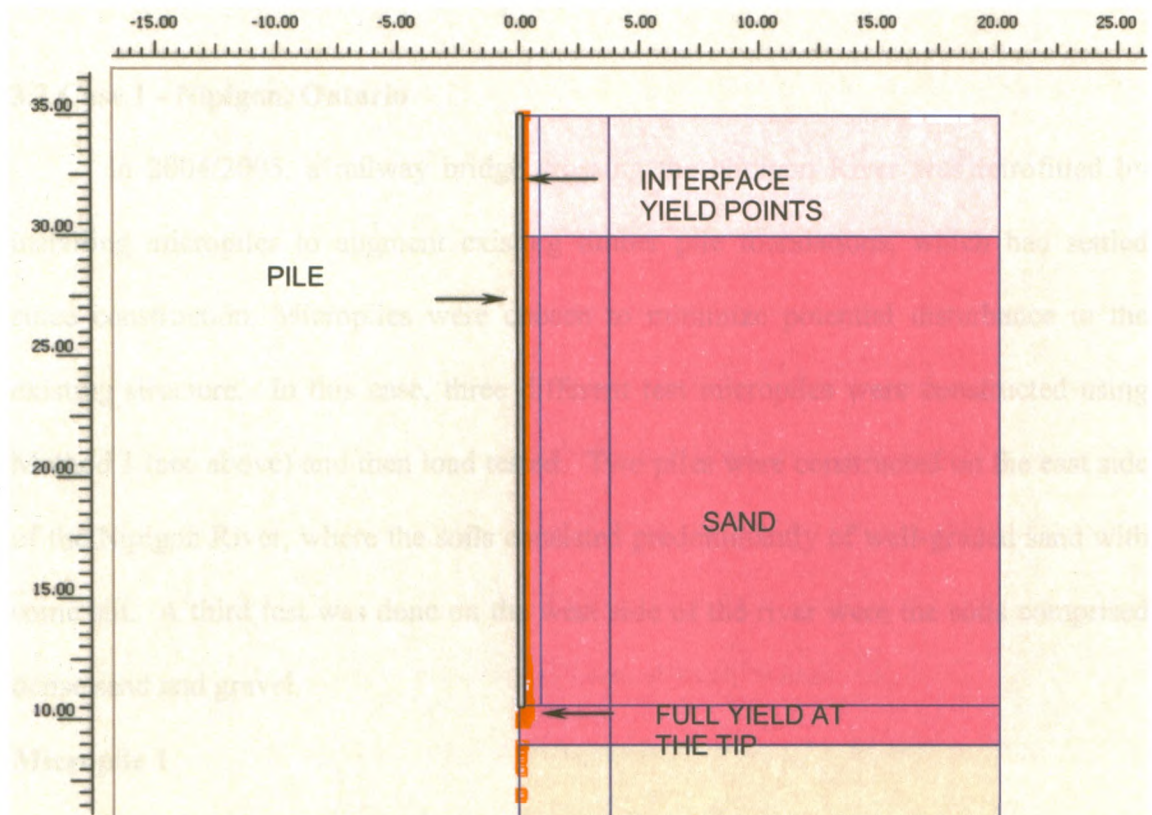


Figure 3.11 Plastic zones (in red) at Point "B"

3.1.5 Strain in the Micropiles

For select micropiles, the internal strain in the pile was calculated using the readings from a Contractometer, which is described in detail in Chapter 2 and by Ramirez (2006). The strain was calculated by subtracting the compression from one node to the next and then dividing it by the distance between nodes. In this Chapter, the measured strain in each micropile is compared with the yield strain of steel and grout to help interpret the pile performance. For the steel components in each pile, the yield strain was estimated by dividing the yield stress of the steel (σ_{ys}) by the elastic modulus of steel ($E_s=200\text{GPa}$). For the grout, the crushing strain was assumed to be 1950 microstrain based on unconfined compression tests (See Chapter 2).

3.2 Micropile Soil Cases

3.2 Case 1 - Nipigon, Ontario

In 2004/2005, a railway bridge crossing the Nipigon River was retrofitted by installing micropiles to augment existing timber pile foundations, which had settled since construction. Micropiles were chosen to minimize potential disturbance to the existing structure. In this case, three different test micropiles were constructed using Method 1 (see above) and then load tested. Two piles were constructed on the east side of the Nipigon River, where the soils consisted predominantly of well-graded sand with some silt. A third test was done on the west side of the river where the soils comprised dense sand and gravel.

Micropile 1

Starting with the micropiles constructed on the east side of the river, Figure 3.12 shows details of the first micropile in this case (Micropile 1), the soil stratigraphy, and

construction details such as the drilling rate, grouting records and pile geometry. Referring to Figure 3.12, the subsurface conditions on the east side comprised 3.5m of compact fill underlain by 1.5m of dense sand. Below this sequence, there was a deep deposit of very dense sand with silt, which extended to a depth of 24m. A layer of hard grey clay was encountered below 24m.

Micropile 1 on the east side comprised a HSS 273×13 hollow structural steel casing filled with grout from the ground surface to a depth of 9.9 m followed by a grouted uncased length from 9.9 m to 24.4 m. Consequently, the pile was terminated in the dense sand with silt at an elevation approximately 2m above the hard clay layer. A 3168 mm² threaded steel bar was centered in the micropile extending from the pile head to the pile tip. The pile was loaded to a maximum load of 1830 kN at which point one of the reaction micropiles failed and the test was stopped

This micropile was constructed using Method 1 and instrumented with a Contractometer to measure internal strain during loading. During construction, the casing was removed in 3m intervals from 24.4m to 9.9m. For each 3m interval, the grout was topped up to replace the volume of the retracted casing. Pressure grouting was done only after the casing was retracted to a depth of 9.9m. The total volume of grout used to build the pile was 2.26m³ of which 2.189m³ was consumed during tremie grouting to fill the drilled shaft, and 0.069m³ was injected into the soil formation during the pressure grouting (see Figure 3.12). Based on the total volume of grout used during construction, the enlarged pile diameter, D' , was at least 345mm.

Figure 3.12 shows: (i) the load-displacement behaviour of Micropile 1, (ii) the pile compression (calculated from the Contractometer measurements) versus pile load, and (iii) the calculated (FE) load-displacement response. Table 3.1 summarizes the

material properties used to obtain the calculated pile behaviour. The FE calculations were performed using an enlarged pile diameter, D' , of 380mm.

From Figure 3.13, it can be seen that initially the actual pile displacement was relatively stiff up to an axial load of about 600 kN after which significant non-linearity occurred. From the pile load test and using Davisson's criterion, the ultimate load of Micropile 1 was about 1800kN. In comparison, the theoretical capacity of this pile (estimated from pile theory) is 3738 kN (see Table 3.9), which is derived from 2486kN (66%) in end bearing and 1252kN (33%) skin friction. Thus, the measured capacity of Micropile 1 was substantially lower than the theoretical capacity from pile theory.

The enlarged diameter, D' , deduced for Micropile 1 was 380mm. This is within 10% of the enlarged diameter estimated from the volume of grout consumed during construction ($D'=345\text{mm}$). Referring to Figure 3.13, the FE analysis undertaken neglecting dilatancy of the Nipigon foundation soil (e.g. $\psi=0^\circ$) gives a load displacement curve with an ultimate load (1500 kN), which is below the ultimate capacity calculated from pile theory but comparable to the actual behaviour. In contrast, a FE analysis undertaken with some dilatancy along the pile-to-soil interface ($\psi=8^\circ$) gives a load displacement curve that is an upper bound to that measured *in situ*. The analysis shown in Figure 3.13 suggests that loads in excess of about 1100kN are carried by the pile due to yielding and dilatancy along the pile-to-soil interface, which increases the lateral stress on the interface. This will be explored further in subsequent pile load tests and cases.

Referring to the measured pile response, at the axial load of 1830kN the measured pile head deflection was 25 mm while compression of the pile (based on Contractometer measurements) was only 5mm. The difference between these

measurements is most likely due to the micropile moving as a unit into the soil mass due to slip along the interface, and bearing failure at the tip. The permanent pile head set after unloading was 23 mm, which is also indicative of plastic deformation.

Figure 3.14 shows the distribution of strain along the length of the pile for each load level. This graph indicates there is constant strain in the micropile above a depth of about 9.9 m where the casing is located. Below 9.9m, the strain begins to decrease with depth. This suggests that there is insignificant skin friction in the upper cased section of the pile. At high loads, the Contractometer indicates that there is tension near the toe; however, this is indicative of the instrument error rather than actual tension in the pile. It can be seen by comparing the measured strain to the structural yield strain of the grout and steel (ϵ_y^g and ϵ_y^s) that the load and consequent strain in the micropile was well below the structural limit of the pile materials. Therefore, it is concluded that the geotechnical capacity of Micropile 1 governed the axial behaviour.

EAST SIDE NIPIGON

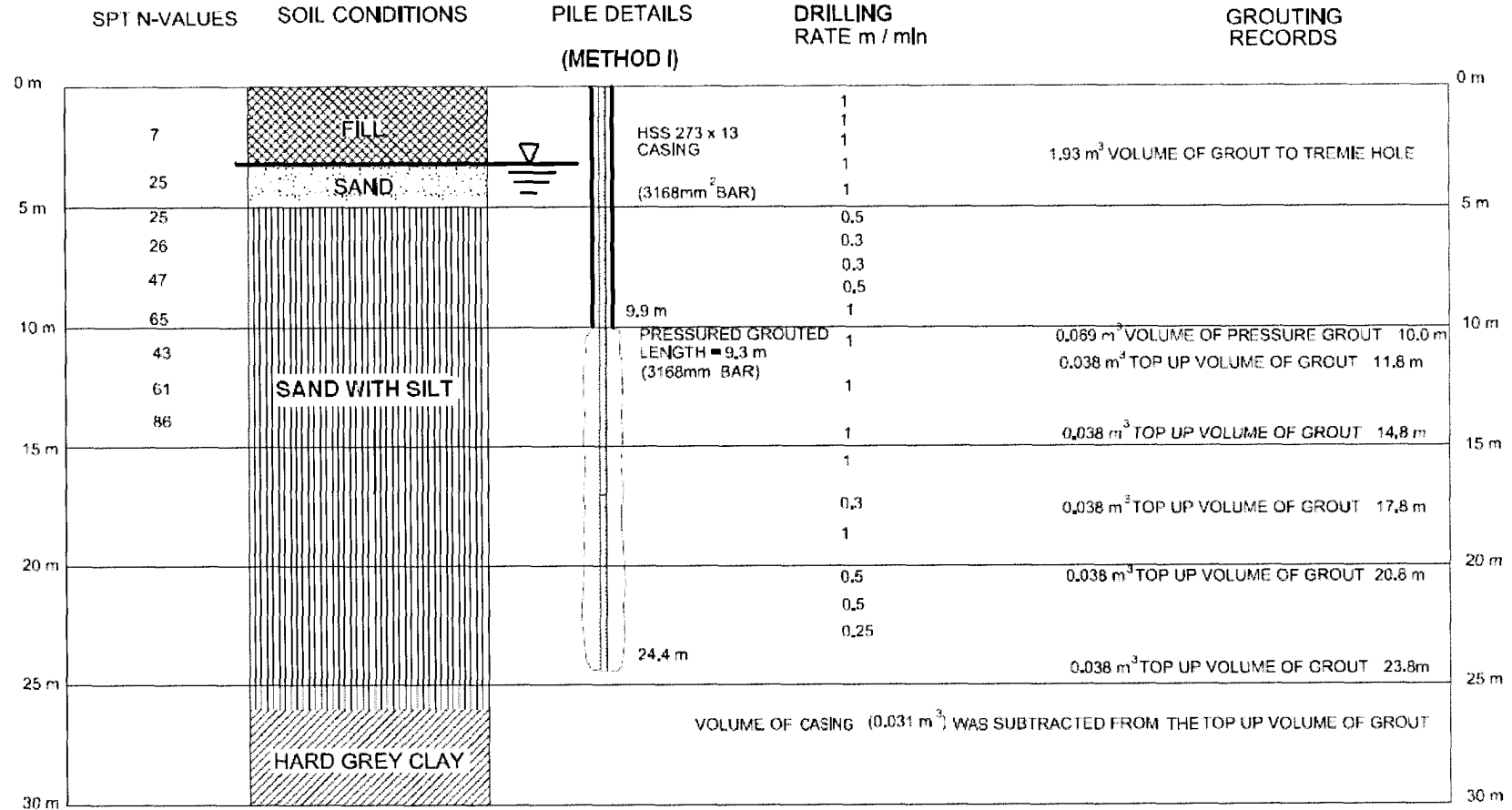


Figure 3.12 Installation Details for East Nipigon-Micropile 1.

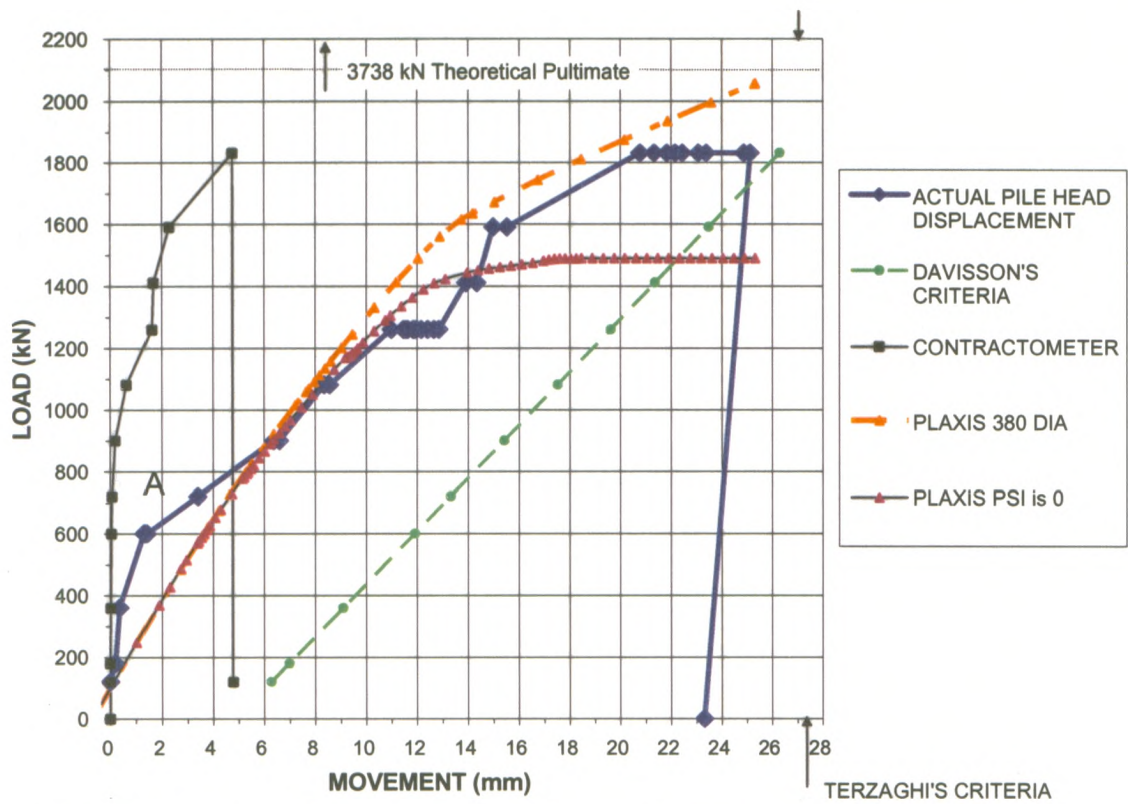


Figure 3.13 Load Displacement Behaviour for the East Nipigon-Micropile 1.

Table 3.1 Parameters Used for the Micropiles at Nipigon.

Material	E MPa	c' kPa	v	Φ' / δ_i	Dry Density Kg/m ³	Ko	ψ
Casing, bar and Grout	33500	32700	0.33	0	1300	0.54	0
Bar and Grout	19600	19100	0.33	0	1300	0.54	0
Silt and Sand	50	2	0.35	38	1000	0.54	8
Stiff Clay	75	100	0.35	0	1000	0.54	0
Top Fill	10	1	0.35	32	1300	0.54	1
Interface along the uncased length	50	2	0.35	38*	1000	0.54	8

* Refers to δ_i

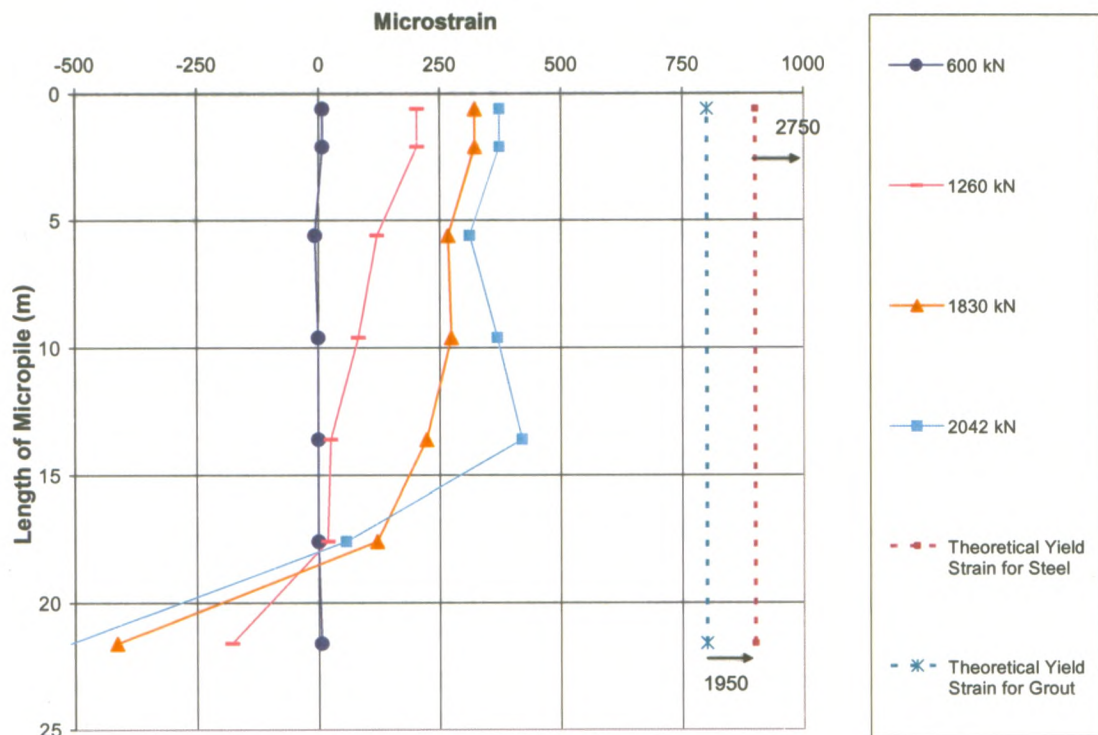


Figure 3.14 Strain Depth for East- Nipigon Micropile 1.

Micropile 2

The second micropile tested at Nipigon (Micropile 2) was a Type D micropile constructed using Method I. The finished pile comprised of a 12.5 m long HSS 273×13 casing from the ground to a depth of 12.5m followed by a pressure grouted section from 12.5m to 27.5m. Unlike Micropile 1, this micropile was pressure grouted in 3 m intervals from a depth of 27.5m to 12.5m and then post grouted 24 hours after the pressure grouting using a TAM installed in the pile. Figure 3.15 shows the soil stratigraphy, pile geometry, and construction details such as drilling rate and grout takes.

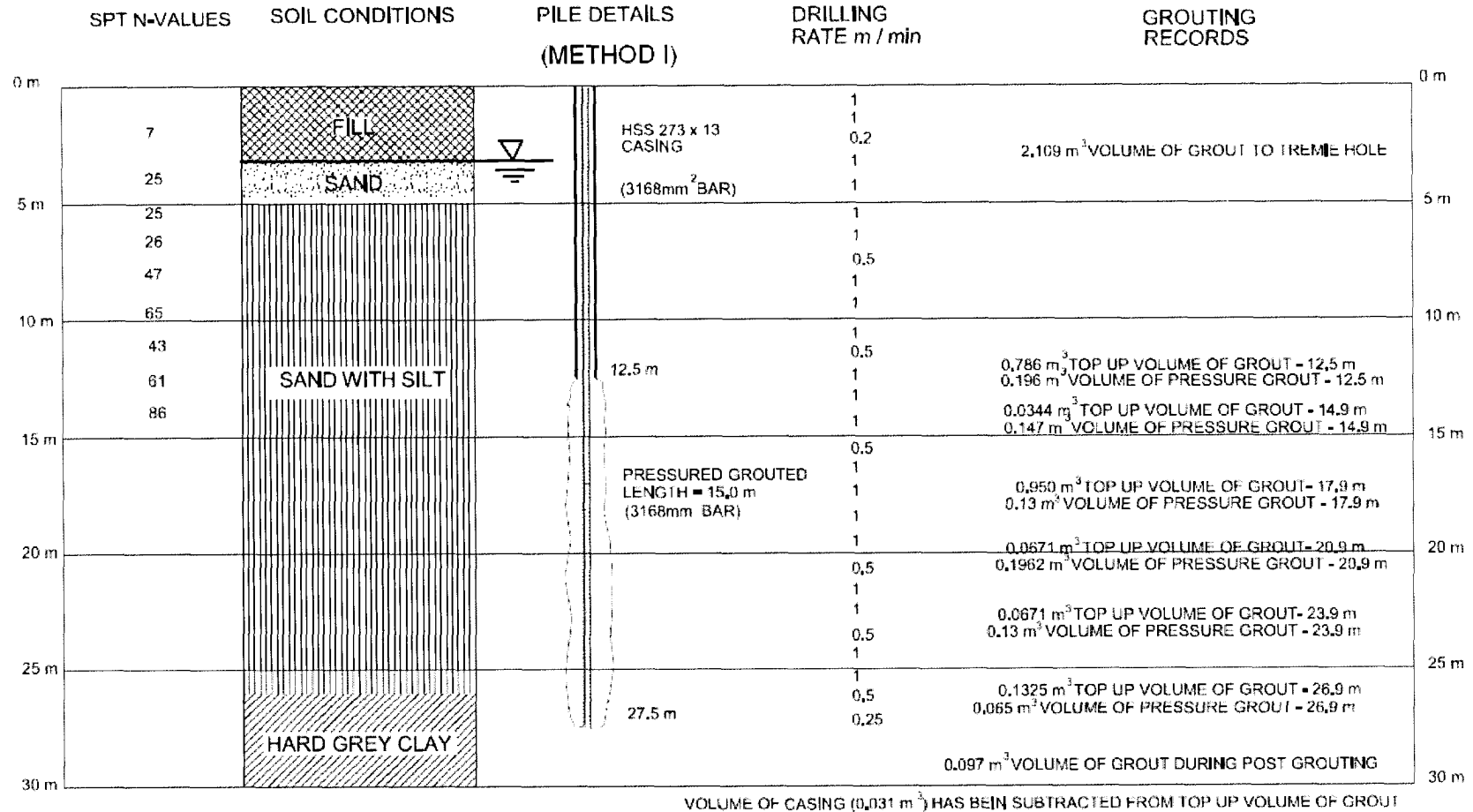
Referring to Figure 3.15, the stratigraphy for Micropile 2 corresponded to that described for Micropile 1 except that Micropile 2 was drilled into the lower hard grey clay layer. As shown below, this had a significant impact on the pile behaviour. During construction of Micropile 2, 2.11m³ of grout was tremied into the bored hole.

Additionally, 2.03m^3 of grout was used in total to top up the grout when the casing segments were retracted from a depth of 27.5m to 12.5m. Then, a total of 0.86 m^3 of grout was injected during the pressure grouting in 3m intervals from 27.5m to 12.5m. Finally, 0.097m^3 of grout were injected through a TAM during post grouting. Micropile 2 was not instrumented with a Contractometer. From the grout volumes consumed during construction, the enlarged diameter of Micropile 2 was at least 490mm.

Figure 3.16 compares the measured load-displacement response of Micropile 2 with the calculated response from FE analysis. In contrast with Micropile 1, Micropile 2 was able to sustain a maximum load of 3063 kN. In addition, the behaviour was nearly linear up to 3063 kN indicating the absence of plasticity in the soil and pile. From the measured response, Micropile 2 had additional capacity compared to Micropile 1. The additional capacity is most likely due to the injection of additional grout during construction (enlarging the pile diameter) and the incremental pressure grouting. Referring to Table 3.9, the theoretical capacity of Micropile 2 is 2695 kN; 707kN (24%) from end bearing and 1988kN (76%) come from skin resistance. This is lower than measured *in situ* capacity of this pile.

As noted above, Figure 3.14 also shows the calculated (FE Analysis) pile load versus deflection, which was obtained using soil properties identical to those used for Micropiles 1 and 3 (see Table 3.2). An enlarged diameter of $D'=500\text{mm}$ was modeled to account for the additional grout injected during construction. From the FE analysis, it can be seen that the higher capacity of Micropile 2 can be attributed to the larger grouted diameter and dilatancy along the pile-soil interface. In this case, there appears to be higher stiffness for Micropile 2 than for Micropile 1, which is attributed to the incremental grouting procedure used for this pile.

EAST SIDE NIPIGON 2ND TEST



57

Figure 3.15 Installation Details for East Nipigon Micropile 2.

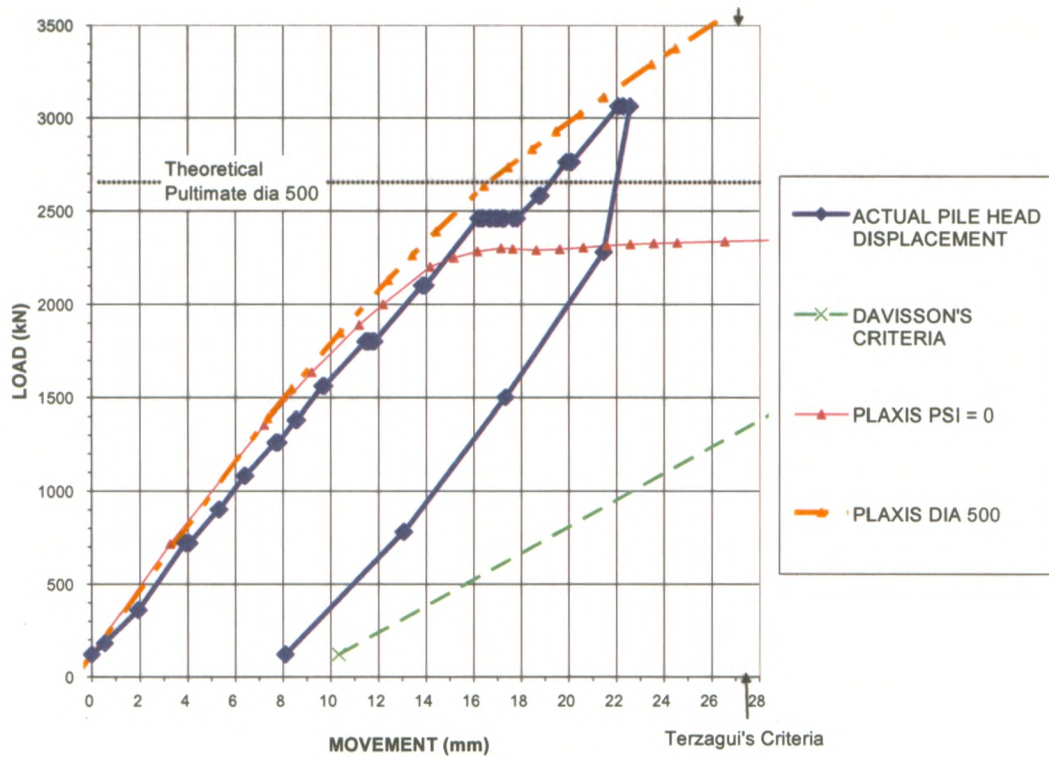


Figure 3.16 Load Displacement Behaviour East-Nipigon Micropile 2.

Table 3.2 Parameters Used for Micropiles 2 at Nipigon.

Material	E MPa	c' kPa	ν	Φ' / δ_i	Dry Density Kg/m ³	Ko	ψ
Casing, bar and Grout	27000	26300	0.33	0	1300	0.54	1
Bar and Grout	19000	18500	0.33	0	1300	0.54	1

Micropile 3

The third micropile tested during the Nipigon Case was constructed on the west side of the river. Micropile 3 was embedded in a pervious layer of sand and gravel with cobbles and it was pressure grouted in 3m intervals and then post grouted giving a Type D micropile. The construction method was identical to that used for micropile 2. Figure 3.17 shows the stratigraphy on the west side of the Nipigon River in addition to the geometry of Micropile 3, and construction details such as the drilling rate and grout takes during construction.

From Figure 3.17, it can be seen that Micropile 3 was 16.3m long. This pile comprised a seven (7) m long HSS 273×13 casing extending from the ground surface to a depth of 7m followed by a grouted section from 7m to 16.3m. A concentric steel bar (3168 mm²) was installed running along the entire length of the pile. During construction of Micropile 3, 2.5m³ of grout was used to tremie fill into the pile shaft and top up the grout when the casing was removed. In addition to this, 0.46m³ of grout was injected during pressure grouting and 0.13m³ was injected through a TAM during post grouting. Based on the total volume of grout used to build Micropile 3, the enlarged diameter was at least 450mm and the theoretical capacity should have been in the order of 2720kN (see Table 3.9).

Figure 3.18 shows the measured load versus pile head deflection up to the maximum applied load of 3000kN; which was 2.5 times the design load. In addition, Figure 3.18 shows both calculated load versus pile head deflection (FE analysis) and total pile compression measured during loading (Contractometer). From Figure 3.18, the measured pile head deflection was approximately 25 mm at a load of 3000 kN. From the Contractometer readings, the corresponding compression of Micropile 3 was 16 mm at 3000kN. In this case, the difference between the pile head deflection and the pile compression may be attributed to deformation of the soil, and elastic and plastic compression of the pile as discussed below. The theoretical capacity of Micropile 3 is 2720kN using an enlarged diameter of 450mm, 646 kN (24%) was estimated from end bearing and 2074 kN (76%) from skin friction. From Figure 3.18, it can be seen that the actual capacity of Micropile 3 was higher than the estimated capacity from pile theory.

The FE results presented in Figure 3.18 were obtained using the same soil parameters as on the east side micropiles. Table 3.3 shows the soil and micropile

parameters used in the finite element analysis. Similar to that done for Micropiles 1 and 2, FE analyses were undertaken for dilatancy angles, ψ , of 0° and 8° , respectively and assuming an augmented diameter of Micropile 3 was 450 mm. The FE results indicate first that a significant component of the pile capacity is derived from post yielding dilatancy on the pile-soil interface. This is illustrated by comparing the curves where ψ of 0° and 8° . In addition, the theoretical pile capacity derived from pile theory lies between the response calculated assuming $\psi=0^\circ$ and $\psi=8^\circ$. This is consistent with the analysis of Micropiles 1 and 2. Consequently both Micropiles 2 and 3 exhibited significantly higher capacity during loading, and notwithstanding differences in the soil stratigraphy, the higher capacity is attributed to the post-grouting methodology which appears to have densified the soil.

To conclude the Nipigon Case, Figure 3.19 shows strains measured in Micropile 3 during loading. It can be seen that for loads exceeding 2100kN, the internal pile strains exceed the yield strain of the grout and steel just below the casing (see strains at 7m depth) suggesting plastic compression. Referring back to Figure 3.18, it can be seen that, after unloading Micropile 3, there was 9mm of permanent compression of the pile. In comparison, there was only 11mm of permanent pile head deflection after unloading. The permanent pile deformation can be attributed to compression of the pile and apparent yielding of the pile below the casing. Lastly, at lower loads, it can be seen that the pile strain (see Figure 3.19) was essentially constant in the cased portion of the pile and that it decreased with depth below the casing. As a result, skin friction in the upper cased section of Micropile 3 appears to be negligible, which is similar to that seen for Micropile 1.

WEST SIDE NIPIGON

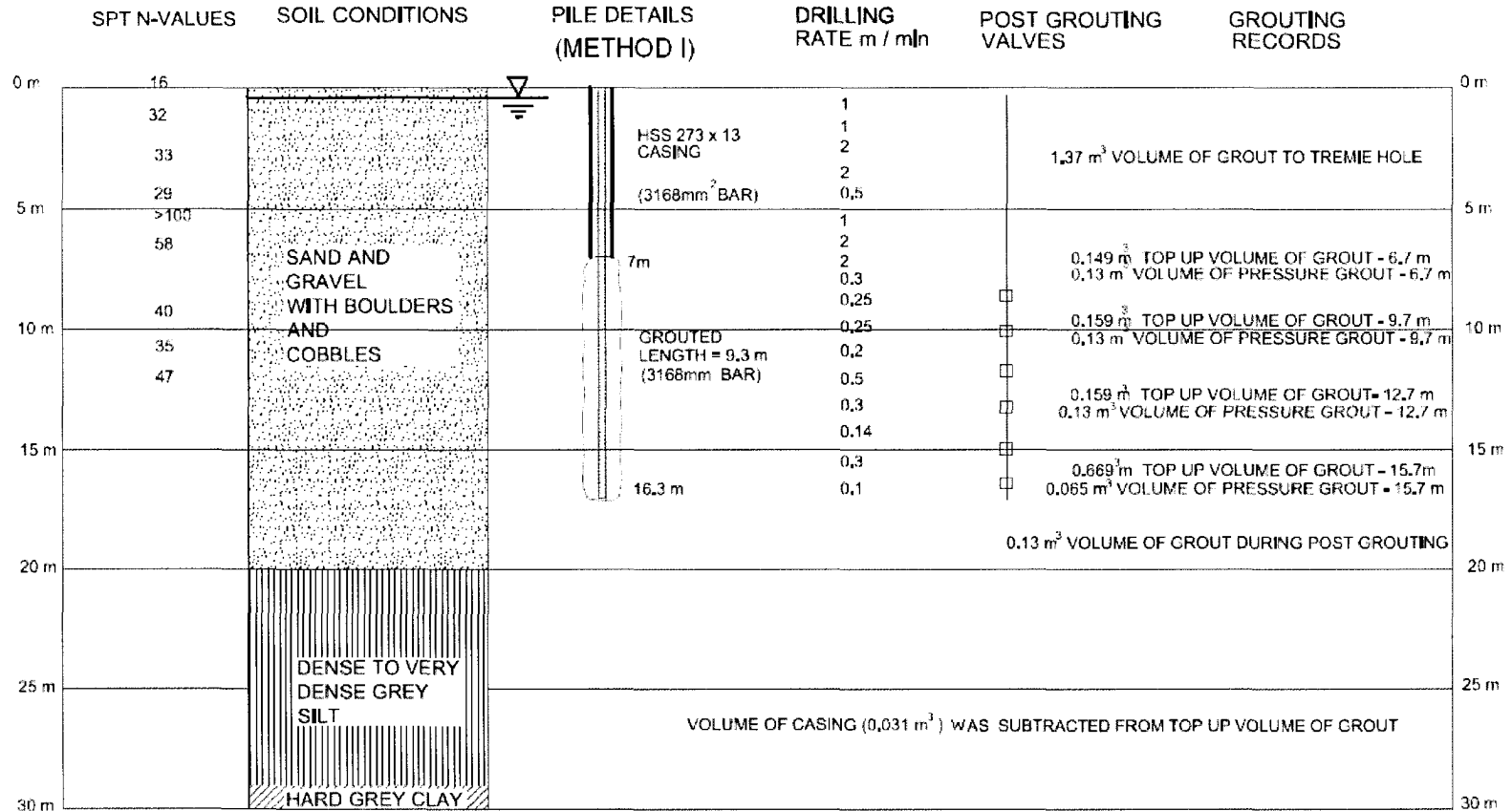


Figure 3.17 Installation Details for the West-Nipigon Micropile 3.

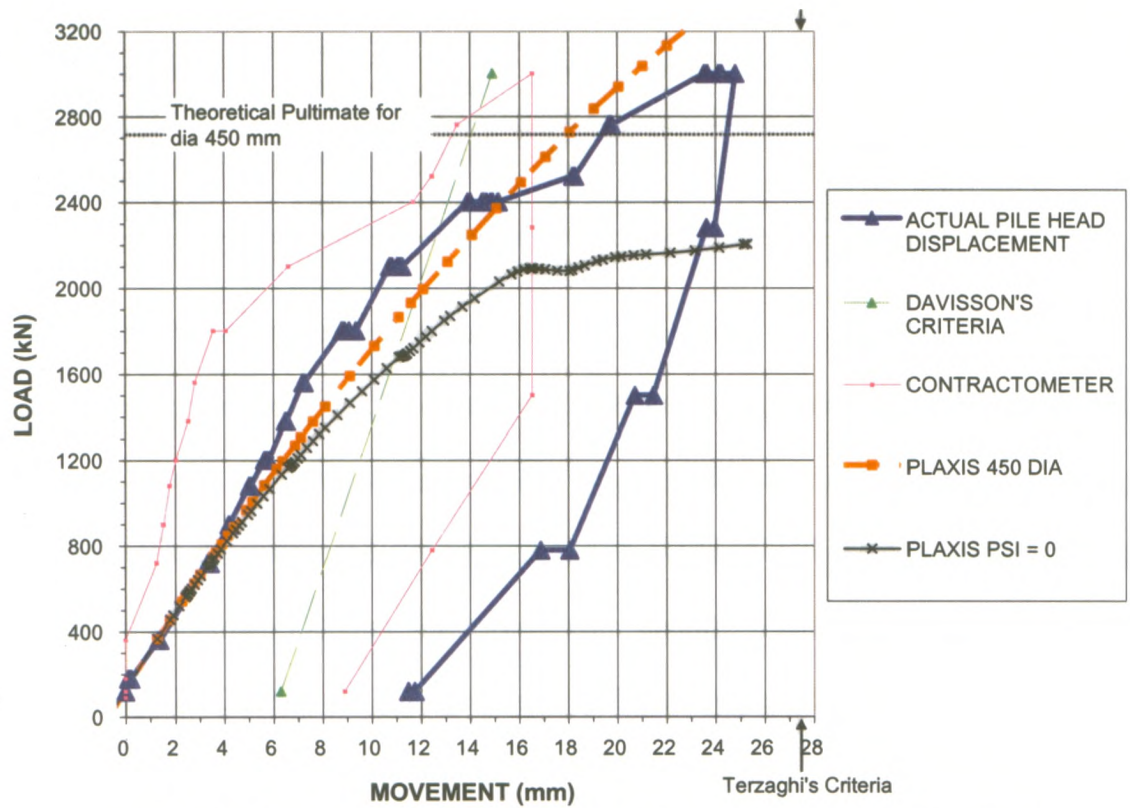


Figure 3.18 Load Displacement Behaviour for West-Nipigon Micropile 3.

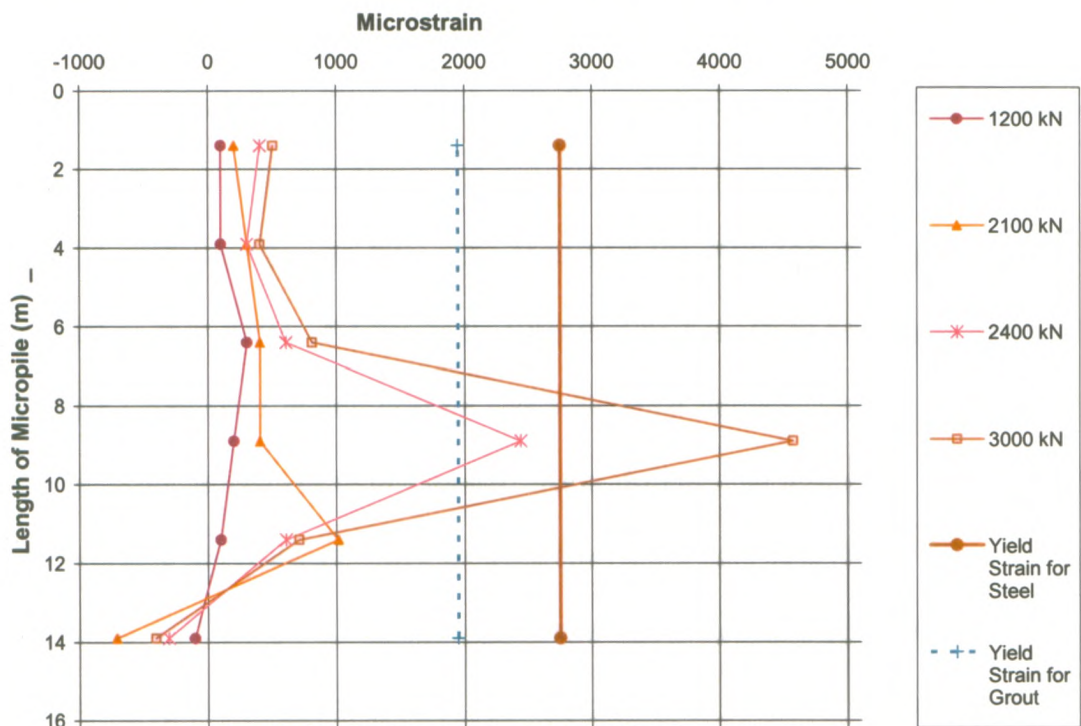


Figure 3.19 Strain Depth for West-Nipigon Micropile 3.

Table 3.3 Parameters Used for Micropile 3 at Nipigon.

Material	E MPa	c' kPa	ν	Φ / δ_i	Dry Density Kg/m ³	Ko	ψ
Casing, bar and Grout	25020	24400	0.33	0	1300	0.54	1
Bar and Grout	19680	19200	0.33	0	1300	0.54	1

3.3 Case 2 - Point Edward, Ontario

The second case involved the retrofit of an existing building in Point Edward, Ontario. At this site, two test micropiles were installed in a soil deposit comprising upper silty sand overlying dense medium to coarse sand with SPT-N values varying from 2 to 33 blows/300 mm (increasing with depth). Figure 3.20 summarizes the stratigraphy for Case 2, the pile geometry and construction details. Contractometers were not installed in the micropiles at this site. Both micropiles (Micropiles 4 and 5) were installed using Method 2 with a hollow core Titan 40/20 bar. These micropiles are Type A micropiles according to the FHWA (2000) manual.

The first micropile in Case 2 (Micropile 4) comprised a HSS 125×12 casing from the ground surface to a depth of 1.5m and then an uncased section from 1.5m to a depth of 12.2m. The second micropile (Micropile 5) comprised a HSS 125×12 casing from the ground surface to a depth of 1.5m and an uncased section from 1.5m to a depth of 13.7m. The Grout used during drilling was a Type 10 Portland Cement mixed with water. The water to cement ratio was 0.6. After drilling, the lean grout was flushed from the borehole and replaced with a grout that had a w/c ratio of 0.45.

Figures 3.21 and 3.22 show the measured and calculated (FE analysis) load-displacement response of Micropiles 4 and 5 respectively. Table 3.4 summarizes the soil parameters used in the FE analysis. A friction angle of 35° was assumed for the

sand and gravel at this site because it comprised rounded to subrounded grains and had relatively low SPT N-values compared to Case 1. Since the grout volumes were not recorded for these piles, the augmented pile diameter was estimated from trial and error using FE analysis and assuming consistent soil parameters for both Micropiles 4 and 5.

Micropile 4

Referring to Figure 3.21, Micropile 4 was tested to an ultimate load of 335 kN. However, this load could not be sustained due to creep and the load relaxed with time until a deflection of 28mm was reached at a load of 300 kN (see Figure 3.21). After removing the axial load, there was 25mm of permanent deformation. Thus the ultimate capacity of the micropile was in the order of 300 kN.

As shown in Figure 3.21, a similar calculated (FE) load-displacement response was obtained using an enlarged pile diameter, D' , of 189mm for the parameters shown in Table 3.4. Figure 3.21 also shows FE calculations performed using $\psi_i = 0^\circ$ and $\psi_i = 2^\circ$. From the FE calculations, it can be seen that the actual capacity of Micropile 4 lies between that estimated from FE analysis assuming $\psi_i = 0^\circ$ and $\psi_i = 2^\circ$. Thus, a portion of the capacity of this micropile appears to be derived from dilation along the pile-soil interface and a portion from pile enlargement. For comparison purposes, the theoretical capacity of Micropile 2 (from pile theory) was 376kN: 205kN from end bearing and 171kN from skin friction (see Table 3.9). The measured load-displacement response of Micropile 4 suggests that a significant portion of the axial capacity is derived from pile enlargement and that dilation effects are less prevalent for the micropiles built in Point Edward (compared to Case 1). This is consistent with the lower SPT-N-value and the absence of pressure grouting.

Micropile 5

Figure 3.22 shows the measured load-displacement response of the second micropile constructed in Case 2 (Micropile 5). The measured response is compared with FE calculations for $\psi_i = 0^\circ$ and $\psi_i = 2^\circ$ and the ultimate pile capacity estimated using pile theory. The enlarged diameter of Micropile 5 was deduced to be 250mm from the measured load-deflection response and using the same soil properties adopted in the analysis of Micropile 4 (see Table 3.4).

Referring to Figure 3.20, Micropile 5 was tested to an ultimate load of 497 kN: the corresponding pile head deflection was 14.8 mm (see Figure 3.22). A permanent deformation of 14.4mm was recorded after removing the applied load. Micropile 5 did not experience load relaxation during the test. From pile theory, the capacity of Micropile 5 is 691 kN (see Table 3.9): 404 kN from end bearing and 287 kN from skin friction. Similar to that seen for Micropile 4, the capacity estimated using pile theory exceeds the measured capacity of Micropile 5. In addition, the measured load displacement response lies between the FE calculations for $\psi_i = 0^\circ$ and $\psi_i = 2^\circ$. Thus, the analysis of Micropiles 4 and 5 are consistent. Since the measured load-displacement response(s) in Case 2 are closest to the FE analysis performed using $\psi_i = 0^\circ$, the influence of dilatancy on the response of the micropiles constructed at the Point Edward site appears to be comparatively less significant than observed at the Nipigon site in Case 1. It is interesting to note that P'_{ult} from pile theory lies between the FE response for non dilatant ($\psi_i = 0^\circ$) and dilant ($\psi_i = 2^\circ$) soil behaviour.

POINT EDWARD, ONTARIO MICROPILE

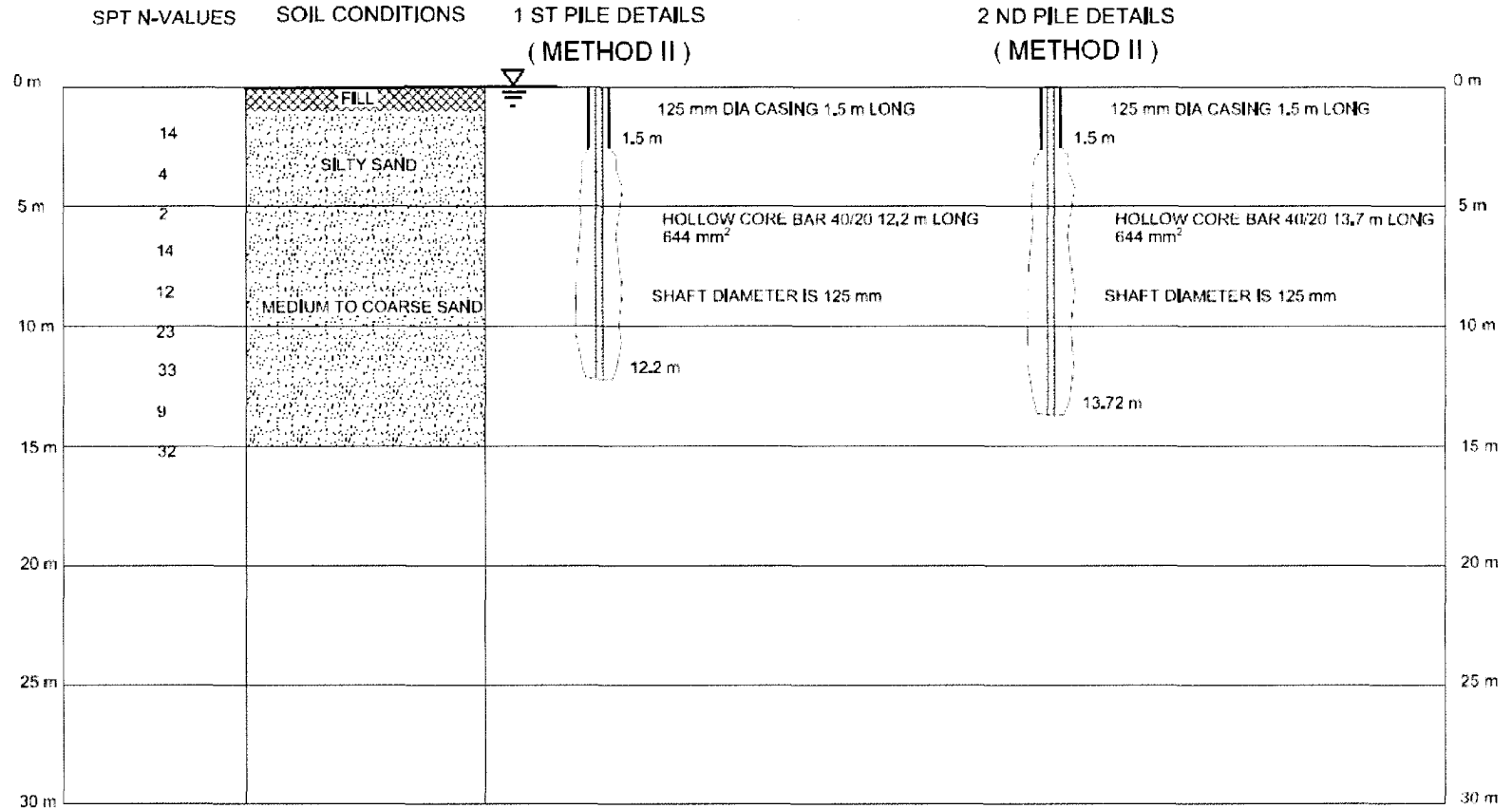


Figure 3.20 Installation Details For The Point Edward Case.

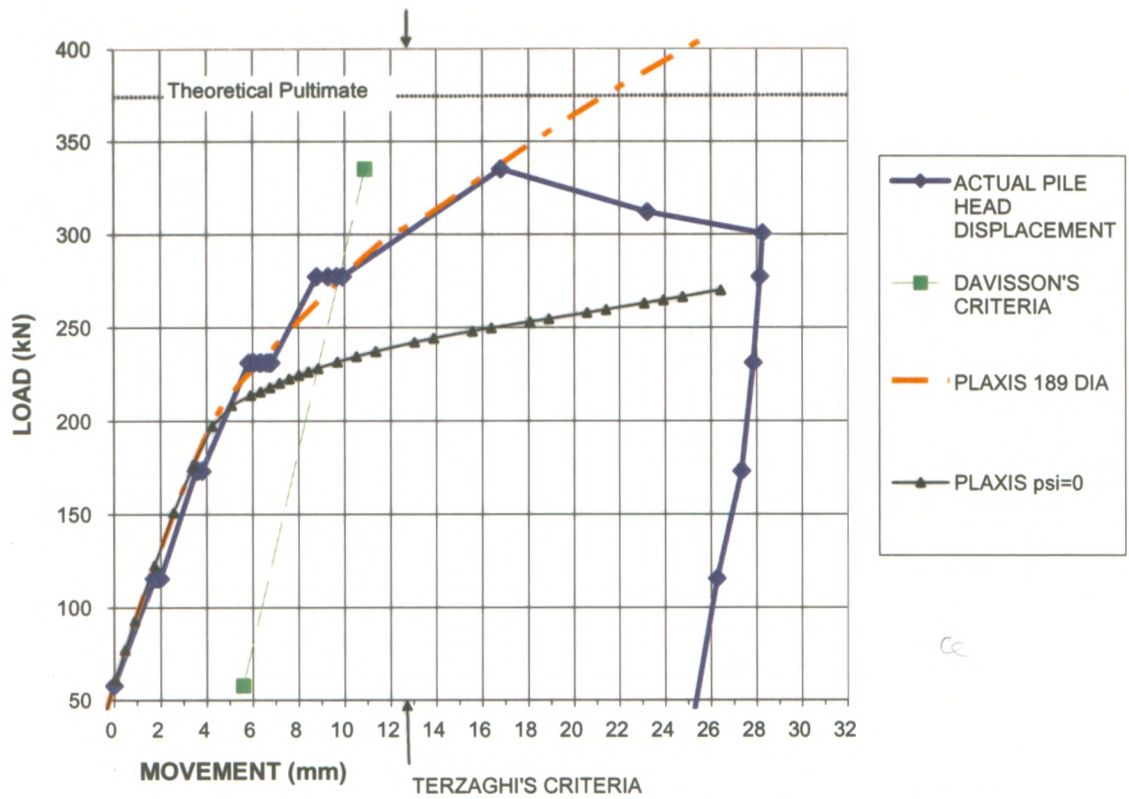


Figure 3.21 Load Displacement Behaviour For Point Edward-Micropile 4.

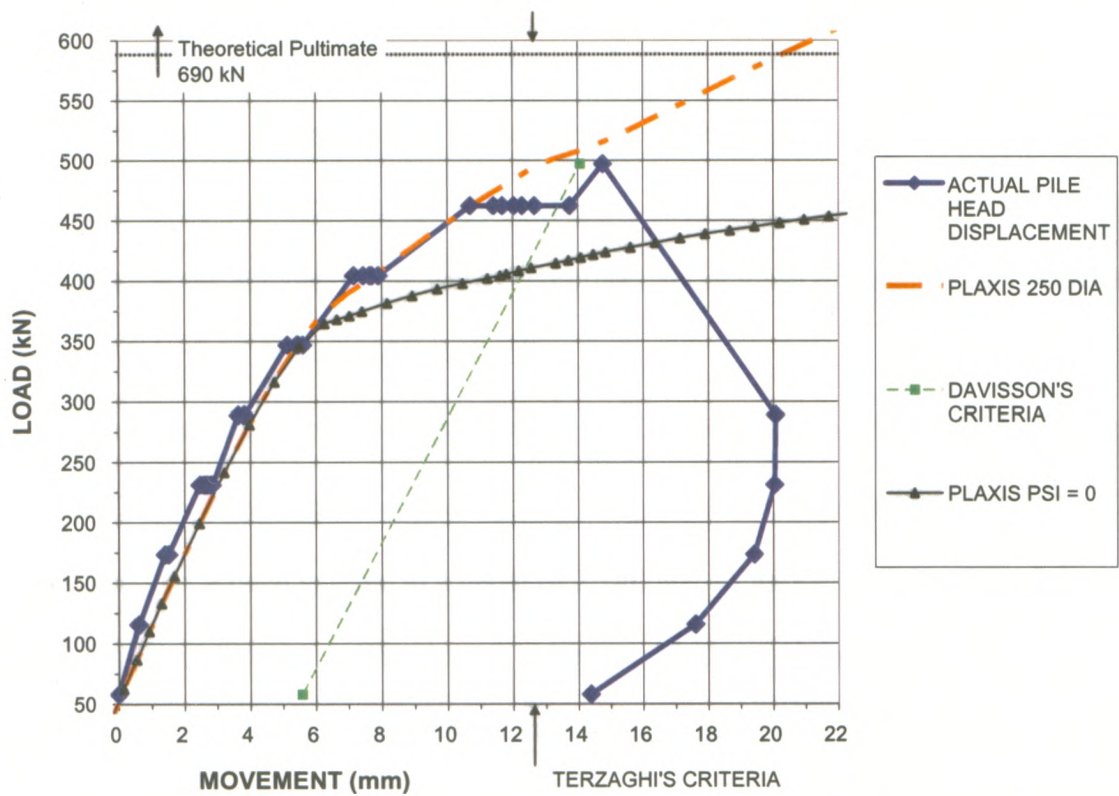


Figure 3.22 Load Displacement Behaviour for Point Edward Micropile 5.

Table 3.4. Parameters used for Point Edward.

Material	E MPa	c' kPa	v	Φ' / δ_i	Dry Density Kg/m ³	Ko	Ψ
Casing, Bar and Grout	31650	30860	0.33	1	2300	0.54	1
Bar and Grout	17190	16760	0.33	1	2300	0.54	1
Silty Sand	10	1	0.35	32	2000	0.54	0
Medium Coarse Sand	30	1	0.35	38	2000	0.54	2
Interface in the Silty Sand	10	1	0.35	32*	2000	0.54	0
Interface in the Medium Coarse Sand	30	1	0.35	38*	2000	0.54	2

* Refers to δ_i

3.4 Case 3 - Kitchener, Ontario

Two micropiles (Micropiles 6 and 7) were installed during the retrofitting of a commercial building in Kitchener, Ontario. Micropiles were used, due to the low headroom available for installation. The Case 3 micropiles were installed through fill and sandy silt till using Method 2 (see Figure 3.23 for installation details); hence both micropiles can be classified as Type A piles according to the FWHA manual. Contractometers were not attached to these two micropiles. Figure 3.23 shows the stratigraphy at the Kitchener site, which comprised 5m of loose to compact fill underlain by a deep deposit of dense sand and silt till.

The first test micropile constructed at the Kitchener site (Micropile 6) comprised a Titan 40/20 hollow core bar extending from the pile head to the pile tip, a HSS 115×11 casing from the ground surface to a depth of 2.7m, and an uncased section from 2.7m to 8.7m. The drill bit had a diameter of 115 mm. The second micropile (Micropile 7) consisted of a 12.2m long 73/45 hollow core bar with a #8 bar embedded in the middle of it, a 2.14 m long HSS 178x11 casing extending from the ground surface to a depth of

2.14m, and an uncased grouted section from 2.14m to a final depth of 12.2 m (see Figure 3.23). The diameter of the drill bit was 178 mm. The following is a description of the pile load test response.

Micropile 6

Figure 3.24 shows the measured and calculated (FE analysis) load displacement response for Micropile 6 in addition to the pile capacity estimated using pile theory (see Table 3.9). The FE calculations were performed using the soil parameters summarized in Table 3.5 and assuming $\psi_i=0^\circ$ and $\psi_i=6^\circ$. Referring to Figure 3.24, Micropile 6 was tested to a maximum load of 687 kN: the corresponding pile head displacement was 13.7 mm. After removing the load, there was permanent deformation of 4.6 mm (plastic). At the maximum load, a creep rate of 1.1mm/hr was measured indicating the pile was not close to the ultimate capacity.

Figure 3.24 shows the calculated response of Micropile 6, which was obtained assuming an enlarged diameter of 172mm and using the soil parameters listed in Table 3.5. From Figure 3.24, it can be seen that there is good agreement between the calculated and measured response of Micropile 6 for the soil parameters and pile geometry used in the FE analysis. The analysis suggests that the as-constructed diameter of Micropile 6 was about 1.5 times larger than the diameter of the drill bit. Referring to Table 3.9, this is consistent with the other micropile cases. From pile theory the ultimate capacity of this pile is 746 kN: 566kN from end bearing and 180 kN from skin friction. Again, as seen with the other cases examined so far, the theoretical capacity lies between that estimated from FE analysis using $\psi_i=0^\circ$ and $\psi_i=6^\circ$. Given that there is reasonable agreement between the calculated and measured behaviour for

$\psi_i=6^\circ$, both dilation and pile enlargement appear to have had a significant impact on the capacity of this micropile.

Micropile 7

The calculated and measured load displacement response of Micropile 7 is shown in Figure 3.25. This micropile was tested to a maximum load of 2314 kN where the corresponding pile head displacement was 24.4 mm. Once the load was removed, there was permanent deformation of 13.8 mm and hence elastic compression of 10.6 mm. The larger permanent deformation recorded suggests there was more plasticity during the loading of Micropile 7 than observed for Micropile 6. At the maximum load of 2314kN, the measured creep rate was 2.2 mm/hr.

As noted above, Figure 3.25 also shows the calculated response of Micropile 7 obtained from FE analysis using $\psi_i=0^\circ$ and $\psi_i=6^\circ$ together with the estimated capacity using pile theory. From pile theory, the capacity of Micropile 7 is about 2584kN: 1985kN from end bearing and 599kN from skin friction. This is slightly higher than the maximum load carried by this pile. The measured response of Micropile 7 is close to that obtained from FE analysis using $\psi_i=6^\circ$. Thus, there is evidence that dilation of the soil and pile-soil interface has had an impact on the capacity of this pile. This is consistent with the dense glacial soils at the site. Although Micropiles 6 and 7 were not loaded to failure, the results and comparisons shown in Figures 3.24 and 3.25 are consistent with Cases 1 and 2 indicating that the micropiles at the Kitchener site were enlarged during construction (relative to the bid diameter) and that a portion of the axial capacity of these piles can be attributed to some dilatancy in the soil and along the pile-soil interface.

KITCHENER, ONTARIO MICROPILE

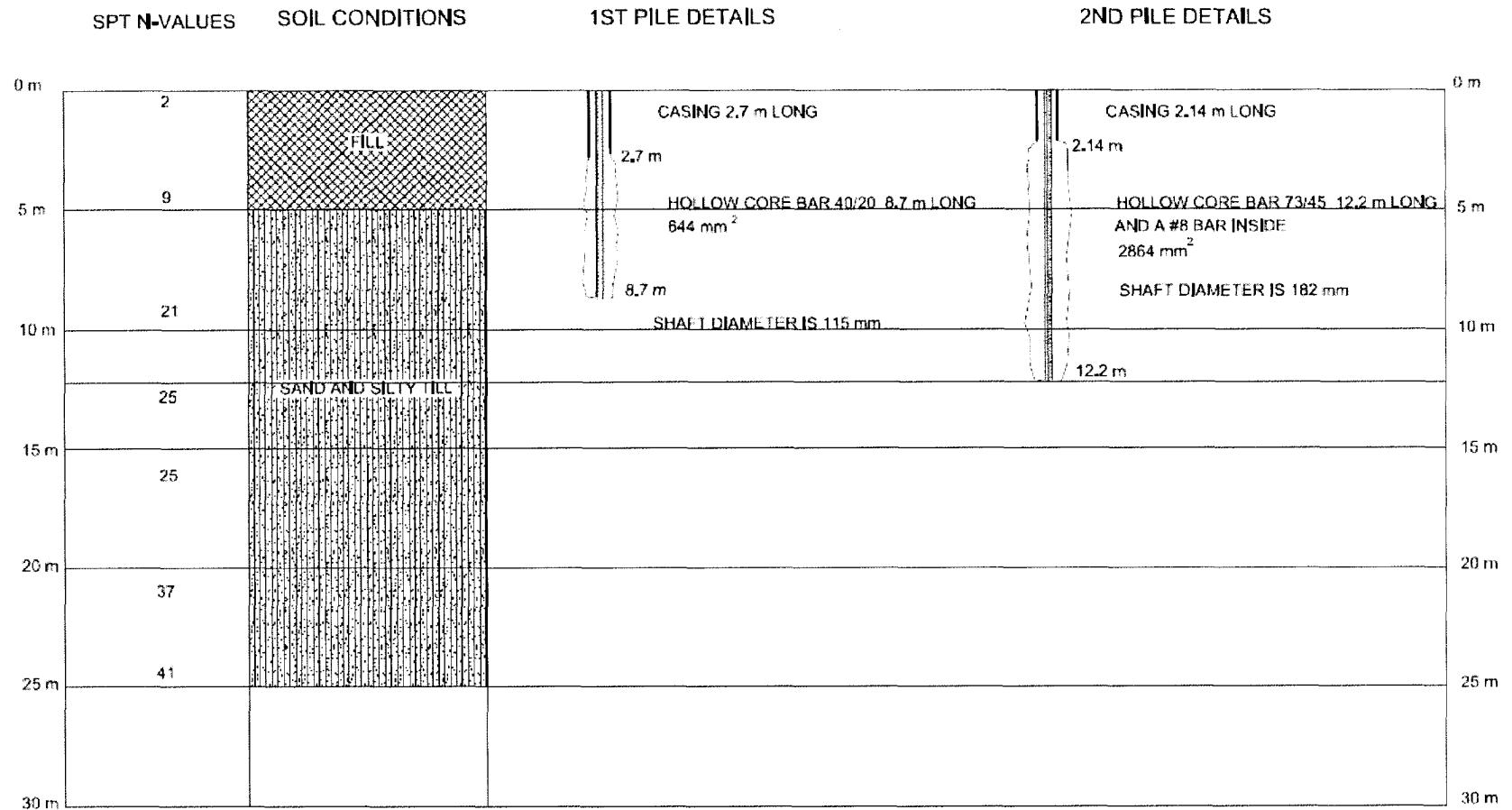


Figure 3.23 Installation Details for Kitchener Micropiles.

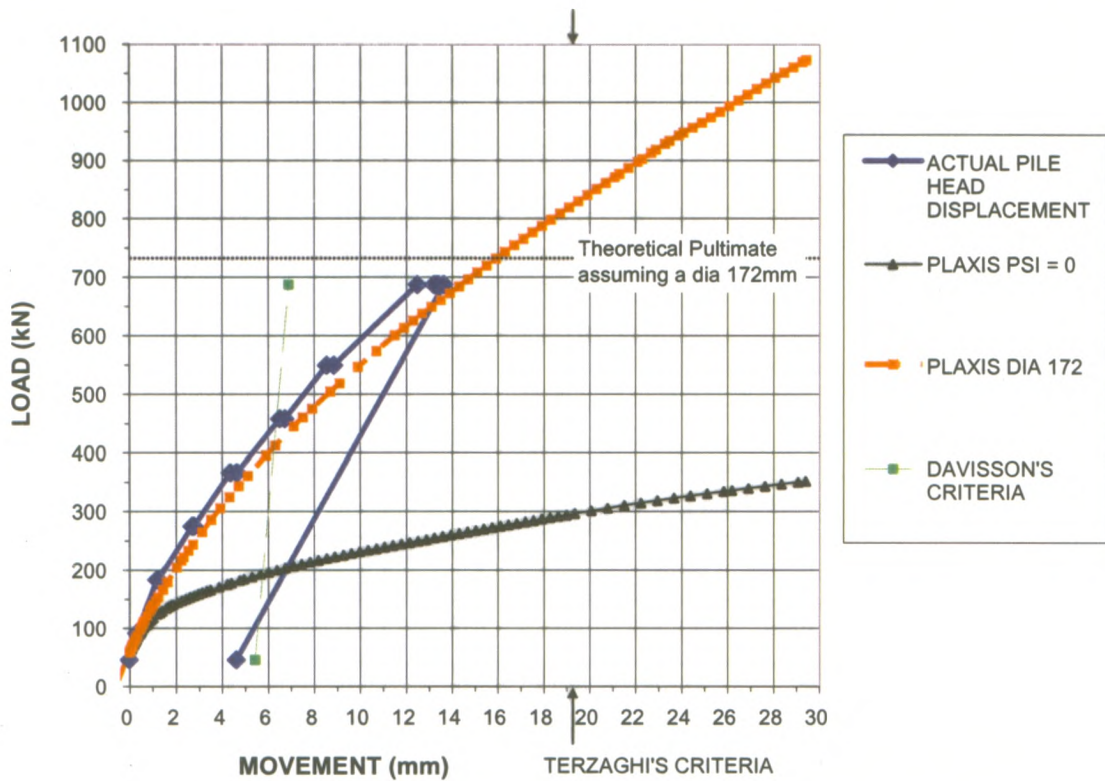


Figure 3.24 Load Displacement Behaviour for Kitchener-Micropile 6.

Table 3.5. Parameters used for Kitchener Micropile 6.

Material	E MPa	c' kPa	v	Φ' / δ_i	Dry Density Kg/m ³	Ko	ψ
Casing, bar and grout section	34000	33150	0.33	1	2300	0.54	1
Bar and grout section	24000	46800	0.33	1	2300	0.54	1
Fill	10	1	0.35	30	2000	0.54	2
Silty Till	250	1	0.35	42	2000	0.54	6
Interface	250	1	0.35	42	2000	0.54	6
Casing Interface 0.1	10	1	0.35	30*	2000	0.54	2

* Refers to δ_i

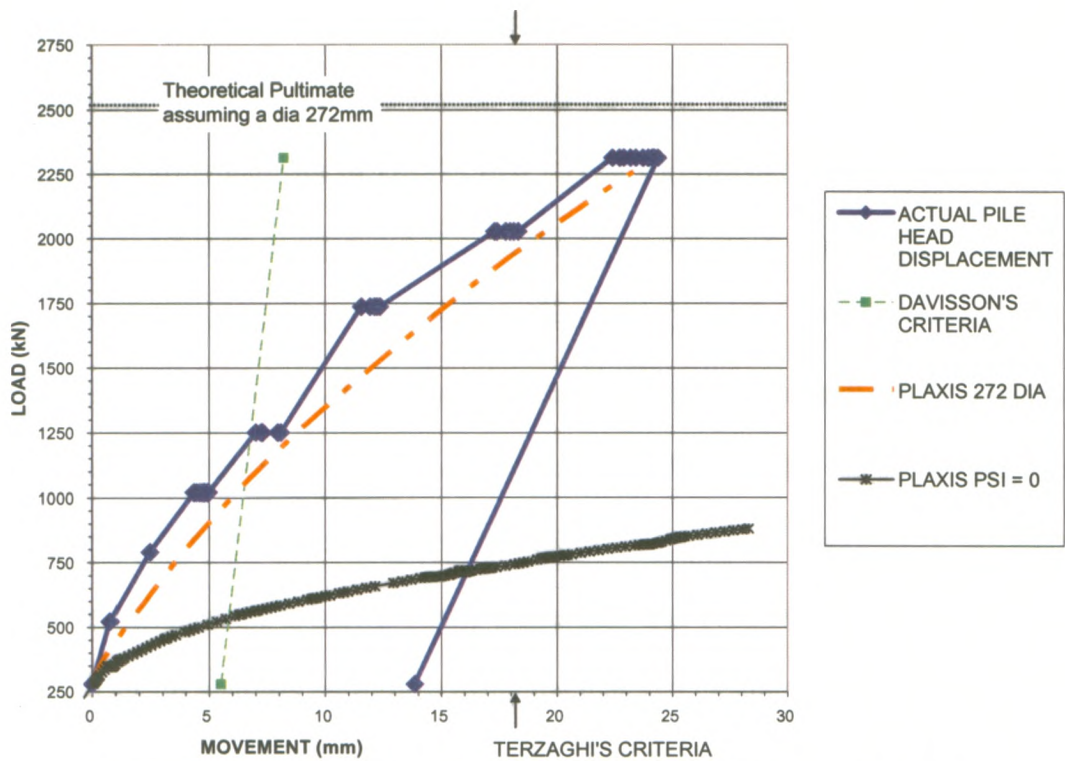


Figure 3.25 Load Displacement Behaviour for Kitchener-Micropile 7.

Table 3.6 Parameters used for Kitchener Micropile 7.

Material	E MPa	c' kPa	v	Φ'	Dry Density Kg/m ³	Ko	ψ
Casing, bar and grout section	34000	33150	0.33	0	2300	0.54	1
Bar and grout section	24250	23600	0.33	0	2300	0.54	1

3.5 Case 4 - Alliston, Ontario

Micropiles were installed at a site in Alliston, Ontario, to limit vibrations during the construction of an addition to an existing commercial building. At this site, one test micropile (Micropile 8) was installed. Micropile 8 was built using a hollow core Titan bar 53/73 and construction Method II. The resultant pile is classified as a Type A micropile according to the FHWA (2000) manual. The soil stratigraphy and micropile geometry are shown in Figure 3.26. The soil deposit in Case 4 comprised brown compact to very dense sand with SPT N-values that varied from 13 to 54 blows/300mm. The Titan 53/73 bar was installed from the ground surface to a depth of 10.6m. The

completed pile had an HSS 168×6 casing extending from the ground surface to a depth of 1.5m followed by an uncased section from 1.5 m to 10.6m. Micropile 8 was drilled using a bit with a diameter of D_o 175 mm. Type 10 Portland cement grout with a w/c =0.5 was used during drilling and also for the structural grout. The grout volumes used during construction were not recorded for this micropile.

Figure 3.27 shows the measured and calculated load-deflection response of Micropile 8. For this pile, an ultimate load of 1343 kN was achieved at a corresponding deflection of 30 mm. When the load was released, there was a permanent deformation of 20 mm and thus the apparent elastic movement was 10 mm. Figure 3.27 also shows the results of FE analysis performed using the material parameters summarized in Table 3.7. FE analyses were done assuming an enlarged diameter of 262 mm diameter, which is roughly 1.5 times larger than the drilled diameter (eg. $D'/D_o = 1.5$). This is consistent with the other micropile cases. In addition, analyses were performed neglecting dilatancy ($\psi=0^\circ$) and assuming $\psi=2^\circ$ and $\psi=3^\circ$. Finally, the theoretical capacity estimated from pile theory is 800 kN: 457kN from end bearing and 343 kN from skin friction.

From Figure 3.27, a consistent interpretation emerges from the micropile cases. Similar to the other pile load tests, the measured load-deflection response of Micropile 8 is closest to the FE analysis performed using some dilatancy for the pile-soil interface and the soil ($\psi=2^\circ$ and $\psi=3^\circ$). In addition, the ultimate capacity estimated from pile theory lies between the FE analysis performed assuming non-dilatant behaviour ($\psi=0^\circ$) and dilatant behaviour ($\psi \neq 0^\circ$). In this case, the theoretical capacity deduced from pile theory (800kN) is lower than can be justified from the pile load test. Using Davisson's

criteria, an ultimate load of 1000kN can be interpreted from the measured load-displacement response whereas Terzaghi's criterion gives 1200kN.

ALLISTON, ONTARIO MICROPILE

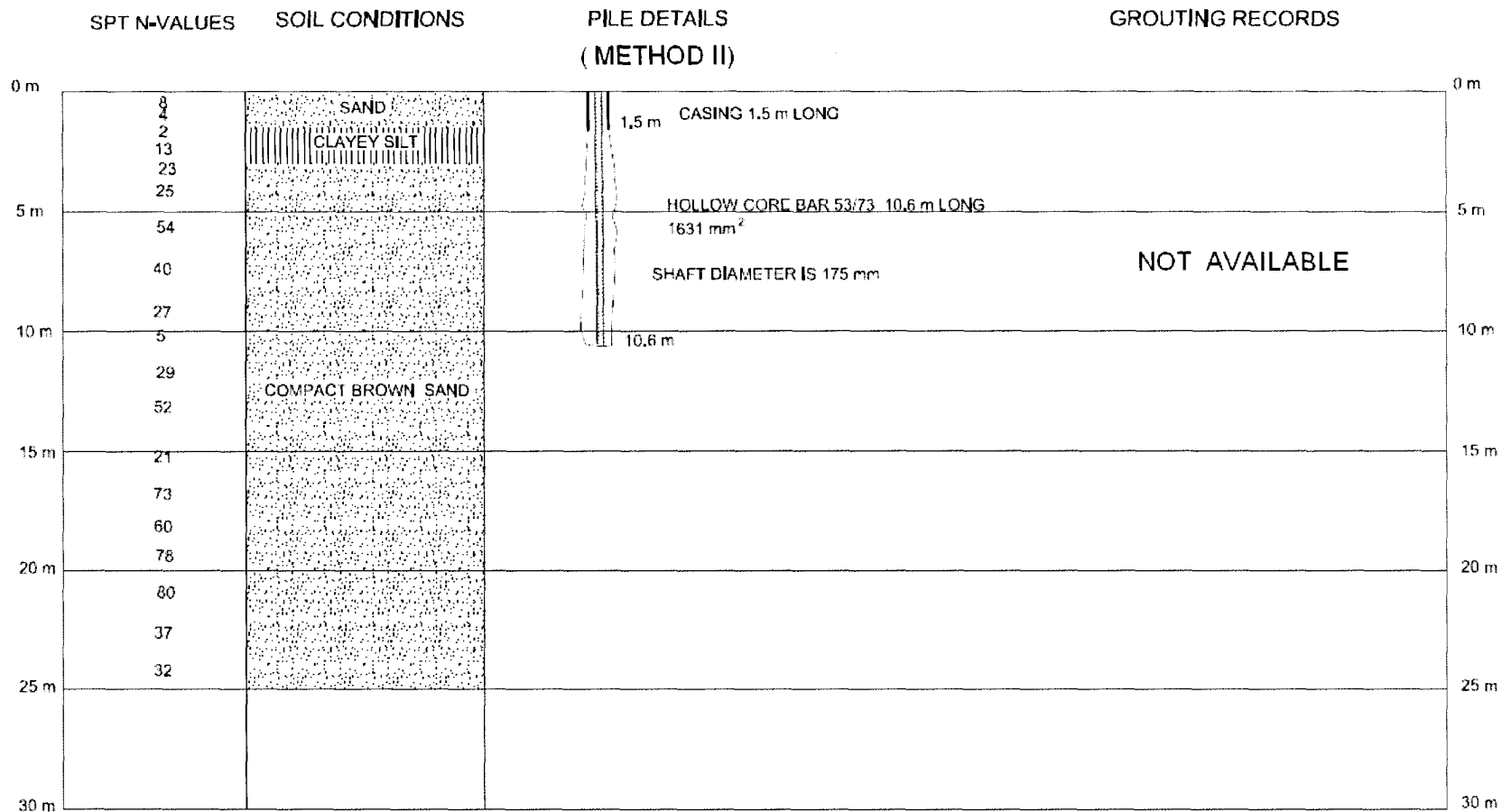


Figure 3.26 Installation Details for The Alliston Case.

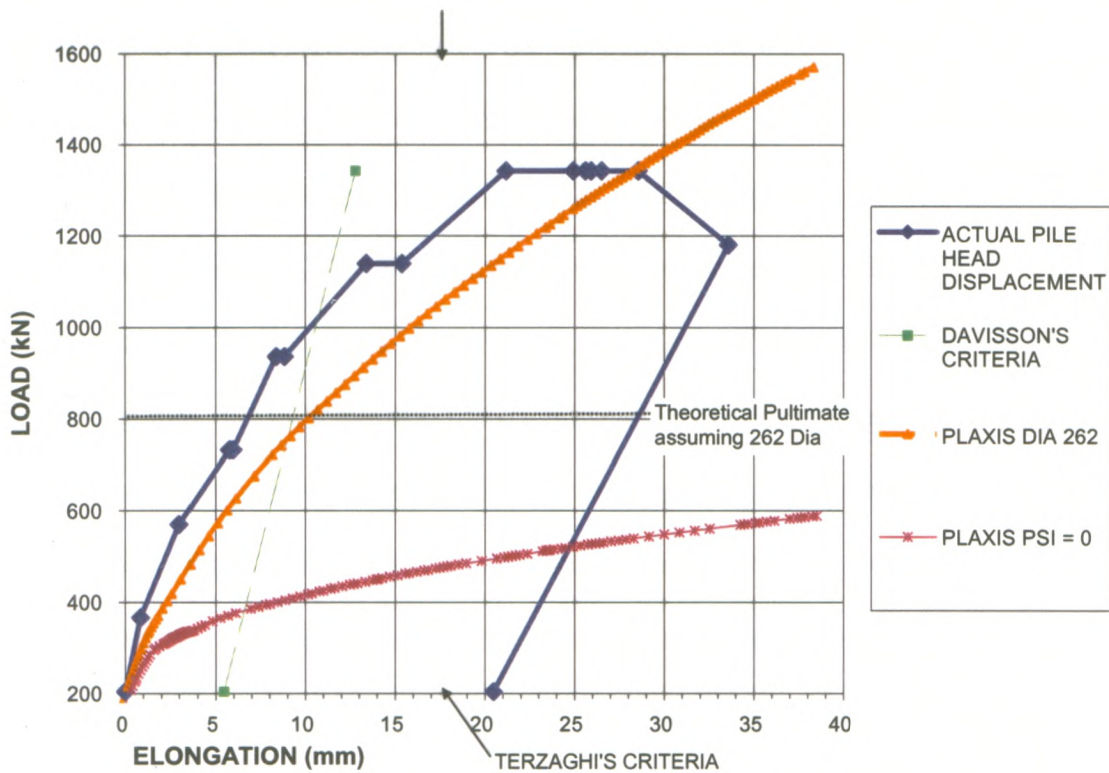


Figure 3.27 Load Displacement Behaviour for Alliston Micropile.

Table 3.7 Parameters used for Alliston Case.

Material	E MPa	c' kPa	v	Φ' / δ_i	Dry Density Kg/m ³	Ko	Ψ
Casing, bar and Grout	31650	30860	0.33	0	2300	0.54	0
Sand	80	1	0.35	41	2000	0.54	3
Fill and Clay silt	10	10	0.35	30	2000	0.54	2
Bar and Grout	21000	20500	0.33	0	2300	0.54	0
Sand Interface	80	1	0.35	41	2000	0.54	3
Fill and Clay Silt Interface	10	10	0.35	30*	2000	0.54	2

* Refers to δ_i

3.6 Case 5 - Pembroke, Ontario

Micropile 9

The last case considered involved the construction of micropiles in Pembroke, Ontario. In this case, micropiles were constructed to support an addition to an existing building due to the presence of boulders in the foundation soil (glacial till), which made

it impractical to install drilled shaft foundations. High capacity micropiles were required in this case to support high tension and compression loads.

Micropile 9 consisted of a 16.5 m long injection bored hollow core Titan bar with a drilling bit diameter of 178mm (D_o). The stratigraphy and pile geometry are summarized in Figure 3.28. This micropile was constructed according to Method II and can be classified as a Type A micropile according to the FHWA (2000) manual. The soil stratigraphy at the Pembroke site comprised 1m of fill underlain by about 2.5m of silty fine sand. A very dense sandy till with boulders was encountered below the upper silty fine sand deposit from 4m to 19.5m depth. The SPT N-values were on average 50 blows/300mm in the upper 5 m of the foundation soil and over 70blows/300mm at depth. During drilling, large boulders were encountered at a depth of 6.2m and 7.8m. The completed micropile comprised an HSS 168x6 casing from the ground surface to a depth of 2.7m followed by an uncased grouted length from 2.7m to 16.5m. A Contractometer was installed in this micropile.

Figure 3.29 shows the load deflection response of Micropile 9, the pile compression versus pile load measured (using the Contractometer), and the results of FE analysis. Referring to Figure 3.29, Micropile 9 was tested to a maximum load of 2609 kN. At an axial load of 2609kN, the measured pile head deflection was 15 mm while the pile compression (Contractometer) was only 11 mm. Thus, only 4mm of pile head deflection can be attributed to deformations of the foundation soil.

Notwithstanding the influence of boulders encountered during the construction of Micropile 9, Figure 3.29 also shows the calculated response of Micropile 9 obtained from FE analysis assuming $\psi=3^\circ$. The FE analysis was undertaken using the material parameters listed in Table 3.8 and assuming an enlarged diameter (D') of 310mm (or

1.74 times the drill bit diameter). The pile diameter enlargement in this case is comparable to that observed in Case1 through 4 inclusive (see Table 3.9). From pile theory, the estimated capacity of Micropile 9 is 8866kN: 7472kN from end bearing and 1393kN from skin friction. Thus, the loads applied to Micropile 9 were well below the geotechnical capacity in this case.

Figure 3.30 shows the pile strain versus depth during loading. From Figure 3.30, it can be seen that the pile strains dissipate rapidly from 4m depth to 8.5m depth. As noted above, large boulders were encountered at a depth of 6.2m and 7.8m. Below 8.5m, there is virtually no strain in the micropile suggesting that 100% of the load had been transferred to the foundation soils by about 8.5m depth. Thus, the boulders appear to have had a significant impact on the response of Micropile 9.

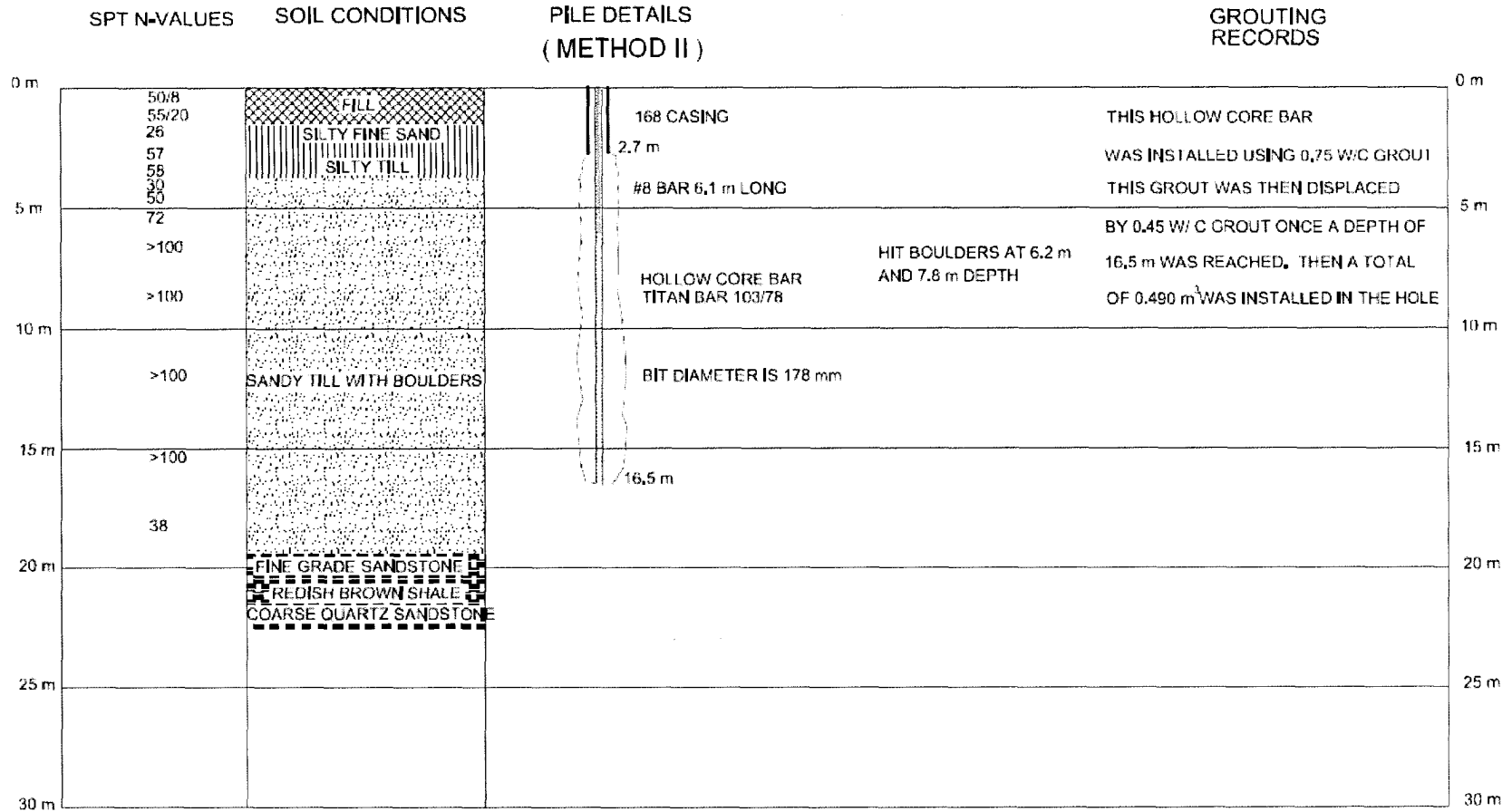
On further examination of Figure 3.30, it can be seen that the strain in Micropile 9 exceeded the yield strain of the grout at a load of 2600kN and a depth of 4m, which is slightly below where the casing terminates. Similar to that seen in the Nipigon case, it appears that yielding occurs in some of the piles examined just below the casing.

Table 3.8 Parameters used for Pembroke.

Material	E MPa	c' kPa	v	Φ'/δ_i	Dry Density Kg/m ³	Ko	ψ
Casing, bar and grout section	43000	42000	0.33	0	2300	0.54	1
Bar and grout section	26100	25500	0.33	0	2300	0.54	1
Fill and Silty Till	100	1	0.35	35	2000	0.54	2
Sandy Till with Boulders	300	1	0.35	45	2000	0.54	3
Interface	300	1	0.35	45*	2000	0.54	3

* Refers to δ_i

PEMBROKE MICROPILE



80

Figure 3.28 Installation Details for Pembroke-Micropile 9.

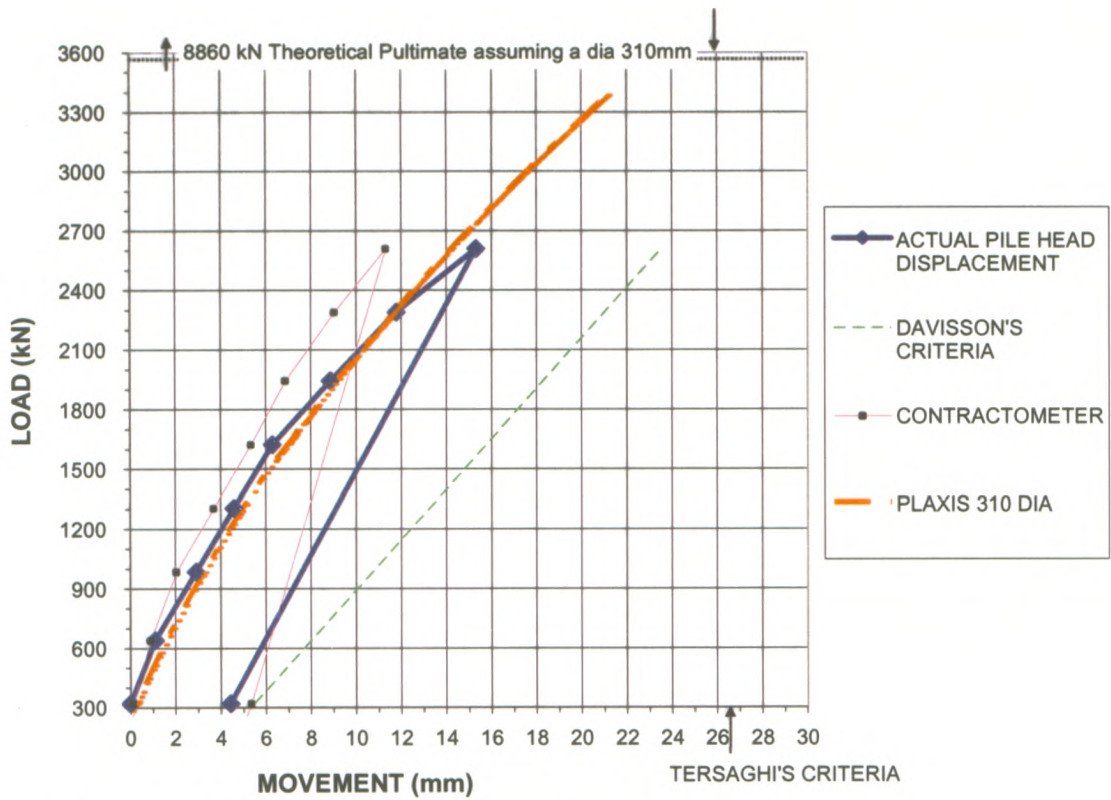


Figure 3.29 Load Displacement Behaviour For Pembroke-Micropile 9.

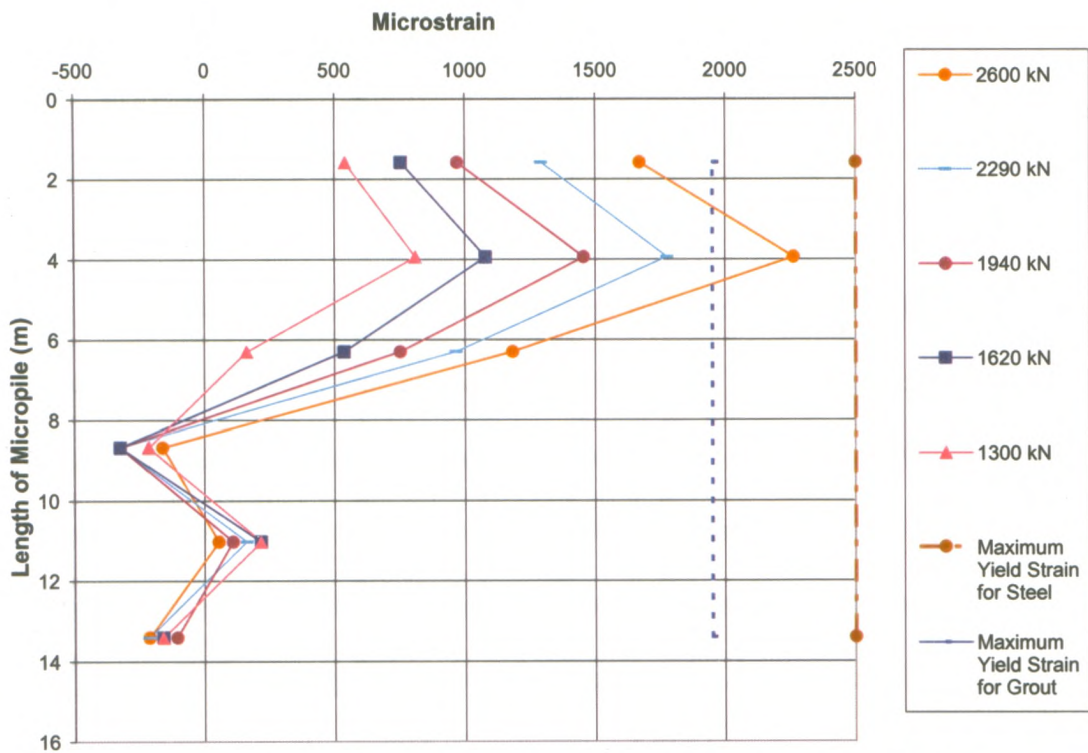


Figure 3.30 Strain vs. Depth Graph for Pembroke-Micropile 9.

Table 3.9 Calculated Theoretical Micropile Capacities

Micropile # and Case Name	Soil Description	bar length (m)	casing length (m)	Pile Dia (m)	L/D ratio	Installation	Phi' from PLAXIS	Max. Load (kN)	Theoretical End Bearing (kN)	Theoretical Friction (kN)	Total Theoretical Capacity (kN)
Micropile 1, Nipigon	Silty Sand N values varying from 25 to 86.	24.4	9.9	0.38	64	Type A	38	1832	2486	1252	3738
Micropile 2, Nipigon	Silty Sand N values varying from 25 to 86.	27.5	12.5	0.5	55	Type D	38	3063	707	1988	2695
Micropile 3, Nipigon	Sand and Cobbles with varying N values from 16 to 58.	16.3	7	0.45	36	Type D	38	3003	2074	646	2720
Micropile 4, Point Edward	Fill from 0 to 1.5m. Silty sand varying from 2 to 34 N.	12.2	1.5	0.189	65	Hollow core bar	36	335	205	171	376
Micropile 5, Point Edward	Fill from 0 to 1.5m. Silty sand varying from 2 to 34 N.	13.72	1.5	0.25	55	Hollow core bar	36	497	404	287	691
Micropile 6, Kitchener	Boreholes varied. Some have fill, some have sand, some have clayey silt varying N values from 18 to > 100.	8.7	2.7	0.172	51	Hollow core bar	42	687	566	180	746
Micropile 7, Kitchener	Boreholes varied. Some have fill, some have sand, some have clayey silt varying N values from 18 to > 100.	12.2	2.14	0.272	45	Hollow core bar	42	2314	1985	599	2584
Micropile 8, Alliston	2.6 m of fill. Below Sand 13 to 54 N values.	10.6	1.5	0.262	40	Type A	35	1143	457	343	800
Micropile 9, Pembroke	Sandy Till with Boulders	16.5	2.7	0.31	53	Type A	45	2609	7472	1393	8866

3.7 Conclusions

This Chapter described 5 cases involving the construction and load testing of 9 test micropiles in pervious granular soils. The measured load-displacement response of each micropile has been presented and compared with calculated behaviour from FE analysis. In some cases, strains in the micropile were also measured. From the results and discussions presented above the following conclusions can be drawn:

- (i) All of the micropiles examined exhibited behaviour that could be explained if an enlarged diameter (larger than the drill bit) was used to analyze the pile response. In some cases, the enlarged diameter could be estimated from the

quantity of grout used to build the pile; whereas, in other cases the enlarged diameter was deduced from FE analysis. Regardless, from Table 3.9, the enlarged diameter was found to vary between 1.4 and 1.8 times that of the drill bit predominantly. From this assessment, it appears the quantity of grout should be carefully recorded during construction of micropiles to evaluate the as-built or bored diameter of micropiles.

- (ii) Each pile exhibited post yield stiffness that could only be interpreted by assuming some pile-soil-interface dilatancy in the FE analyses. As a result, it is concluded that some of the axial response of the micropiles examined in this Chapter came from dilatancy in the soil and on the pile-soil interface.
- (iii) The axial capacity calculated for each micropile from pile theory was found to lie between that estimated from FE analysis for the non-dilatant case ($\psi=0^\circ$) and the dilatant case ($2^\circ \leq \psi \leq 6^\circ$). As a result, it is concluded that some of the pile capacity *in situ* can be attributed to dilatant effects.
- (iv) For cases where a Contractometer was installed in the pile, the Contractometer measurements indicated constant strains along the casing length suggesting insignificant load transfer to the surrounding soil around the casing.
- (v) In Micropiles 3 and 9 there was evidence of structural yielding just below the casing (measured) suggesting a possible weak point in these piles.

CHAPTER 4

**CASE STUDIES
OF
ROCK
MICROPILES**

4.0 Case Studies of Micropiles Tested in Rock

This Chapter presents the response and evaluation of 7 full-scale micropiles socketed into rock and then load tested. Most of the micropiles described below were socketed into the Georgian Bay and Queenstone Shale formations which are the predominant rock formations in the Greater Toronto Area (Ontario, Canada). One micropile was socketed into granitic rock in Northern Ontario. Four of the micropiles were instrumented with a Contractometer to measure internal compression of the pile during loading.

The primary objective of this Chapter is to evaluate the distribution of load in micropiles socketed into rock using elastic solutions for rock sockets published by Pells and Turner (1979). Since only one of the test micropiles was tested to failure, the secondary objective of this Chapter is to estimate the minimum pile-to-rock bond developed in each case. For each case, the soil stratigraphy, micropile geometry, installation details and load-deflection response is presented. For the four test piles that were instrumented with a Contractometer, the variation of strain in the micropile with depth is presented and assessed using elastic theory.

4.1.1 Methodology

Problem Geometry

The geometry of a micropile socketed into rock is as shown in Figure 4.1. Typically these micropiles consist of a casing that is installed in a bored hole through the overburden soil and seated into the rock. The bored diameter in the overburden is often slightly larger than the bored diameter in the rock socket. In some cases, a central steel bar is installed the whole length of the micropile. However, the central steel bar can also be installed at the bottom of the pile having sufficient overlap with the casing (typically at least 3 to 4 metres) to develop the bond capacity between the bar and the grout. The

bored shaft is then filled with tremied grout. Hence, the cross-section of the micropiles presented in this Chapter tends to vary along the length of the micropile.

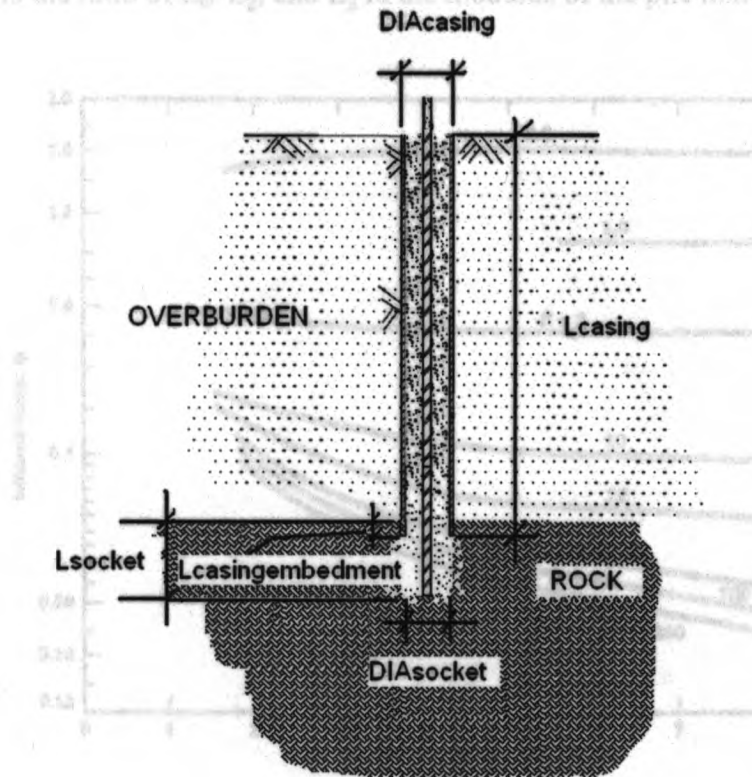


Figure 4.1 Elastic Settlement Influence Factors (after Polls and Turner)
Figure 4.1 General Geometry of Rock Micropiles.

Above the rock socket, the load-displacement response is also assessed assuming the

File Load Tests

micropile behaves as a free column (e.g. $\Delta = PL/AE$) using:

For each case presented below, pile load tests were conducted according to the

$$\Delta = cL_{ovb} = PL_{ovb} / (A_s E_s + A_g E_g) \quad [4.2]$$

performance test procedures described in the Post-Tensioning Institute Manual (PTI where P is the constant load in the pile (assumed), L_{ovb} is the length of the pile above the rock socket, A_s is the area of the steel in the overburden, E_s is the elastic modulus of

found in Chapter 3 and are not repeated here. steel (200,000MPa), A_g is the area of grout inside of casing, E_g is the elastic modulus of

grout. Although in Chapter 2 testing showed that E_g is approximately 16GPa, in the

First, each pile load test is evaluated using equation 4.1 for a rock socket:

rock micropile cases, a higher value E_g 30GPa was used to account for the confinement

$$\Delta = Q I_p / B E_d \quad [4.1]$$

of the grout inside the steel casing. Equations 4.1 and 4.2 are superimposed to obtain

where Q is the pile head load, I_p is the influence factor from Figure 4.2, B is the diameter of the socket, E_d is the deformation modulus of the rock mass surrounding the pile shaft, R in Figure 4.2 is the ratio of E_d/E_g , and E_g is the modulus of the pile material (grout).

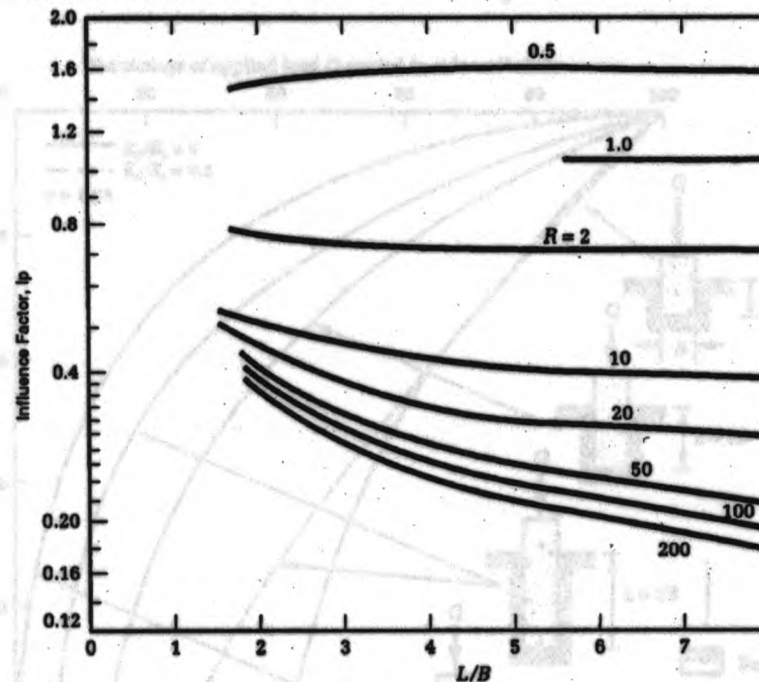


Figure 4.2 Elastic Settlement Influence Factors (after Pells and Turner)

Above the rock socket, the load-displacement response is also assessed assuming the micropile behaves as a free column (e.g. $\Delta = PL/AE$) using:

$$\Delta = \epsilon L_{ovb} = PL_{ovb} / (A_g E_g + A_s E_s) \quad [4.2]$$

where P is the constant load in the pile (assumed), L_{ovb} is the length of the pile above the rock socket, A_s is the area of the steel in the overburden, E_s is the elastic modulus of steel (200,000MPa), A_g is the area of grout inside of casing E_g is the elastic modulus of grout. Although in Chapter 2 testing showed that E_g is approximately 16GPa, in the rock micropile cases, a higher value E_g 30GPa was used to account for the confinement of the grout inside the steel casing. Equations 4.1 and 4.2 are superimposed to obtain

theoretical load versus displacement for the piles described below. Finally, the distribution of strain in the pile versus depth below the rock level is compared with elastic solutions for rock sockets (Pells and Turner 1995) assuming $E_d/E_g=1$ (see Figure 4.3), where E_d is the elastic modulus of the rock and E_g is the elastic modulus of grout.

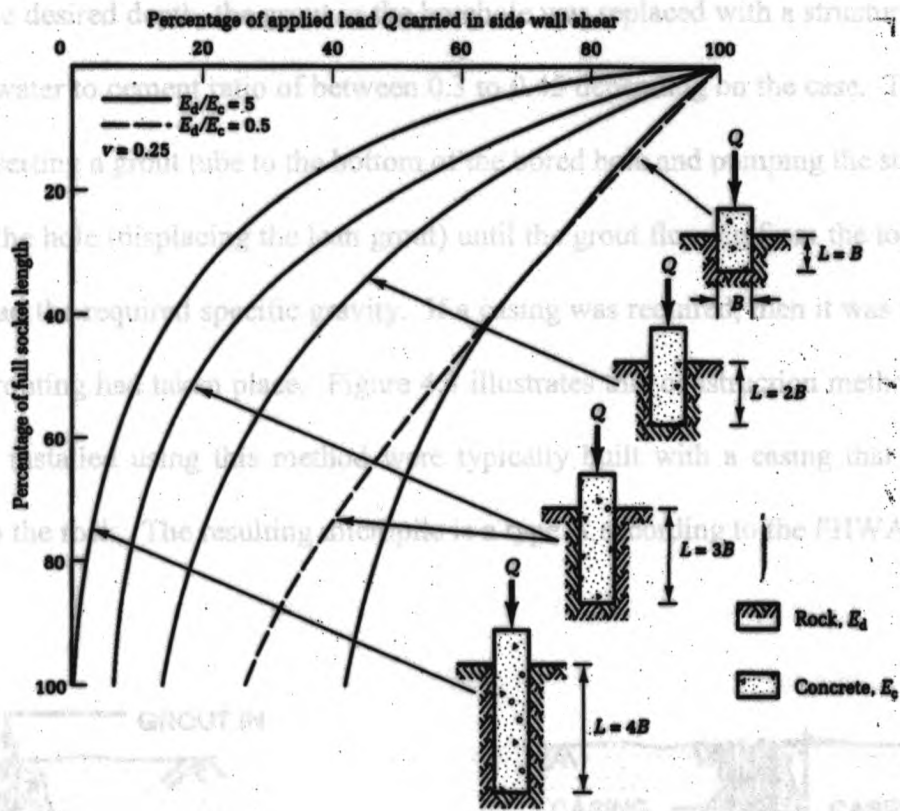


Figure 4.3 Distribution of Side wall Shear (Pells and Turner 1995)

Note $E_c = E_g$

4.1.2 Rock Micropile Installation Methods

Two different installation methods were used to construct the micropiles presented in this Chapter as described in the following sections.

Injection-bored, hollow-bar

The first installation method is referred to as the injection-bored, hollow-bar method as described in Chapter 3. For this method, a hollow threaded steel bar with a

disposable bit at the tip was advanced through the overburden by rotation and percussive drilling. The drilling fluid comprised a high water to cement ratio, w/c, grout (typically w/c=0.6) that was injected through the hollow bar, jetted out the bit and flushed to the ground surface. The grout was continuously circulated during the drilling. After reaching the desired depth, the grout in the borehole was replaced with a structural grout that had a water to cement ratio of between 0.3 to 0.45 depending on the case. This was done by inserting a grout tube to the bottom of the bored hole and pumping the structural grout into the hole (displacing the lean grout) until the grout flowing from the top of the borehole had the required specific gravity. If a casing was required, then it was inserted after the grouting had taken place. Figure 4.4 illustrates this construction method. The micropiles installed using this method were typically built with a casing that did not extend into the rock. The resulting micropile is a type A according to the FHWA (2000) manual.

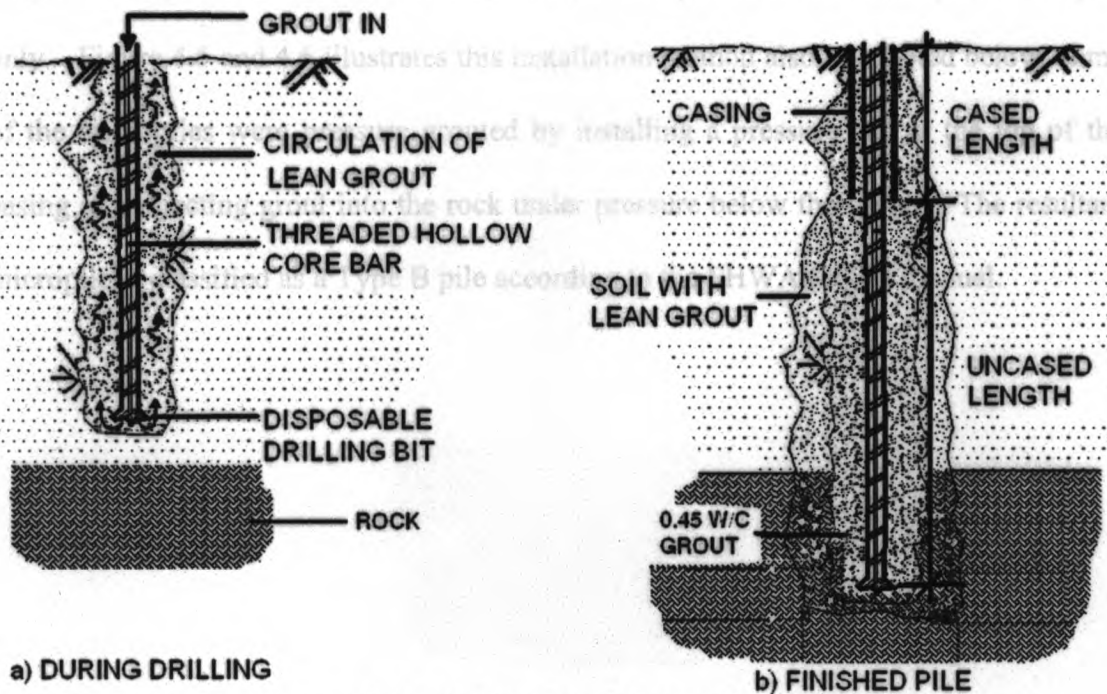


Figure 4.4 Injection Bored Hollow Core Bar.

Rotary Duplex Drilling

The second installation method (and most common) was used for piles where the casing extended through the overburden and into the rock (typically about 300 mm into the rock). With this method, a borehole was advanced through the overburden and 300m into rock using a rotary duplex drill rig equipped with a retractable drilling bit and a down the hole hammer. The retractable bit was used to under ream the casing drilling a slightly larger hole than the casing. The casing was advanced behind the bit using rotary action. Water was used as a flushing medium for the cuttings.

After advancing the casing into the rock (typically 300mm), a smaller drill bit was used to drill into rock to the required rock socket depth. After retracting the smaller bit, a threaded solid bar was inserted into the pile and centered and the shaft was filled with tremied grout. As noted below, in some cases, the solid bar extended the entire length of the pile whereas in other cases the bar was placed in the lower part of the pile only. Figure 4.5 and 4.6 illustrates this installation method also. As noted below, some of the micropiles were pressure grouted by installing a pressure cap at the top of the casing and injecting grout into the rock under pressure below the casing. The resultant micropile is classified as a Type B pile according to the FHWA (2000) manual.

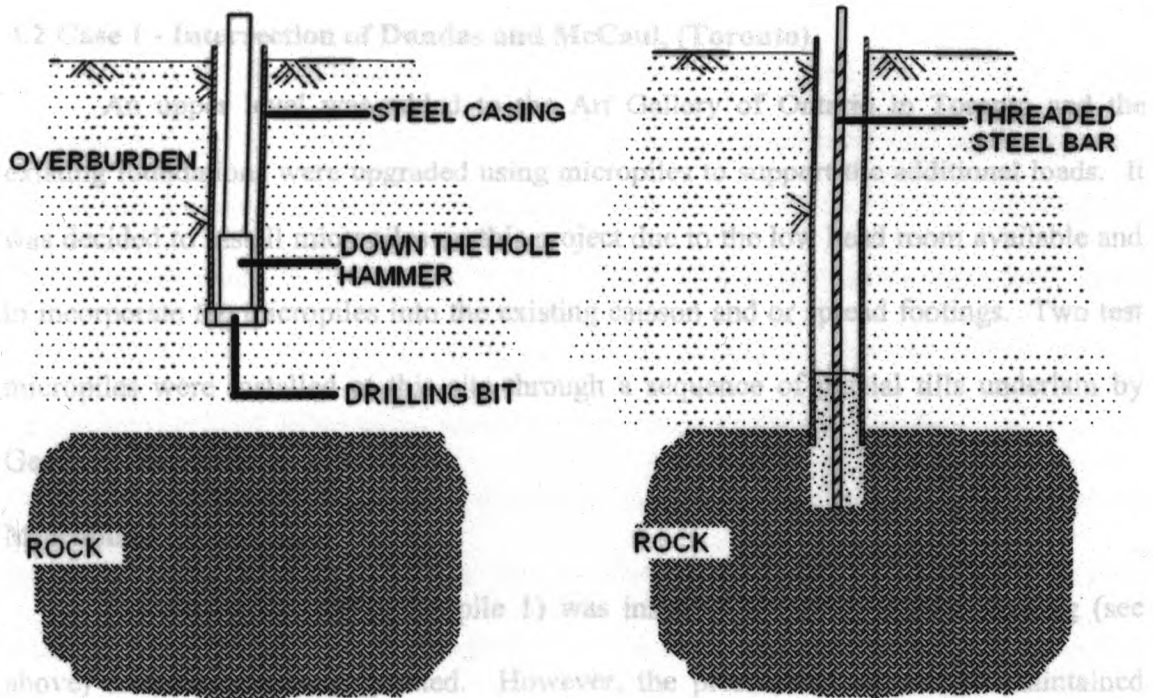


Figure 4.5 Installation of a Rotary Duplex Micropile in Rock.

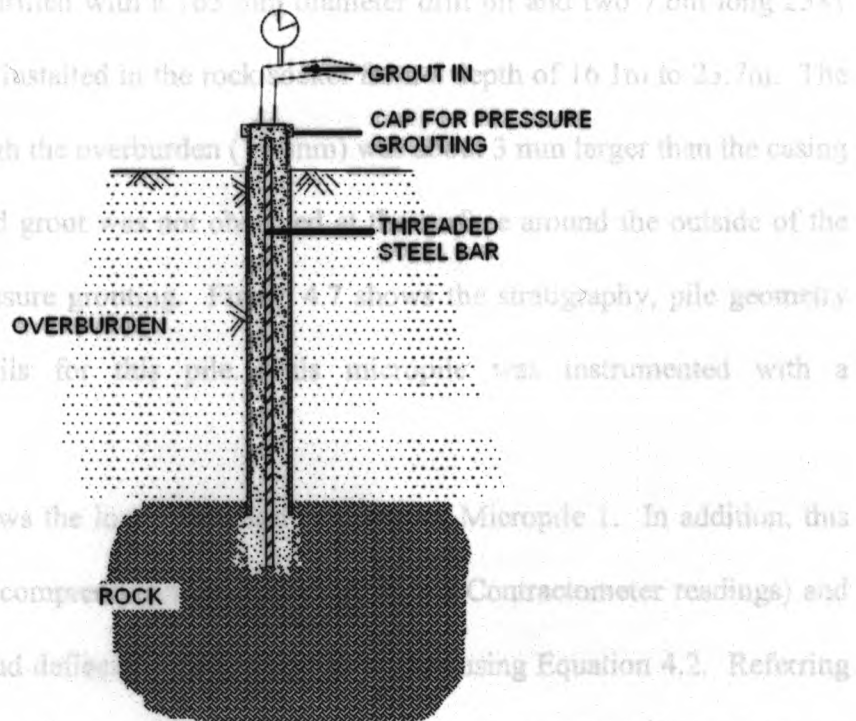


Figure 4.6 Installation of Micropile in Rock - Pressure Grouting.

4.2 Case 1 - Intersection of Dundas and McCaul, (Toronto)

An upper level was added to the Art Gallery of Ontario in Toronto and the existing foundations were upgraded using micropiles to support the additional loads. It was decided to install micropiles on this project due to the low head room available and to incorporate the micropiles into the existing caisson and or spread footings. Two test micropiles were installed at this site through a sequence of glacial tills underlain by Georgian Bay shale.

Micropile 1

The first micropile (Micropile 1) was installed by rotary duplex drilling (see above) and then pressure grouted. However, the pressure could not be maintained during grouting due to cross communication with a nearby borehole. Micropile 1 consisted of a 23.7 m long, HSS 193×11 casing embedded 600 mm into the bedrock. The rock socket was drilled with a 165 mm diameter drill bit and two 7.6m long 2581 mm² (each) bars were installed in the rock socket from a depth of 16.1m to 23.7m. The drilled diameter through the overburden (196mm) was about 3 mm larger than the casing diameter (193mm) and grout was not observed at the surface around the outside of the casing during the pressure grouting. Figure 4.7 shows the stratigraphy, pile geometry and installation details for this pile. This micropile was instrumented with a Contractometer.

Figure 4.8 shows the load-deflection response of Micropile 1. In addition, this figure shows the pile compression versus load (from the Contractometer readings) and the theoretical pile head deflection versus load estimated using Equation 4.2. Referring to Figure 4.7, the load-deflection response of Micropile 1 was essentially linear up to the maximum applied load (4000kN). This response was more stiff from no load up to 1300

kN most likely due from end bearing contribution from the pile cap. During the test, the pile compression (Contractometer) versus load was stiffer than the overall pile head response and slightly lower than the theoretical compression estimated using Equation 4.2. It appears that the difference between the pile compression and pile head deflection is due to deformation in the pile socket. Given the nearly linear behaviour, these deformations appear to be elastic in nature notwithstanding that there was about 5mm of permanent pile head deformation recorded after removing the axial loads.

Table 4.1 shows the strains calculated from the Contractometer readings along the casing length and the theoretical strains. The axial strain in the pile above the rock socket is generally close to that deduced from linear elastic theory for an unsupported column ($\epsilon = P/AE$). Figure 4.8 shows the pile strain versus depth during loading. In addition, the strain in the pile drops abruptly to zero at about the rock level. This is consistent with the socket behavior shown in Figure 4.2. At the tip of the pile, however, the strains increase abruptly and at an axial load of 3465kN, the strain exceeds the yield strain of both steel and grout. Such behaviour suggests that the tip of the pile has yielded at high loads, which considering the zero strain above only be possible if there is negligible end bearing at the tip of the pile due to either debris in the borehole after drilling or loss of grout at the tip into the rock formation (e.g. a defect at the tip).

Table 4.1 Theoretical and Measured Strains along the casing for Micropile 1

Load	Measured Strain* ($\mu\epsilon$)	Theoretical Strain** ($\mu\epsilon$)
1724	630	760
2608	950	1200
2980	1100	1370
3465	1260	1600

* Deduced from Contractometer measurements

** From Equation 4.2

ART GALLERY OF ONTARIO IN TORONTO

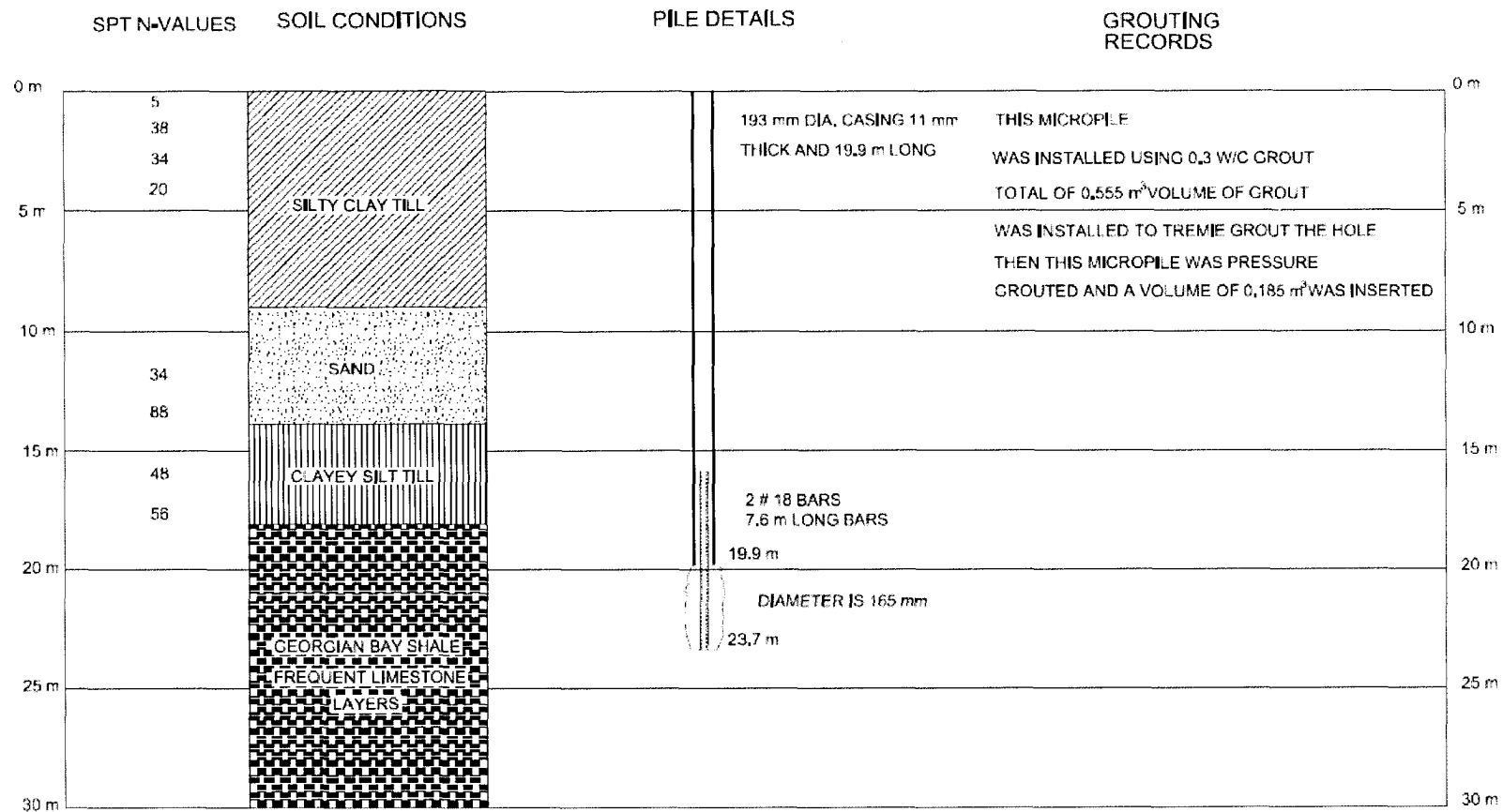


Figure 4.7 Installation Details for AGO-Micropile 1.

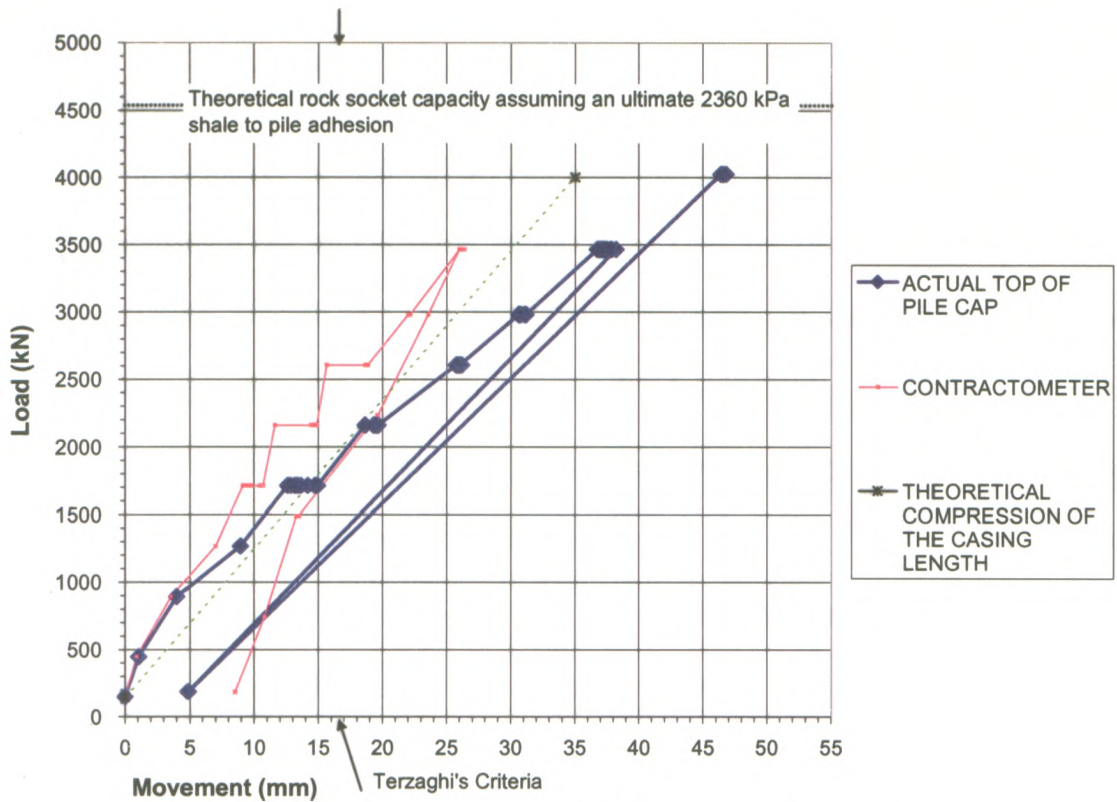


Figure 4.8 Load Displacement for AGO-Micropile 1.

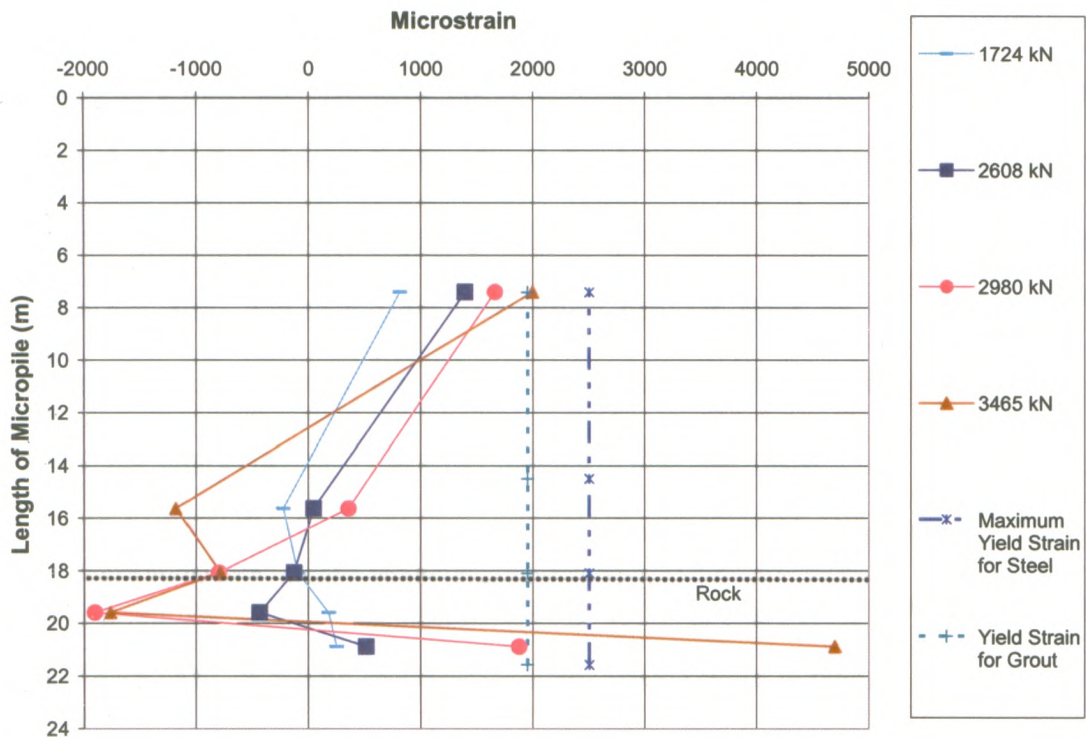


Figure 4.9 Strain vs. Depth Graph for AGO-Micropile 1.

Micropile 2

The second micropile tested at this site (Micropile 2) consisted of a 19.5 m long HSS 273×13 casing embedded 600 mm into the rock (see Figure 4.9). The rock socket was drilled using a 241 mm diameter bit and three 2581 mm² bars were installed in the rock socket from a depth of 14.9m to 23.7m. This micropile was tremie grouted and then pressure grouted. The casing was observed to heave upward by 250 mm when the grout pressure was applied suggesting low rock permeability. To complete the construction, the casing was pushed back into place.

Micropile 2 was tested to 7000 kN. The load displacement graph is shown in Figure 4.10, which also shows the pile compression versus load and the theoretical pile head compression estimated using Equation 2. Referring to Figure 4.10, the measured pile head deflection was essentially linear up to the maximum load of 7000kN. Although the pile compression versus load is slightly non-linear, there is generally good agreement between the measured pile compression and the theoretical pile compression estimated using Equations 4.1 and 4.2. At the maximum axial load of 7000kN, the pile head displacement was 54 mm whereas the measured pile compression was only 36mm (Contractometer). Given the good agreement between Equation 4.1 and 4.2 and the measured pile compression, the difference between the pile head displacement and the pile compression is indicative of deformations in the rock socket.

Table 4.2 illustrates the comparison between the calculated strains along the casing of the micropile from the Contractometer readings as well as the theoretical strains $\epsilon = P/AE$. It can be seen that the compressive strain in the pile above the rock is lower than that deduced from the theoretical equation. The pile strain versus depth is plotted in Figure 4.12. In the bedrock, the socket strains quickly reduce to zero in

accordance with Figure 4.3. However, at the tip of the micropile, the strain is high and it exceeds the yield strain of the grout and steel used to construct the rock socket. Although this behaviour could be due to instrument error, it is believed that this indicates the absence of end-bearing at the tip of the pile due to either debris in the bottom of the borehole or grout loss (into joints in the rock) at the tip. (Note there is zero strain in the socket above the tip).

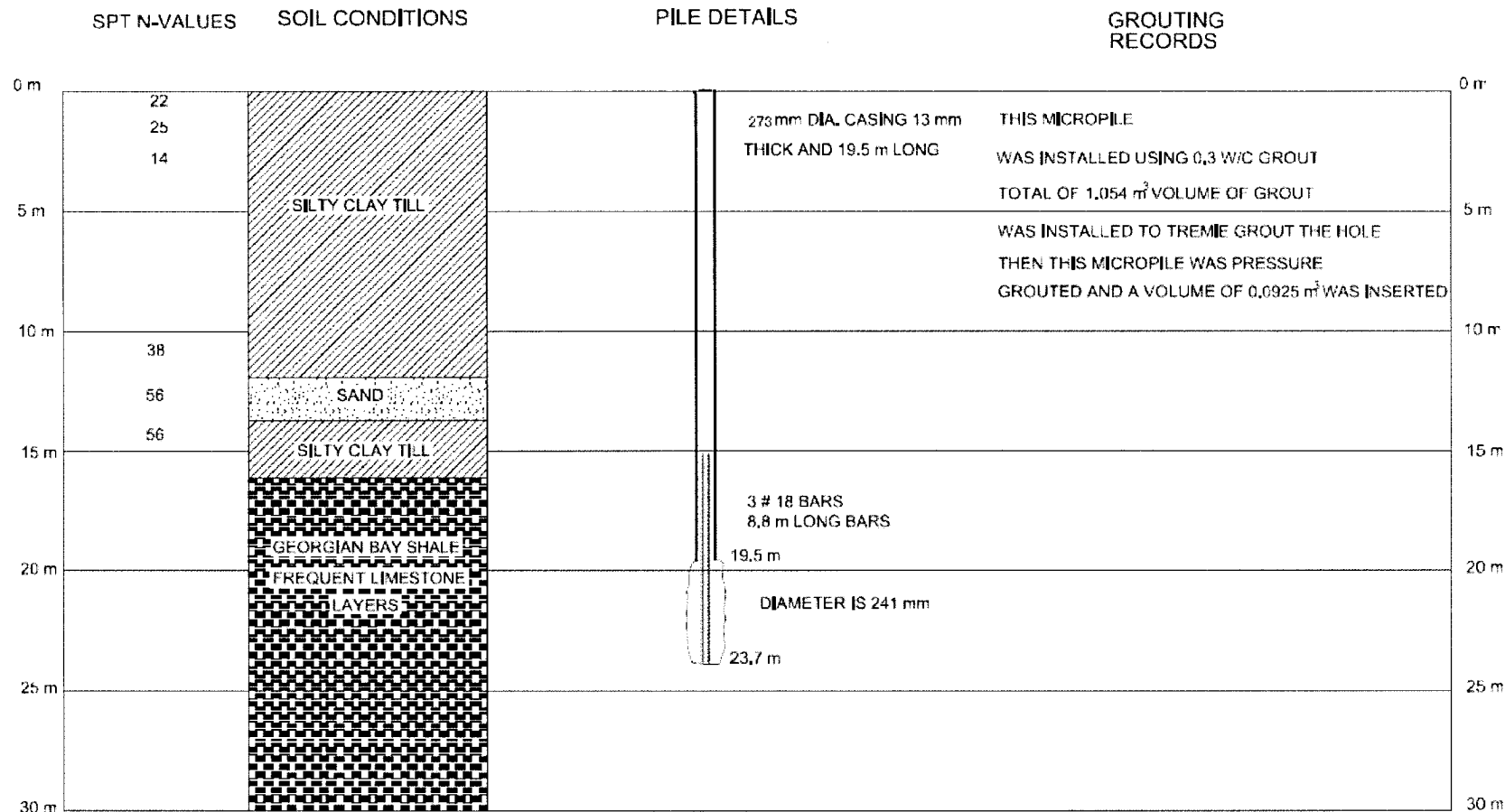
Table 4.2 Theoretical and Measured Strains along the casing for Micropile 2

Load	Measured Strain* ($\mu\epsilon$)	Theoretical Strain** ($\mu\epsilon$)
1490	-	300
2235	-	475
2980	180	665
4470	400	1050
7000	810	1700

* Deduced from Contractometer measurements

** From Equation 4.2

ART GALLERY OF ONTARIO IN TORONTO



98

Figure 4.10 Installation Details for AGO- Micropile 2.

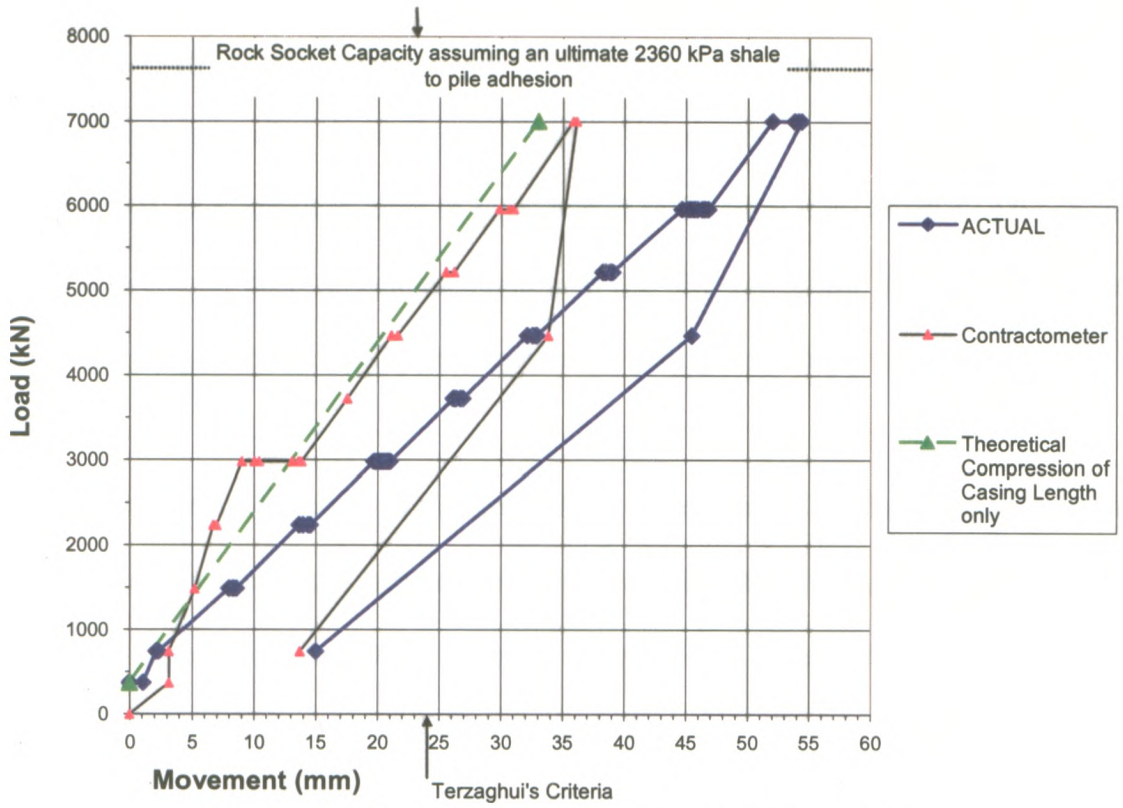


Figure 4.11 Load Displacement for AGO-Micropile 2.

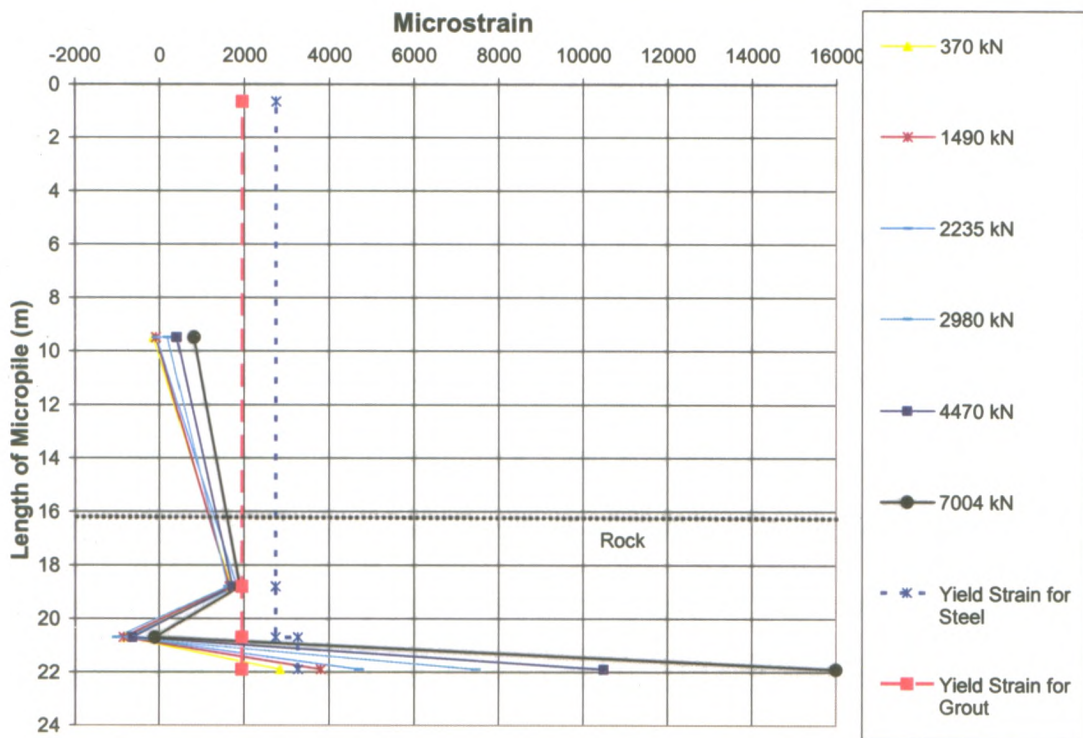


Figure 4.12 Strain vs. Depth for AGO-Micropile 2.

4.3 Case 2 - Micropile in Metamorphic Rock in Thunder Bay, Ontario

The second case involved installation of micropiles through very soft clay and socketed into Metamorphic Rock at a paper mill in Thunder Bay, Ontario. Micropiles were the preferred deep foundation solution at this site due to low overhead clearance. One test micropile (Micropile 3) was constructed and tested at this site.

Micropile 3

This test micropile was constructed by rotary duplex drilling method, tremie grouted and then pressure grouted only in one stage to give a Type B micropile according to the FHWA (2000) manual. Micropile 3 consisted of a 36.3 m long HSS189×11.5 casing socketed 300mm into the rock. The borehole through the overburden was drilled with a diameter (192mm) slightly larger than the casing. The rock socket was drilled 4.5 m deep into the rock below the end of the casing using a 143mm diameter drill bit. A concentric (3168 mm²) steel bar was installed in the pile extending from a depth of 32.3m to 40.8m. After installation of the pile, the casing was capped at the surface and grout was injected under pressure through the casing. The total volume of grout used for tremie grouting the pile was approximately 1.57m³ and 0.948m³ of grout was injected presumably into the bedrock during the pressure grouting.

Figure 4.14 shows the measured load-displacement response of Micropile 3, and the measured and theoretical (Equations 4.1 and 4.2) pile compression versus load. The micropile was test loaded to a maximum load of 2900 kN. At an axial load of 2900kN, the measured pile head deflection was 60 mm while the measured pile compression (Contractometer) was 53 mm. Referring to Figure 4.14, it can be seen that the load-displacement response and the theoretical and measured pile compression versus load

are all very close. The response reported in Figure 4.15 suggests that the pile behaved as a free column in the overburden and that deformations in the rock socket were negligible.

Figure 4.15 shows the measured strain in Micropile 3 versus depth. This figure shows that the response of Micropile 3 was very close to the ideal response. In the overburden, the strain in the pile is equal to the theoretical elastic strain $\epsilon = P/AE$. This is also noted in Table 4.3 where the theoretical as well as the calculated strains from the Contractometer are shown. At about the rock level, the strains in the micropile abruptly drop to zero in accordance with the classic socket behaviour reported in Figure 4.2. However, unlike the sockets in softer rock (see Case 1), there is no evidence of yielding at the tip of Micropile 3, which indicates better socket performance in this case.

Table 4.3 Theoretical and Measured Strains along the casing for Micropile 3

Load	Measured Strain* ($\mu\epsilon$)	Theoretical Strain** ($\mu\epsilon$)
1096	320	409
1811	680	820
2530	1300	1230
2906	1630	1450

* Deduced from Contractometer measurements

** From Equation 4.2

BOWATER IN THUNDERBAY, ONTARIO

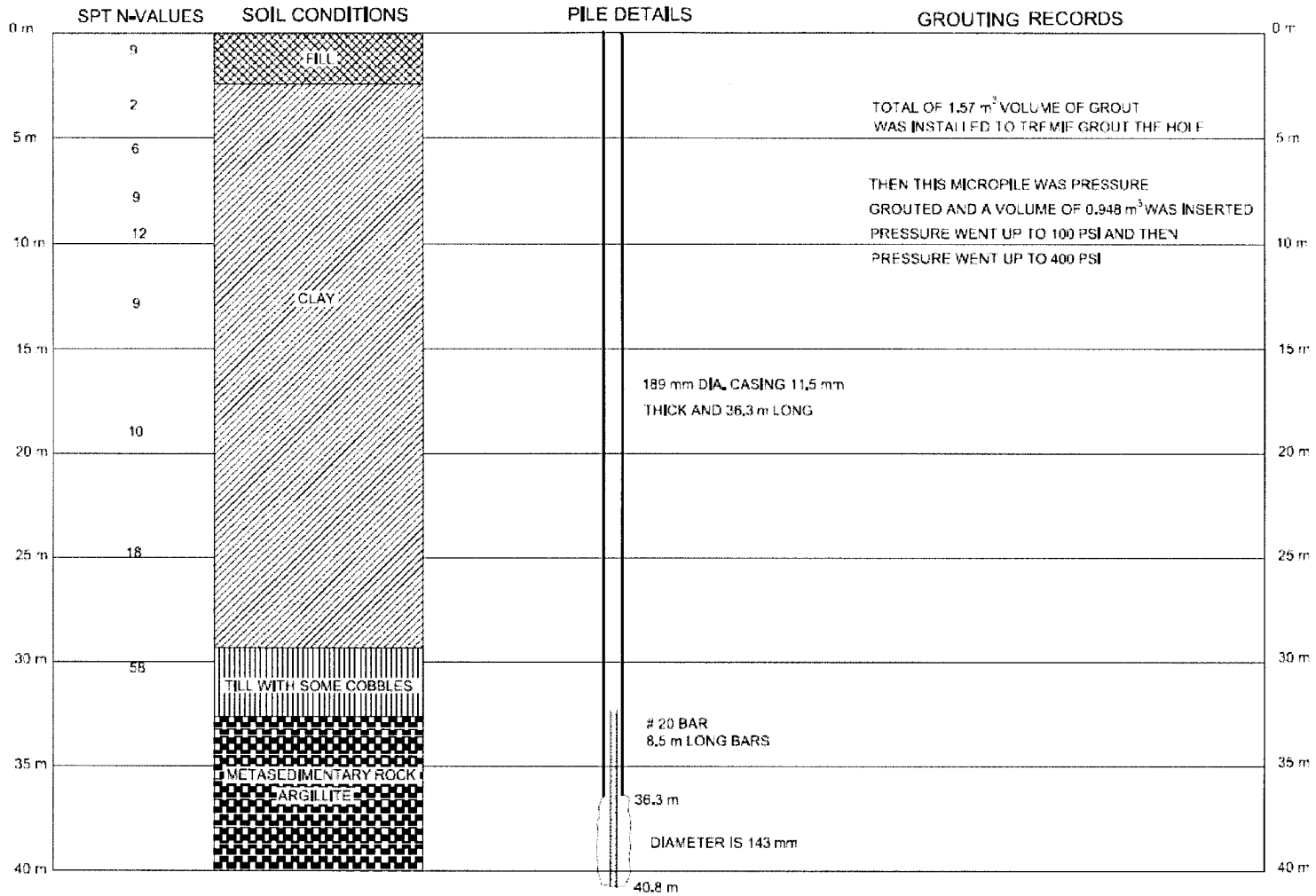


Figure 4.13 Installation Details for Thunder Bay-Micropile 3.

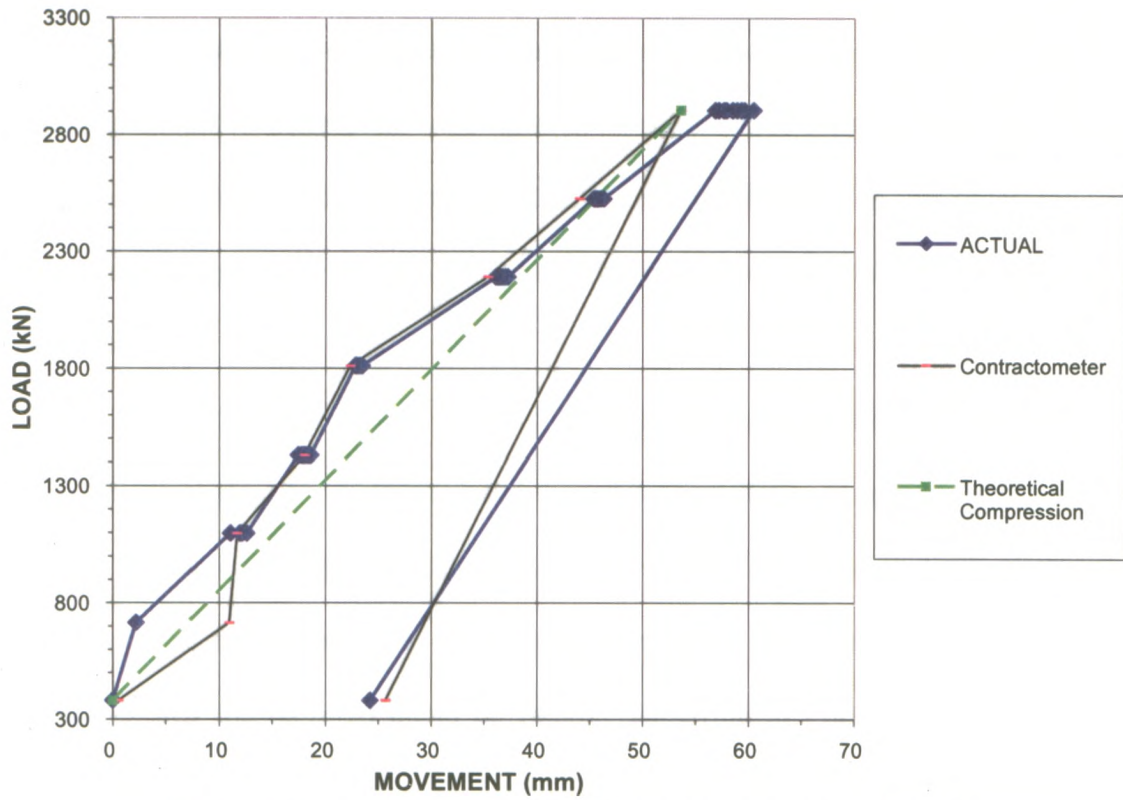


Figure 4.14 Load Displacement for Thunder Bay-Micropile 3.

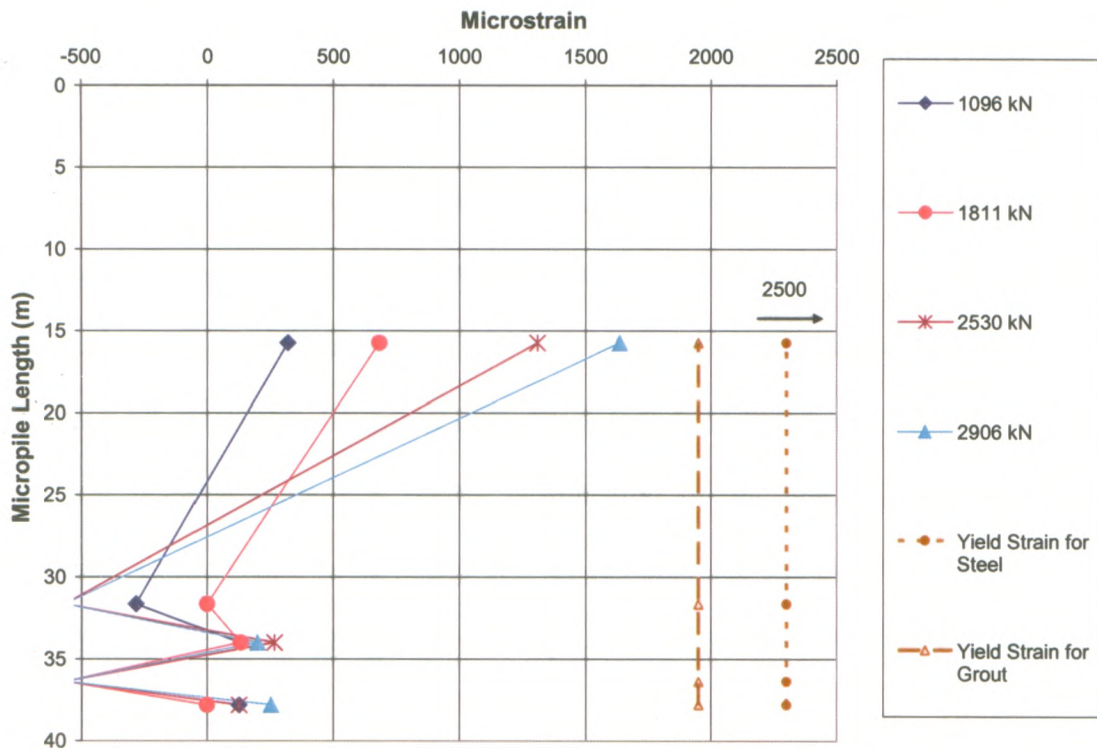


Figure 4.15 Strain vs. Depth for Thunder Bay-Micropile 3.

4.4 Case 3 - Intersection of Yonge and Dundas Toronto Micropile

Case 3 involved the expansion of an existing building at the corner of Yonge and Dundas in Toronto. Micropiles were again used to retrofit existing pile raft foundations due to the low head room available additional pile installation. In this case, one test micropile (Micropile 4) was installed and load tested as described below.

Micropile 4

The tested micropile was installed through silty clay glacial till and embedded into Georgian shale. A casing was used during the installation and water was used for drilling. The water mixed in with the shale and produced a mud like material around the whole length of the pile surface. This mud like material was not cleaned out once the drilling reached the required depth of 14.3m. Referring to Figure 4.16, Micropile 4 consisted of a 14.3 m long (HSS 194x11) casing and a 3168 mm² concentric bar embedded into Georgian Bay Formation with approximately a 5m long (143mm Diameter) socket. This micropile was tremie grouted and pressure grouted according to Method 2.

Figure 4.17, shows the load deflection graph for this micropile. The maximum test load was 2644 kN where one of the reaction micropiles failed. At the maximum load the measured pile head deflection was 12.0 mm while the Contractometer only measured 4.3 mm. The difference indicates deformation in the rock socket. When the load was released there was plastic deformation of 2.7 mm. The measured and theoretical elastic compression of the pile are less than the pile head displacement at all loads therefore this is another case that suggests the load was shed in the rock socket and not in the overburden.

The strain versus depth plot in Figure 4.18 as well as Table 4.4 indicates that this micropile was tested below its structural capacity. It also shows that above a depth of 6 m the strain is constant confirming that there was insignificant load transfer to the surrounding soil. From a depth of 6 to 8 m there is a reduction of strain and hence there is some load shedding along this length. Below 8 m (approximate rock level) the strain is generally negligible which again is consistent with classic socket behaviour (see Figure 4.3).

Table 4.4 Theoretical and Measured Strains along the casing for Micropile 4

Load	Measured Strain* ($\mu\epsilon$)	Theoretical Strain** ($\mu\epsilon$)
881	110	160
1762	330	500
2644	560-700	820

* Deduced from Contractometer measurements

** From Equation 4.2

THE EATON CENTRE TORONTO, ONTARIO

106

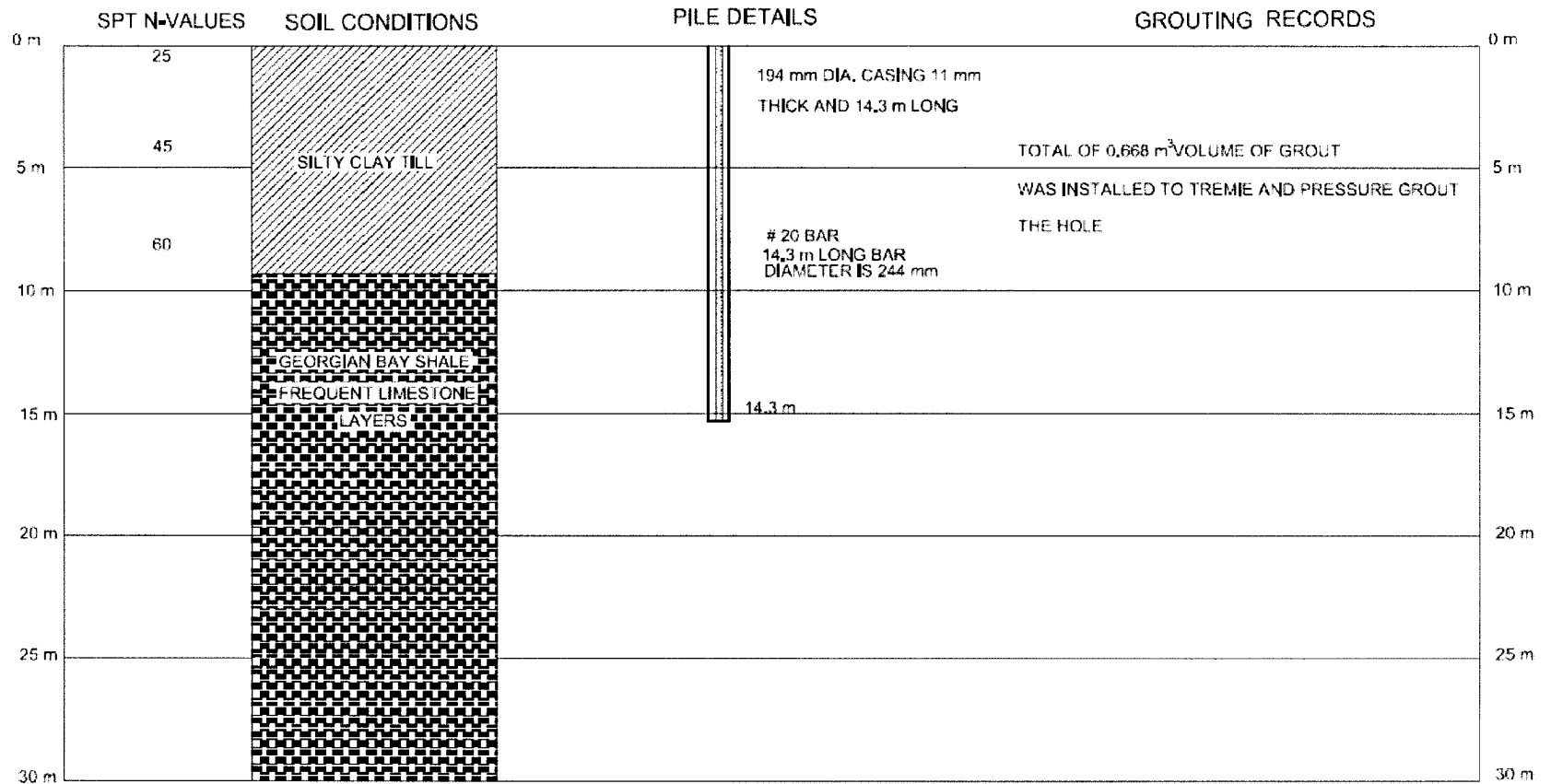


Figure 4.16 Installation Details for Yonge and Dundas Toronto Micropile.

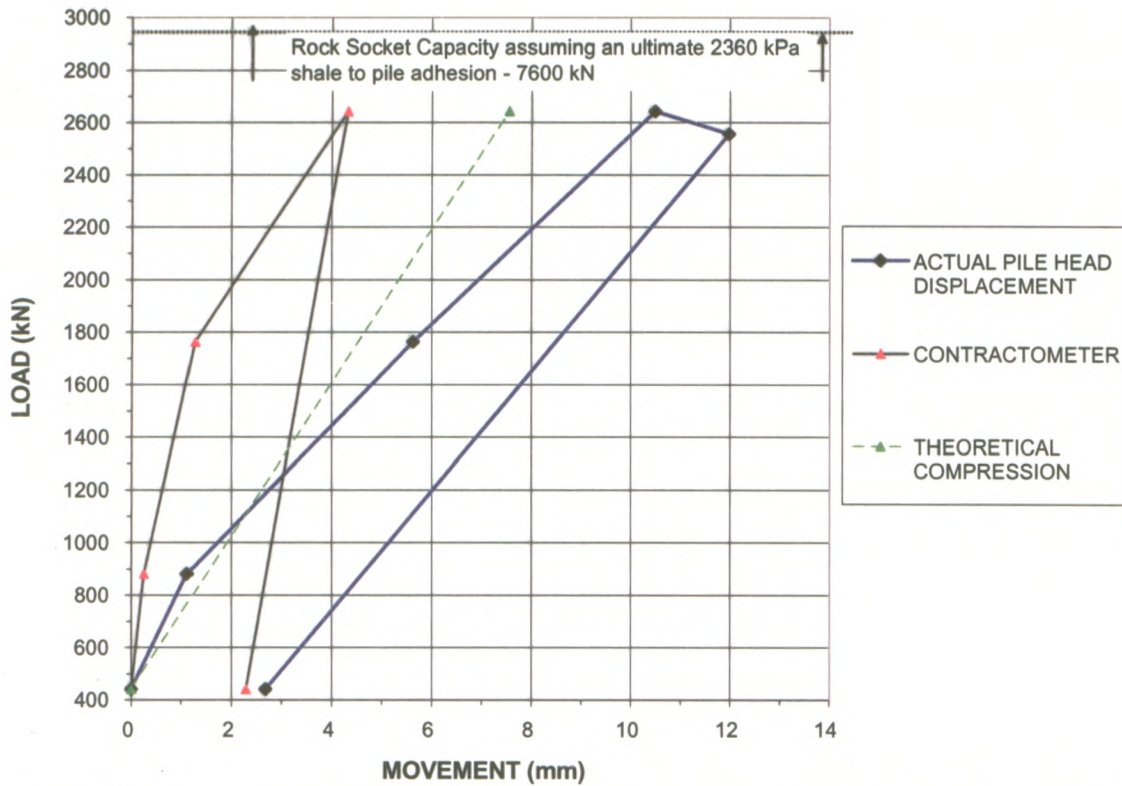


Figure 4.17 Load Displacement Behaviour for Yonge and Dundas Toronto Micropile.

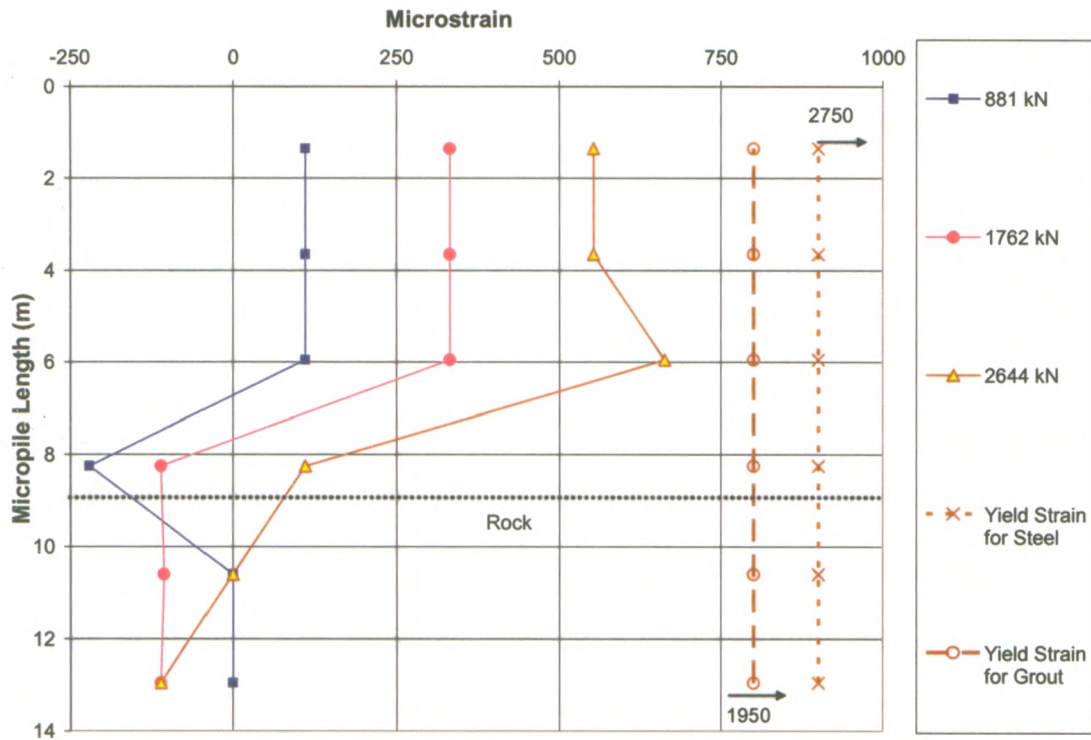


Figure 4.18 Strain vs. Depth Graph for Yonge and Dundas Toronto Micropile.

Confirmation Cases

The preceding cases involved micropiles that were instrumented with a Contractometer during testing. These piles exhibited free column response above the rock and classic socket behaviour in the rock. The following 4 cases are micropiles that were embedded in rock, but were not instrumented with a Contractometer. A brief description of the stratigraphy, geometry of the micropile and installation will be provided in text format only. Each case will also include the load deflection plot. The measure load-displacement response is compared with that deduced using equations 4.1 and 4.2 to confirm the behaviour seen above for the instrumented piles.

4.5 Case 4 – Tip Top Lofts, Toronto

Micropile 5

This micropile (5) was constructed in close proximity to the lakefront in Toronto. Micropiles were installed in an existing building due to seismic upgrading and additional loads resulting from addition of 3 floors above. Because of the seismic requirements, most of the micropiles were installed at a 15% incline and hence the tested micropile was also inclined.

Micropile 5 was installed through a 5 m deep deposit of loose fill overlaying a layer of silty sand with SPT N-values that varied from 6 and 13 blows/ 300mm. This micropile consisted of a 7.2 m long HSS 193x11 casing embedded 300mm into the Georgian Bay Formation. Micropile 5 had a 3.5 m long rock socket. The main steel reinforcement bar comprised 2-3168mm² bars which were installed from ground level to a depth of 10.5m. This micropile was constructed using the rotary duplex drilling method.

Micropile 5 was tested to a maximum load 4000 kN where creep rate of 0.9 mm per hour was measured (See Figure 4. 19). From Figure 4.14, it can be seen that there is good agreement between the theoretical compression of the casing length only and the actual pile head compression.

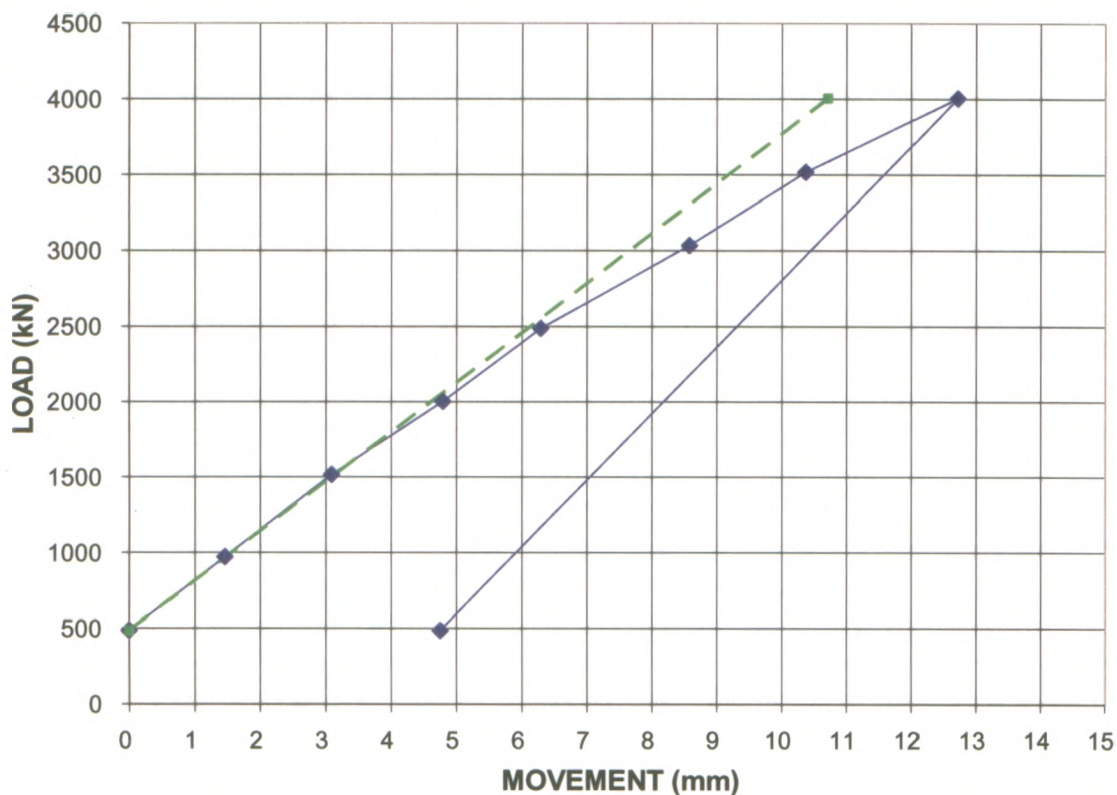


Figure 4.19 Load Displacement Behaviour for Bathurst and Lakeshore Toronto Micropile.

4.6 Case 5 - Exhibition Place, Toronto

Micropile 6

This case involved the only micropile in the Georgian Bay Formation tested to failure. Micropile 6 consisted of a hollow core bar titan bar 73/53 with a #10 bar inside and a 2.15 m long HSS 219x7 casing from the ground surface to a depth of 2.15m. There was an uncased section from 2.15m to the tip at 8.5m. It was drilled through 6.5

m of silty clay with SPT-N values varying from 12 and 36 blows/ 300mm and a 2m-long-175-dia-rock socket. It was constructed by hollow core bar method.

Figure 4.20 illustrates the load displacement for Micropile 6. It was tested to an ultimate load of 2590 kN. At the ultimate load (2590kN), creep rate of 5.3 mm/hour was recorded. From figure 4.20 the actual pile head deflection deviates from the theoretical compression at 1000 kN, indicating there was slippage in the rock socket. Below 1000kN, the pile head response suggests $\delta = PL/AE$ is an adequate idealization for Micropile 6.

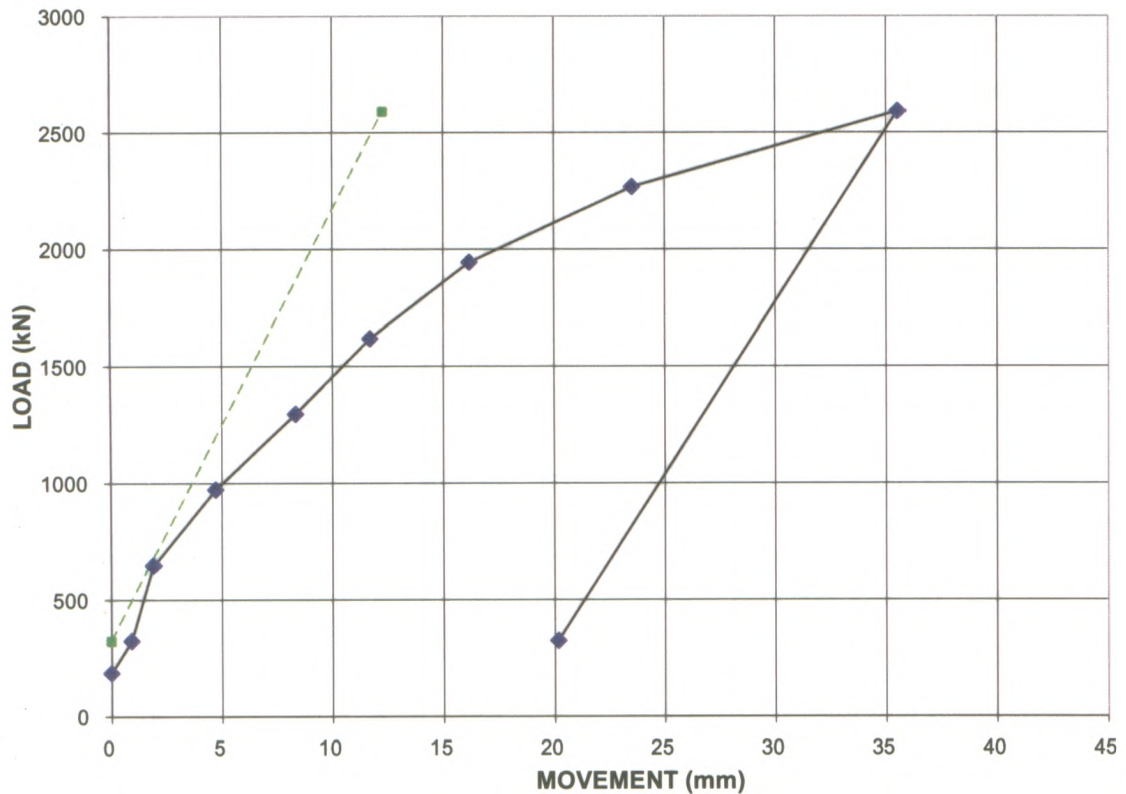


Figure 4.20 Load Displacement Behaviour for Exhibition Place Toronto Micropile

4.7 Case 6 - Mississauga, Ontario

Micropile 7

The last micropile considered was constructed through a clayey silt with SPT N values that varied from 10 to 58 blow/ 300mm from the ground surface to the rock level

(3.2m deep). The Queenston Formation was encountered below 3.2m depth. The pile had a bored diameter of 152mm and it comprised of a No.14 bar ($A_s = 1452 \text{ mm}^2$) that extended from the ground surface to a depth of 5.2m. As such, the pile comprised a 3.2m long section through overburden (clayey silt) and a 2m into the Queenston Formation.

The load-displacement response during the pile load test is presented in Figure 4.21. From Figure 4.21 it can be seen that the measured response of Micropile 7 was close to the theoretical compression estimated from Equations 4.1 and 4.2 up to a load of about 300 kN. Above 300kN, the actual load-displacement response of the pile head exhibited some non-linearity indicative of yielding within the rock socket. At a maximum load of 599 kN a creep rate of 0.2 mm per 30 minutes was recorded. For loads up to 300 kN, however, the response of Micropile 7 is comparable to that of the free column as seen in the other 6 cases.

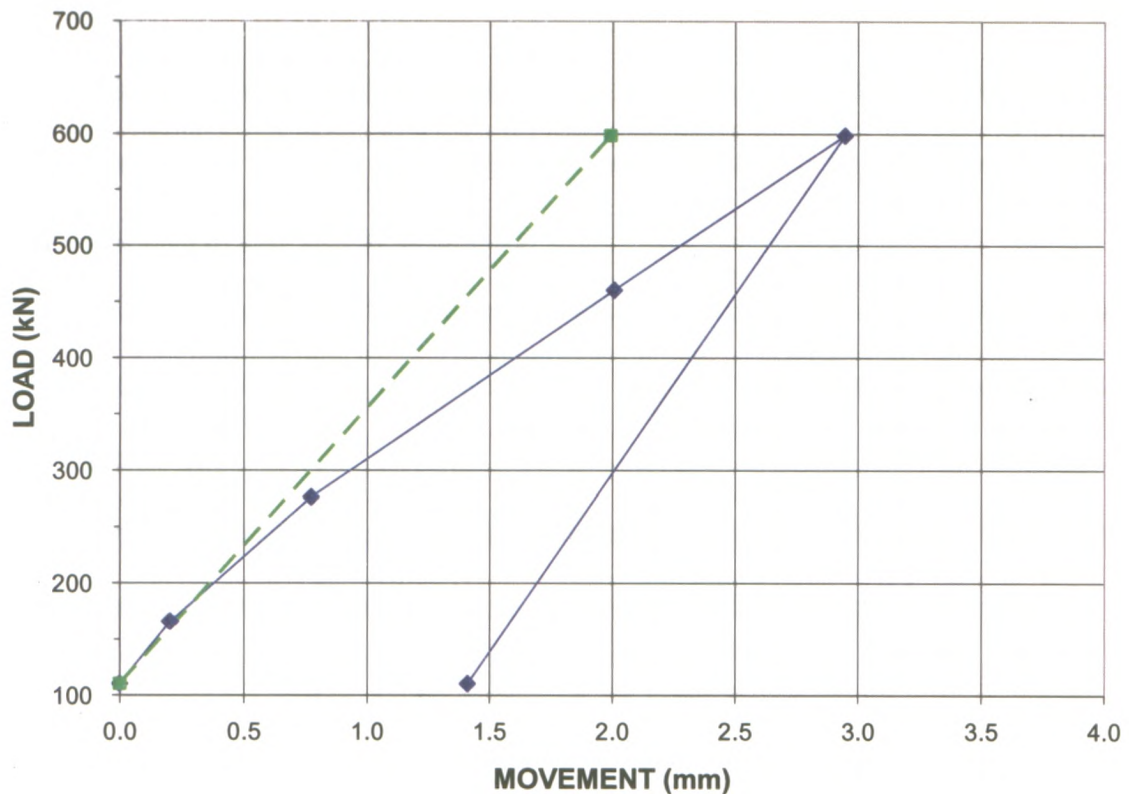


Figure 4.21 Load Displacement Behaviour for Mississauga Micropile.

4.9 Conclusions

This Chapter has presented the results of instrumented and non-instrumented micropiles that were socketed into rock. From the data and analyses presented above, the following conclusions can be drawn:

1. Based on the response of the instrumented micropiles, the section of pile in the overburden soil above bedrock behaves like a free column. The measured strains in this section were essentially constant and close to that predicted using Equation 4.2. This response is confirmed by the non-instrumented cases (e.g. no Contractometer).
2. The strains in the hard rock socket drop rapidly to zero below the rock level. This is consistent with classic rock socket behaviour (see Figure 4.2)

3. In soft rock, there is evidence suggesting the tip of the micropiles studied in this case yield during loading and that there is a possible defect and/or debris in the borehole at the tip. Such behaviour was not observed in the one micropile installed in hard rock (see Case 2).
4. Clearly construction techniques can affect the axial capacity of a micropile as seen in Case 3 where using water had a negative effect in the friction along the rock socket.
5. Finally, some yielding of the rock sockets was observed for piles socketed into weak rock such as the Georgian Bay formation and the Queenston Formation.

CHAPTER 5
SUMMARY AND CONCLUSIONS

5.1 Summary

Chapter 2 provided an overview of micropiles, including the history of micropiles, current design and construction practices, and typical approaches to the analysis of load data. Details of the Contractometer and the properties of grout measured from unconfined compression tests were described in Chapter 2. Chapter 3 described and analyzed five cases of micropiles constructed in cohesionless soils. The description of each case included details of the construction method, the stratigraphy, grout volumes consumed during drilling (in some cases) and the geometry of each micropile. The analysis of micropile load tests consisted of closed-form solutions from pile theory as well as finite element analysis using the software PLAXIS. Four of the tested micropiles were instrumented with a Contractometer to obtain strain measurements along the length of the micropile. The strain measurements provided additional insight into the performance of the piles.

Next, Chapter 4 describes detailed testing and analysis of 8 micropiles socketed into rock. Four of these cases had Contractometers embedded in the piles to measure strain during loading. In most of the cases, it is shown that a classic rock socket is mobilized in hard rock and in soft rock. There is also evidence of yielding of the pile at the tip in soft rock only. Also, in this Chapter a series of confirmation pile tests are described involving micropiles socketed in rock, but that were not instrumented with a Contractometer during the load tests.

Finally, it is the purpose of Chapter 5 to summarize all conclusions made from the analysis and observations contained in this thesis and suggest potential areas for future research.

5.2 Conclusions

In total 16 instrumented micropiles were analyzed using closed-form solutions, and FE analysis. From the analysis as well as the Contractometer readings it was found that construction technique is one of the main factors influencing the adhesion between the grout and the rock or soil. Mainly from the finite element analysis it was found that dilation of the interface and soil surrounding the micropiles provides additional capacity. The comparison of closed-form solutions and actual pile capacities indicate that end bearing can provide more than 25% of the total capacity. The cases of micropiles embedded in rock demonstrate that there is high strain in the tip of micropiles in soft rock. Each of these statements will be furthered discussed and recommendations for further studies will be provided below.

The drilling methodology, as well as the grouting technique of micropile affects the capacity mechanism for micropiles. For example, micropiles often have additional capacity from enlargement (diameter) due to grouting and drilling techniques. It was also noticed from many of the strain versus depth diagrams that the strain was constant along the length of the casing of micropiles. This is considered to be caused by installation of the casing in a hole with a bored diameter that is slightly larger than the casing. This leaves a very small annulus between the drilled diameter and the outside of the casing; which the grout cannot penetrate. For the Case I (Nipigon) it was demonstrated that pressure grouting in several stages as well as post grouting dramatically improved the capacity of the micropiles. Also for Case 5 (Pembroke) the capacity of the micropile mostly came from the boulders that were encountered while drilling. For the first case in the rock micropiles it was shown that poor flushing of

water resulted in a muddy coating outside of the casing which lead to very low adhesion in the rock.

Additional capacity of the micropiles was obtained from dilation along the pile-to-soil interface. This was proven by analyzing cases using FE analysis ignoring dilation and then with dilation. This FE analysis indicated that dilation provided additional post yield capacity which may not be accounted for when analyzing micropiles with conventional pile theory.

Although the literature indicates that it is conservative to ignore end bearing in micropiles, since their cross section is typically small (compared to caissons), it is good practice to account for end bearing to gain a better understanding of how much of the load is sustained in friction and how much is sustained in end bearing. In all of the soil cases presented in Chapter 3, end bearing component accounted for more than 25% of the total capacity.

The load-deflection plots from the micropile tests show that Davisson's criterion is not always accurate when estimating the ultimate capacity of micropiles from pile load test results. In addition, the estimation of pile deflection cannot always be calculated using Poulos and Davis solutions since the slenderness of some micropiles lies outside the range of parameters reported in their graphs.

Some of the micropiles socket in rock and presented in Chapter 4 indicate that there are large strains near the pile tip. Some causes may be that the tip of these micropiles was not cleaned well and there was crushing of cuttings while the test was taking place.

5.3 Recommendations

For future work in micropiles, it is recommended that close inspection of installation of micropiles be done. In particular it is recommended to closely quantify the grout volumes when micropiles are being installed to estimate enlarged diameters. It is very important to note abnormalities while drilling such as boulders hit or how cuttings are being flushed out of the hole in order to quantify the factors affecting end bearing as well as side friction. It is also recommended to further research on quantifying the contribution from end bearing and side friction in micropiles. Hopefully, one day a test with an Osterberg-cell can be done to determine the contribution from end-bearing and side friction considering end-bearing modulus as well as the friction modulus. It is also recommended that further instrumentation of micropiles be undertaken to continue to understand how existing as well as future drilling methodologies and grouting procedures hinder or enhance the capacities of micropiles.

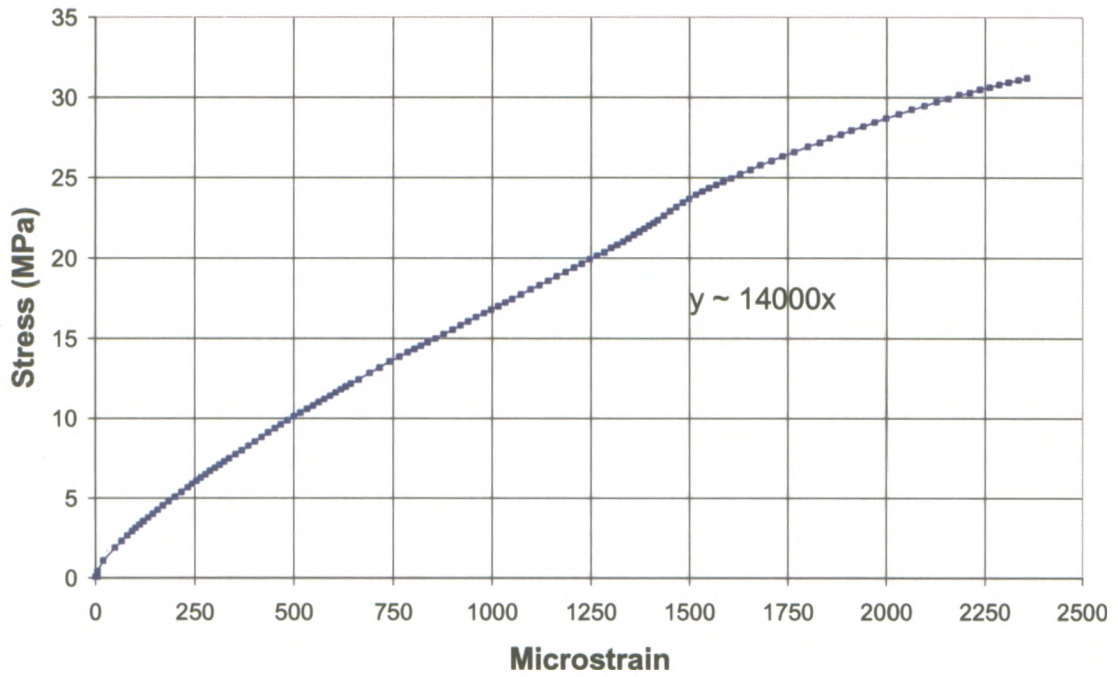
REFERENCE

- ASTM D 1143. Standard Test Method for Piles Under Static Axial Compressive Load. American Society for Testing and Materials.
- ASTM C 109-64 Standard Method of Test for Compressive Strength of Hydraulic Cement Mortars (using 2-in. Cube specimens).
- Bruce.J, Ramirez.D and P.Lausch (2005). “The SMART Contractometer – Its Application to Micropile Quality Assurance”. Proceedings of the ADSC – Geo Cubed: Comprehensive AQ/QC Technical Conference, Dallas, TX.
- Cadden. A., Bruce. Et. Al. (2004). “Current Practices and Future Trends in Deep Foundations: A special Geotechnical Publication Honouring George G. Goble”
- Donald P.Coduto. Foundation Design Principles and Practice. 2001. Second Edition. Prentice Hall New Jersey.
- Fellenius.H.B (1980). The Analysis of Results from Routine Pile Load Tests. Ground Engineering. September pages 19 to 31.
- Fellenius H.B. (2002). Determining the Resistance Distribution in Piles. Part I. Notes on Shift of No-Load Reading and Residual Loads. Geotechnical Instrumentation News. Volume 20 No 2. Pages 23 to 27.
- FHWA (1997). Drilled and Grouted Micropiles: State-of-Practice-Review. Report No. FHWA-RD-96-016/019. United States Department of Transportation, July 1997. Volume II.
- FHWA (2000). Micropile Design and Construction Guidelines Implementation Manual Priority Technologies Program. Publication No. FHWA-SA-97-070. United States Department of Transportation, June 2000.
- Itasca Consulting Group (2005). Theory and Background Manual. Third Edition.
- Jessee A., F.Barry Newman (2004). Compressive Strength Testing of Micropile Grout. Foundation Drilling ADSC: The International Association of Foundation Drilling. September/ October issue Pages 24 to 34.
- Lizzi, Fernando (1982). The static Restoration of Monuments basic criteri-case histories. Stengtheing of buildings damaged by earthquakes. Sagep Publisher. Genova.
- Lizzi, Fernando (2002). Micropiles: Fifty Years Ago and Now. Conference proceedings for International Workshop on Micropiles in Venice, Italy.

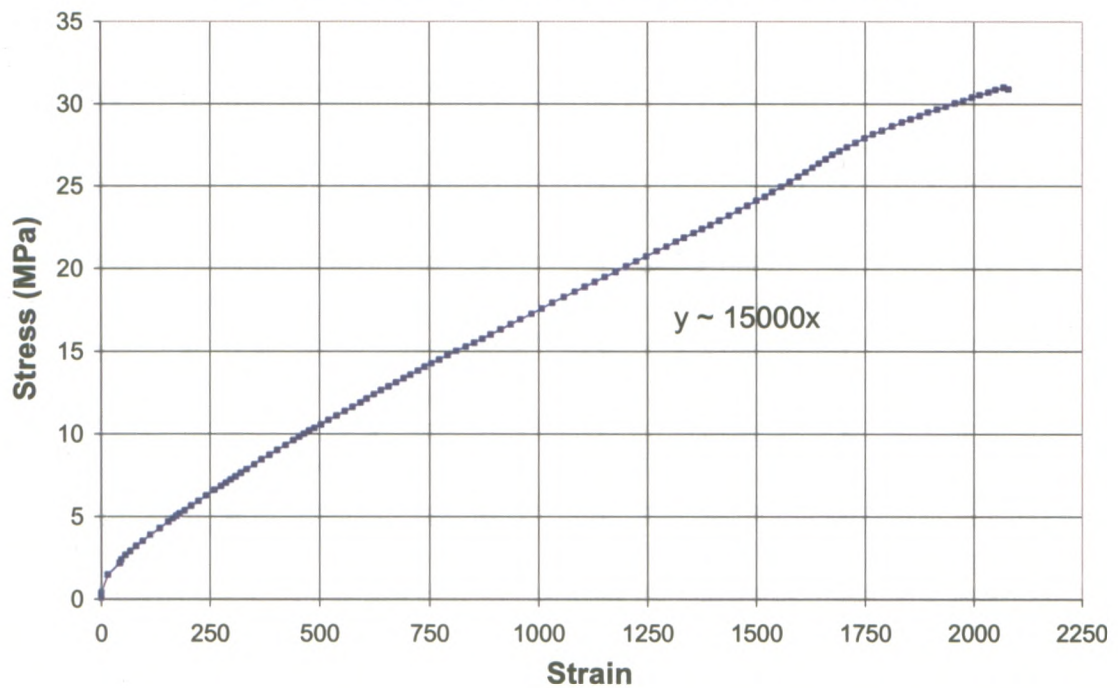
- MJ Tomlinson (1995). *Foundation Design and Construction*. Sixth Edition. Longman Scientific & Technical, New York.
- Muni Budhy. *Soil Mechanics and Foundations*. 2000. John Wiley & Sons.
- Peter Rosenberg and Noel L.Journeaux (1976). Friction and end bearing tests on bedrock for high capacity socket design. *Canadian Geotechnical Journal*. Volume 13, pages 325 to 332.
- P.J.N. Pells and R.M. Turner (1979). Elastic Solutions for the design and Analysis of Rock-socketed piles. *Canadian Geotechnical Journal*. Volume 16, Pages 481 to 486.
- Poulos, H.G and E.H Davis (1980). *Pile Foundation Analysis and Design*. Series in Geotechnical Engineering. New York.
- Post Tensioning Institute (2004). *Recommendations for Prestressed Rock and Soil Anchors*. Fourth Edition. USA.
- Ramirez.D “What we have learned about Micropile Behaviour from Field Instrumentation” (2006). *Proceedings of the International Society of Micropiles*. Schrobenhausen, Germany
- Russo.G (2004). Full-Scale Load Tests on Instrumented Micropiles. *Geotechnical Engineering* 157 Issue GE3. Pages 127 to 135.
- R.Whitlow (1995) . *Basic Soil Mechanics*. Third Edition. Addison Wesley Longman Limited, Harlow Essex, England.
- Seidel.J. (2002). The Magazine of the Deep Foundations Institute Deep Foundations. Fall 2002 pages 29 to 32.
- S.-S.Jeon (2004). Interpretation of Load tests on Minipiles. *Geotechnical Engineering* 157 Issue GE2. Pages 85 to 90.
- Townsend, F.C., Anderson, J.B Rahelison. L (2001). *Evaluation of FEM Engineering Parameters from Insitu Tests*. Florida Department of Transportation.

APPENDIX A GROUT COMPRESSION RESULTS

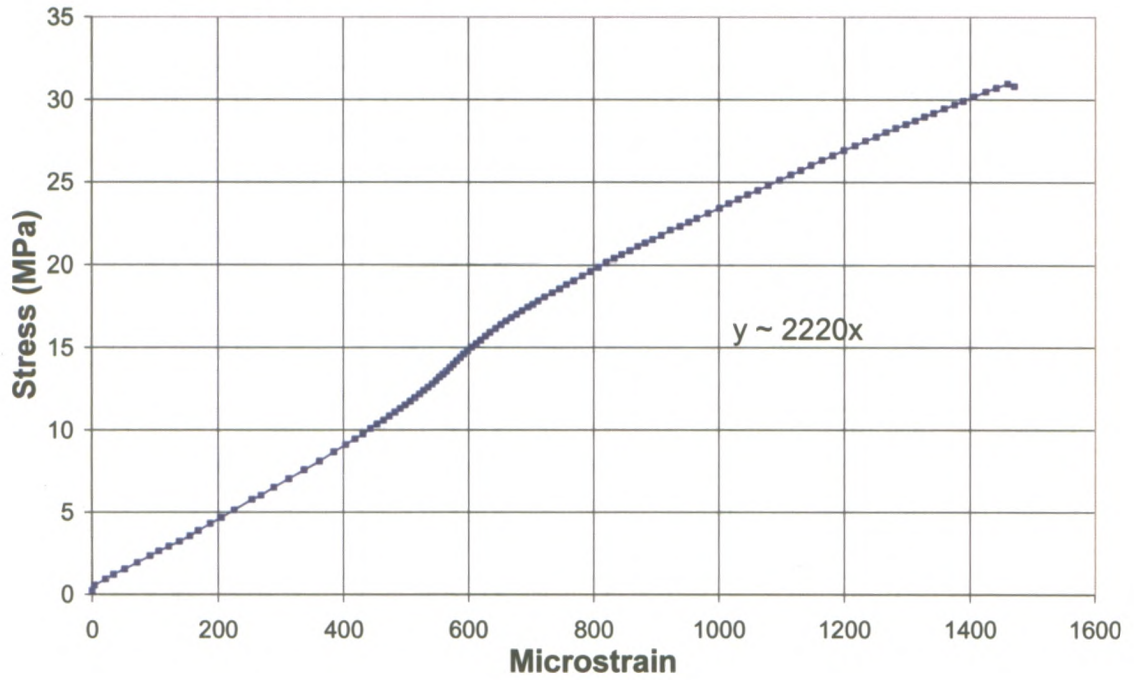
Compression Grout Test after 7 Days



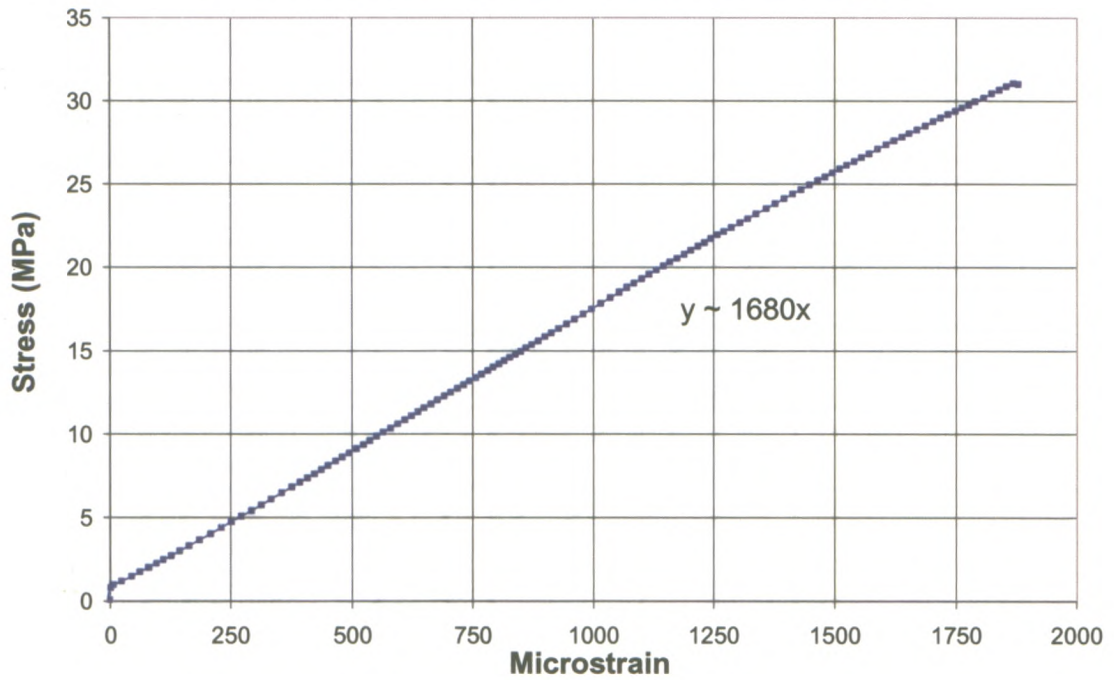
Compression Grout Test After 7 Days



Compression Grout Test After 24 Days

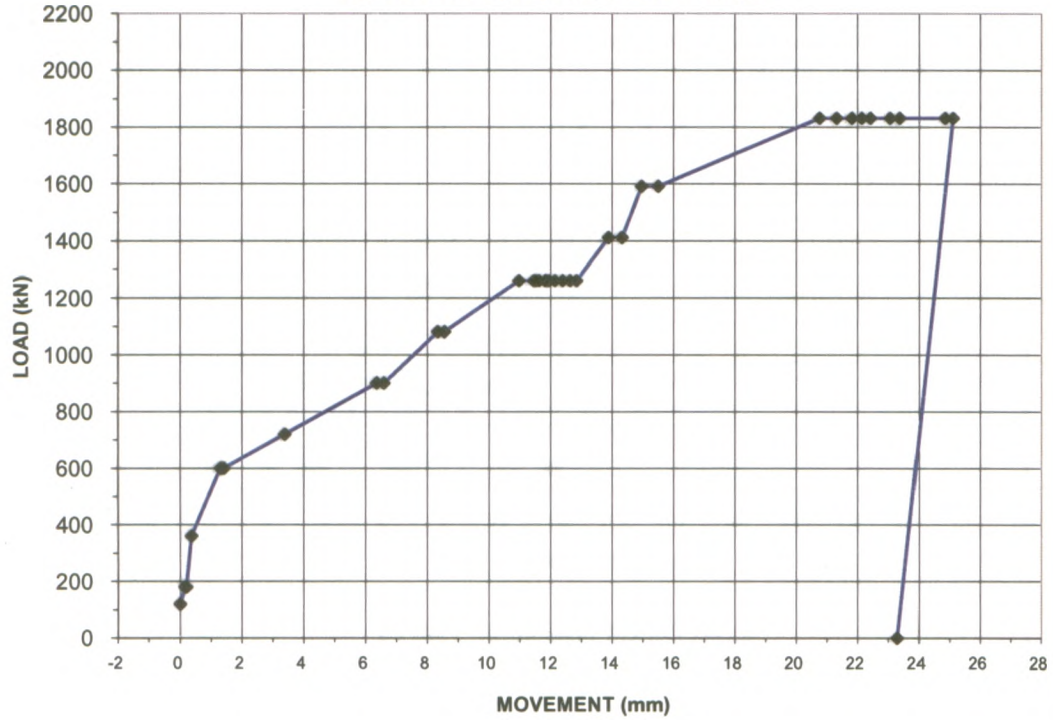


Compression Grout Test after 24 Days

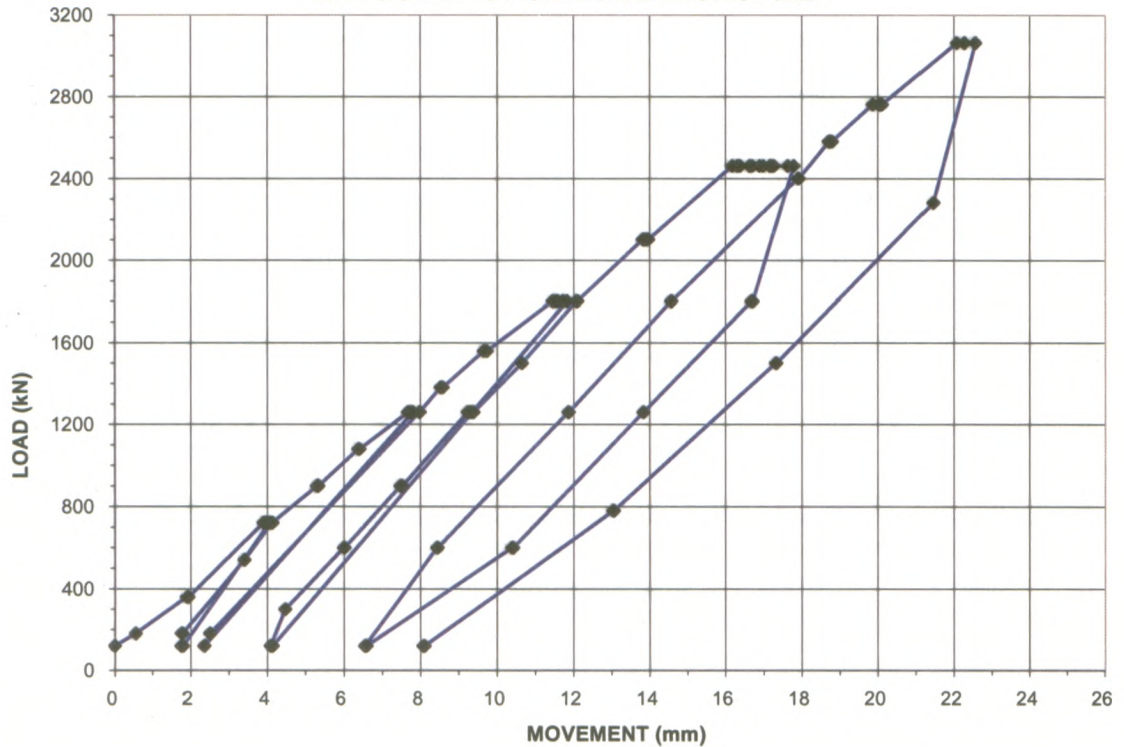


APPENDIX B RAW LOAD TEST RESULTS

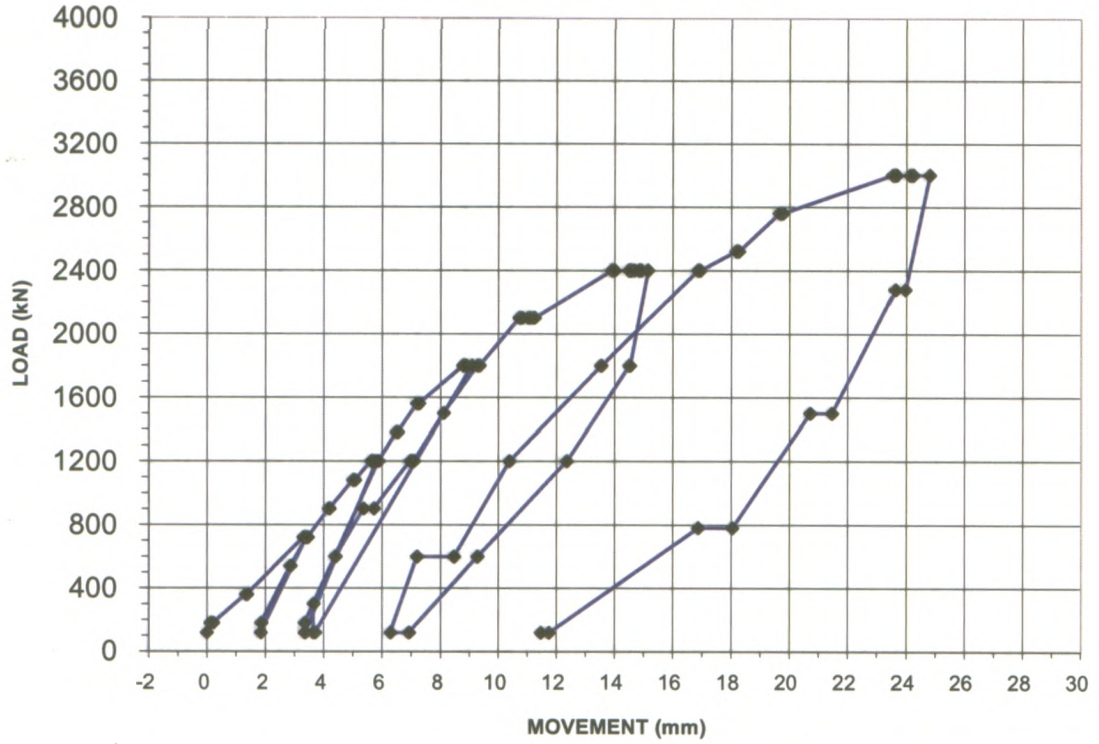
NIPIGON MICROPILE EAST SIDE



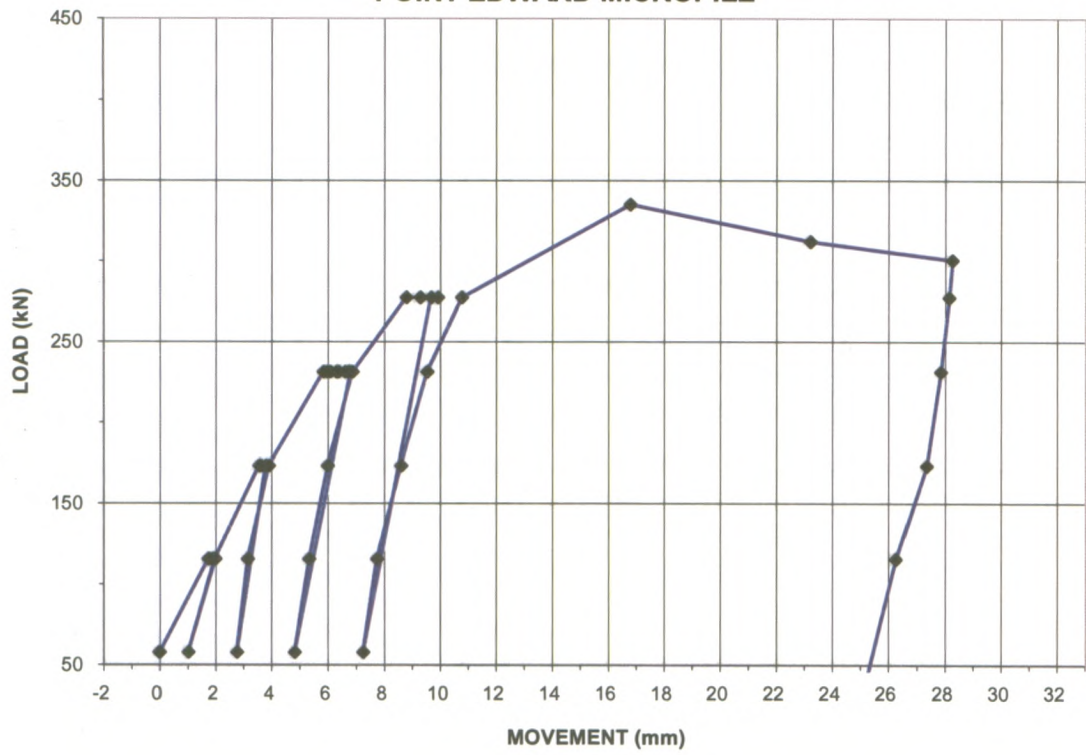
NIPIGON EAST SIDE 2ND MICROPILE



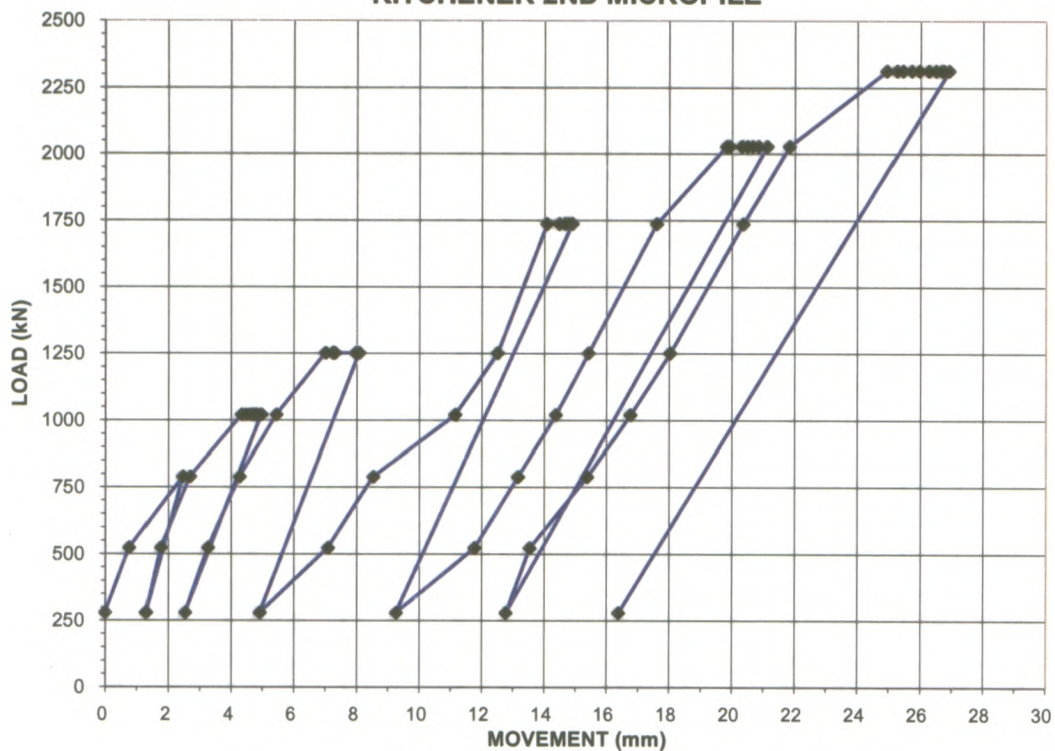
NIPIGON MICROPILE WEST SIDE



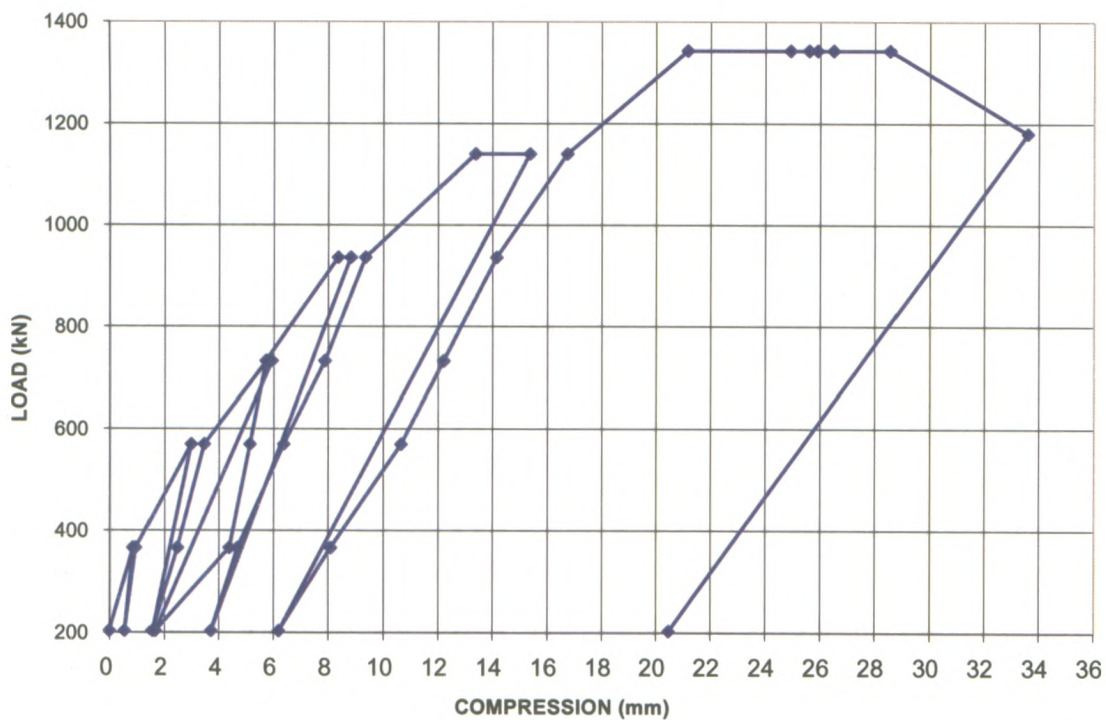
POINT EDWARD MICROPILE



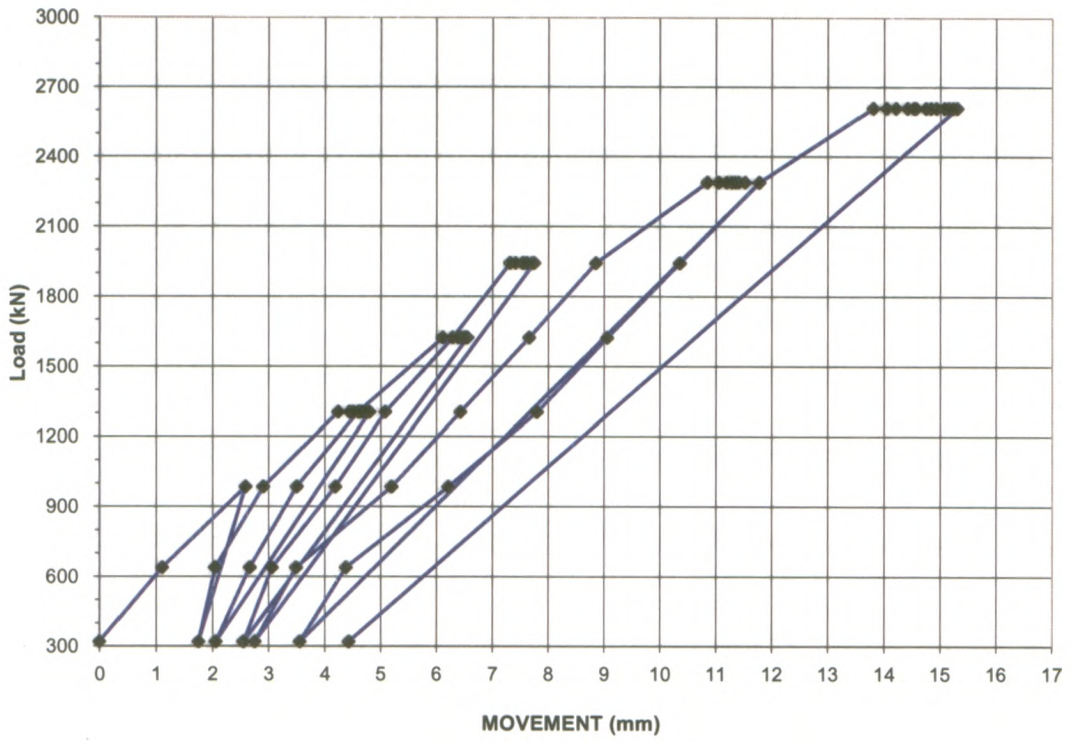
KITCHENER 2ND MICROPILE



ALLISTON MICROPILE



PEMBROKE MICROPILE



APPENDIX C

SENSITIVITY ANALYSIS

This section analyzes the response of micropile 1 (refer to Chapter 3). This micropile is embedded in a deposit of cohesionless soil. The micropile is 273 mm diameter and 24.4m long micropile. The upper 9.9 m of the micropile is cased (HSS 273x13). The soil properties assumed in the FE analysis are listed in Table C1. The groundwater table is situated 3 m from the ground surface. The following is a discussion of the influence of ψ_i , ϕ'_s , E_s and K'_o on the pile response during loading.

Table C1. Parameters Used for the Micropiles at Nipigon.

Material	E MPa	c' kPa	v	Φ'/δ_i	Dry Density Kg/m ³	Ko	Ψ
Casing, bar and Grout	33500	32700	0.33	0	1300	0.54	0
Bar and Grout	19600	19100	0.33	0	1300	0.54	0
Silt and Sand	50	2	0.35	38	1000	0.54	8
Stiff Clay	75	100	0.35	0	1000	0.54	0
Top Fill	10	1	0.35	32	1300	0.54	1
Interface along the uncased length	50	2	0.35	38*	1000	0.54	8

* Refers to δ_i

Figure 1 shows the impact of ψ_i on the micropile response from FE calculations. Point A is the yield point as defined in Chapter 3. It can be seen from Fig. 1, that ψ_i governs the slope of the load-deflection curve after reaching Point 'A'.

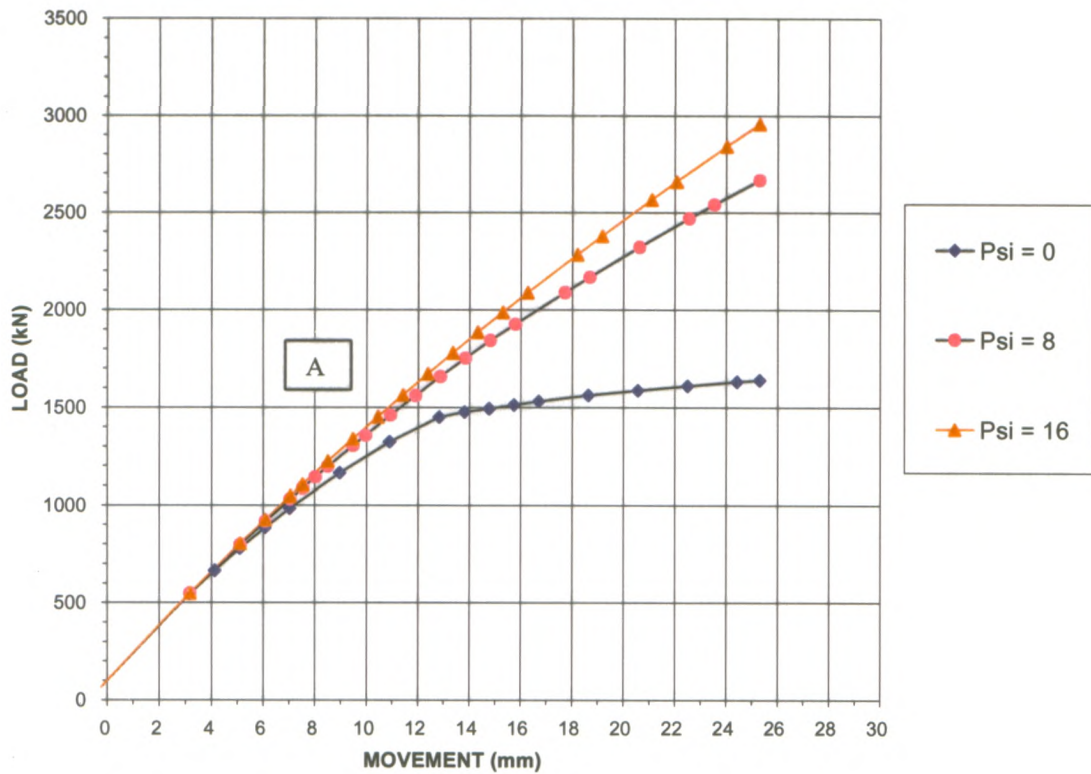


Figure C1. Sensitivity Analysis for psi angle

In Figure 2 it is shown that when Phi is doubled the maximum load achieved at a displacement of 24 mm is increased by 2.2 times. When the Phi angle is doubled again the load achieved at a displacement of 24 mm is increased by 3.6. This suggests that Phi angle is very sensitive parameter in the load deflection results from the Finite Element Analysis.

Figure 2 illustrates the influence of ϕ'_s on the response of a typical micropile. From Figure 2, it can be seen that increasing ϕ'_s increases the ultimate pile capacity (for $\psi_i=8^\circ$).

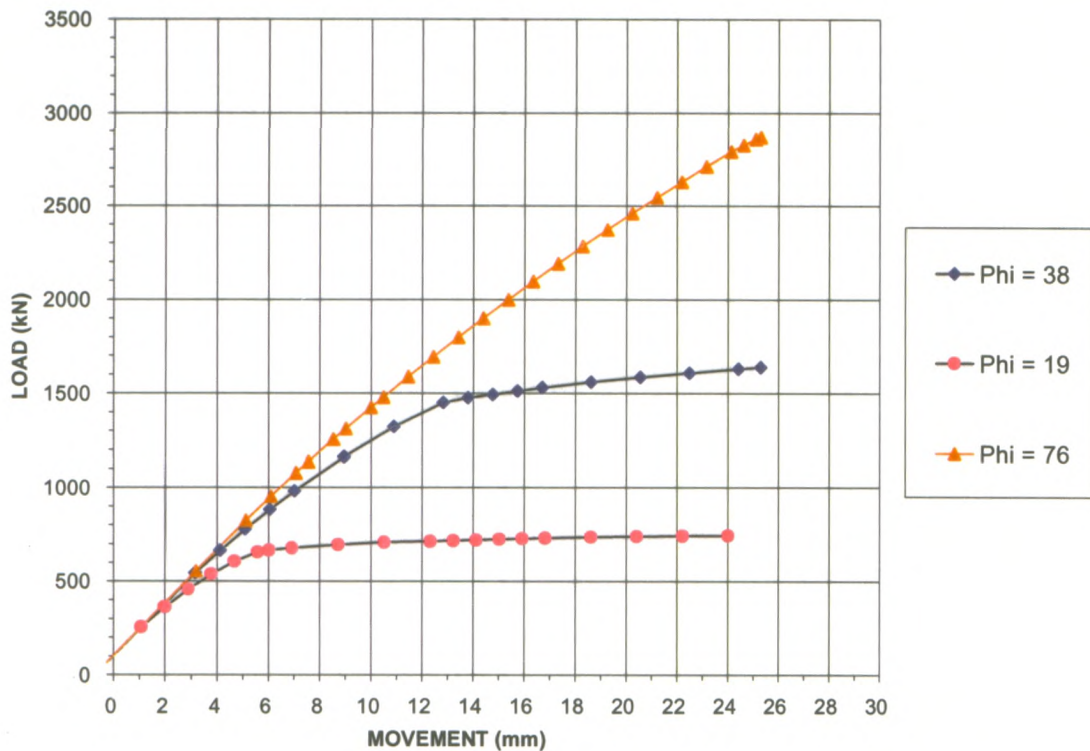


Figure C2. Sensitivity Analysis for phi angle

Figure 3 illustrates the influence of soil modulus of Elasticity. Referring to Fig. 3, it can be seen that when the Elastic Modulus is doubled the maximum load achieved at a displacement of 24 mm is increased by 10%. When the Elastic Modulus is doubled again the load achieved at a displacement of 24 mm is increased by 20%. This suggests that the Elastic Modulus is not a very sensitive parameter in the load deflection results from the Finite Element Analysis. The primary influence of the elastic modulus is to increase the slope of the load-deflection curve for loads up to 1200 kN.

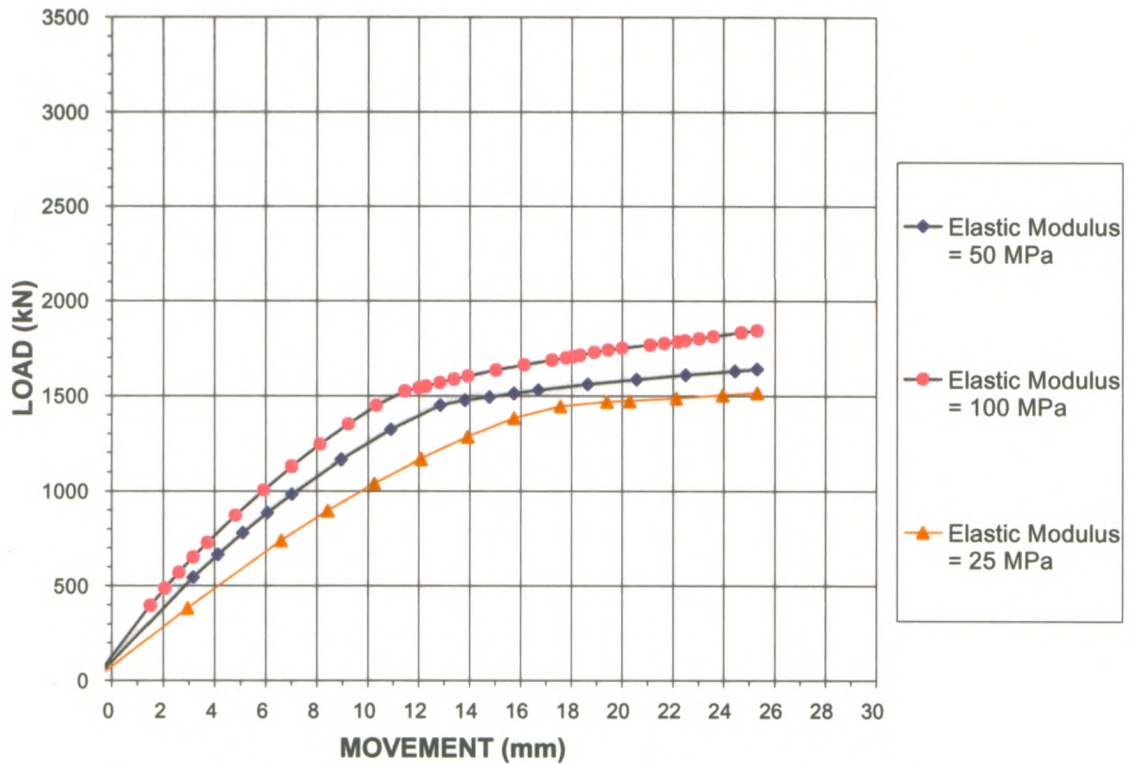


Figure C3. Sensitivity Analysis for Elastic Modulus

Figure 4 illustrates the influence of the pile diameter on the calculated pile response. From this figure, it can be seen that when the Diameter of the pile is doubled the maximum load achieved at a displacement of 24 mm is increased by 2.2 times. When the diameter of the pile is doubled again the load achieved at a displacement of 24 mm is increased by 4.5 times. This shows that the diameter of the pile has a major impact on the ultimate pile capacity as well as on the initial slope of the load-deflection curves.

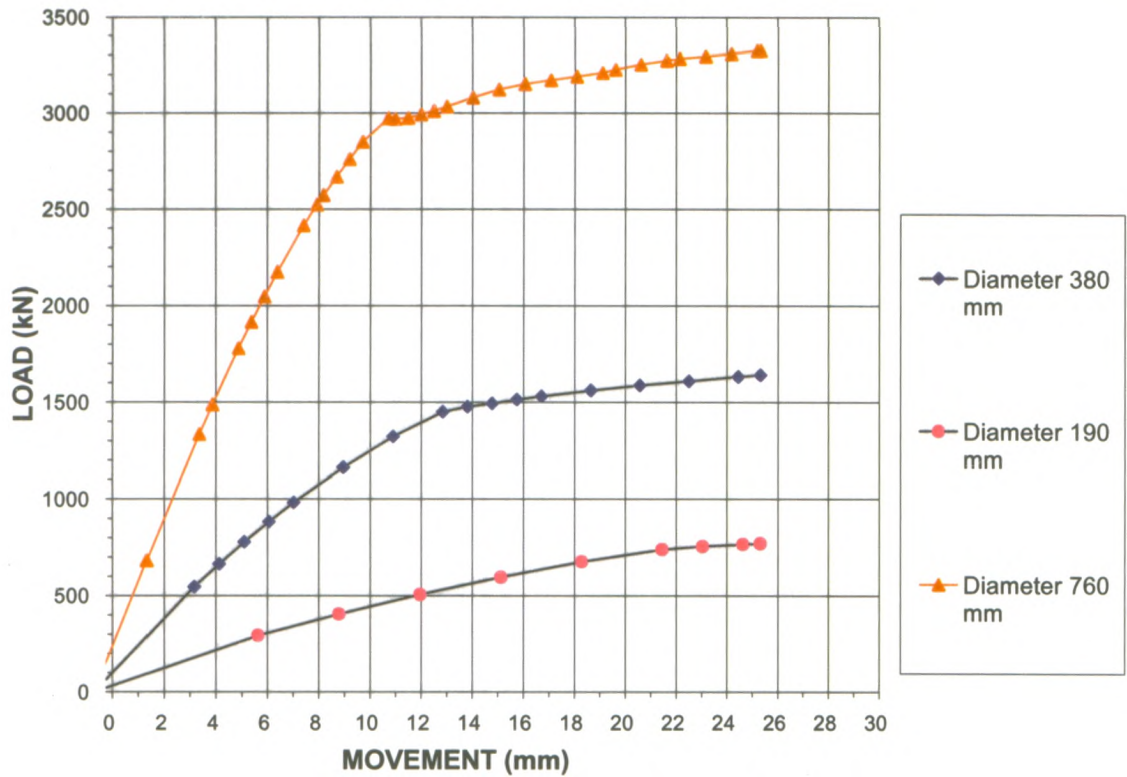


Figure C4. Sensitivity Analysis for Diameter of the pile

To conclude, Figure 5 shows the impact of K'_o on the pile load-displacement response. The analyses shown in Figure 5 indicate that when the coefficient of at rest pressure is doubled the maximum load achieved at a displacement of 24 mm is increased by 20%. When K'_o is doubled again the load achieved at a displacement of 24 mm is increased by 40%. Thus, the load displacement response is moderately sensitive to K'_o .

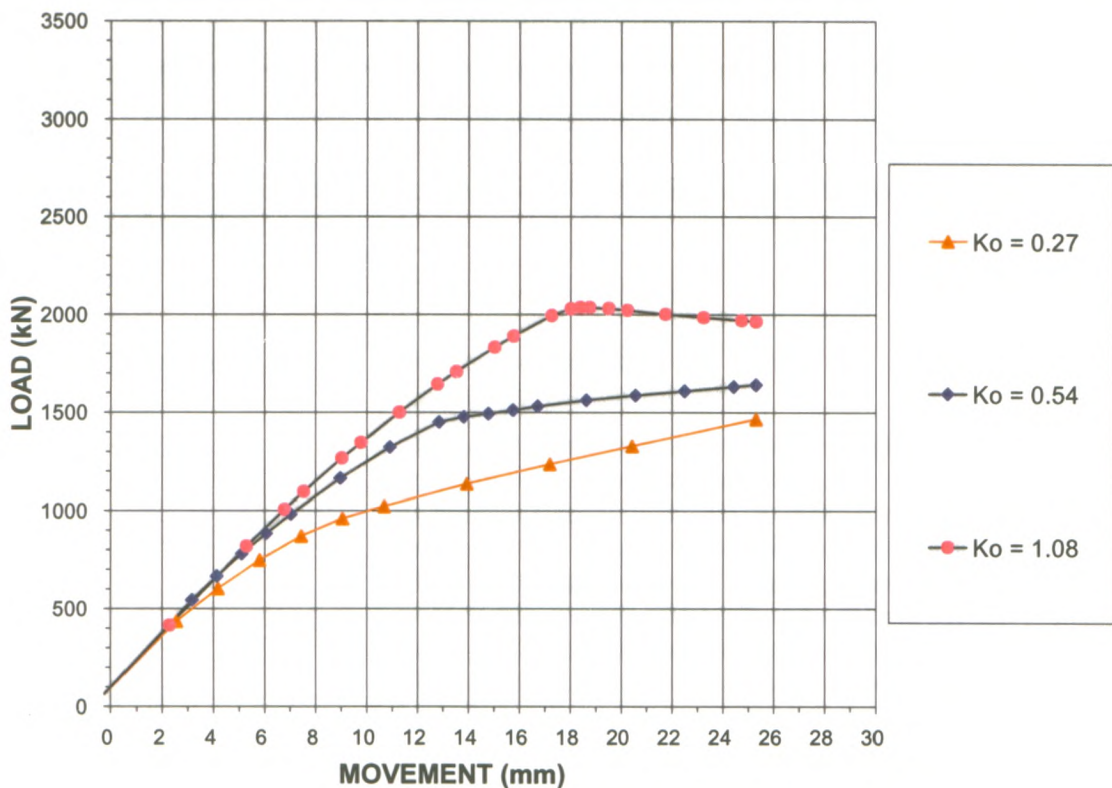


Figure C5. Sensitivity Analysis for the K_o

In summary, the primary variables affecting the pile load-displacement response are ϕ , ψ , and D . Changes in these parameters have a significant impact on both the calculated stiffness and the axial capacity of micropiles. K'_o is a secondary parameter. Changes in the value of K'_o tend to cause moderate changes in the micropile response. The calculated behaviour of micropiles is least sensitive to changes in the elastic modulus of the soil. This parameter has a negligible impact on the ultimate capacity of a micropile but a significant impact on the initial slope of the load-deflection curve.